

LAYERWISE HIGHER-ORDER FINITE ELEMENTS

LAYERWISE HIGHER-ORDER FINITE ELEMENTS  
FOR LAMINATED COMPOSITE MATERIAL  
STRUCTURES

(積層複合材料構造の多層・高次変形有限要素法解析)

鈴木 浩 治

平成9年度 東京大学 博士学位論文

LAYERWISE HIGHER-ORDER FINITE ELEMENTS  
FOR LAMINATED COMPOSITE MATERIAL  
STRUCTURES

( 積層複合材料構造の多層・高次変形有限要素法解析 )

by

KOHJI SUZUKI ( 鈴木 浩治 )<sup>†</sup>

Thesis submitted in partial fulfillment  
of the requirements of the degree of Doctor of Engineering  
in Naval Architecture and Ocean Engineering,  
Division of Engineering, Graduate School,  
University of Tokyo

( 東京大学 大学院 工学系研究科 船舶海洋工学専攻 )

Thesis supervisors : Professor Isao Kimpara and Professor Kazuro Kageyama

( 指導教官 金原 勲 教授 影山 和郎 教授 )

Copyright © 1997 by Kohji Suzuki

December 19<sup>th</sup>, 1997 ( 平成9年 12月 19日 )

<sup>†</sup> JSPS Research Fellow

## Acknowledgements

First of all, I can scarcely express my appreciation and gratitude to the two thesis supervisors, Professor Isao Kimpara and Professor Kazuro Kageyama, for their supports and encouragements throughout my graduate student days. Professor Kimpara showed me not only plenty of interesting examples concerning numerical analysis of composite materials, but also his valuable works relevant to my study. He also gave me a lot of opportunities for attending many related conferences in and out of the country, joining a couple of collaboration projects and whatever. Professor Kageyama has been so patient with me, although the progress of my research was very slow and I could hardly meet his demands. His prominent sense of engineering and enthusiasm for research have been amazing me and then encouraging me. Furthermore, I am always impressed by their deep insight into composite material technologies and sciences.

I am also greatly indebted to the five referees of the University of Tokyo, the two thesis supervisors, Professor Isao Kimpara and Professor Kazuro Kageyama, and Professor Hideomi Ohtsubo, Professor Yutaka Toi and Associate Professor Katsuyuki Suzuki, for reading the manuscript, making their valuable comments and suggesting much better improvements of this thesis work.

In addition, I have to thank Mr. Toshio Suzuki and Mr. Isamu Ohsawa, Research Associates of Giso Lab., for their helpful advises on my research. When I was in trouble, I used to go and ask Mr. Suzuki, and he would always willingly help me. It was the most pleasant and significant time for me to chat with him at lunch. Mr. Ohsawa was very kind of me. He kindly gave me a lot of practical information on composite materials, especially testing methods and know-hows for operating the experimental apparatuses. I will never forget such a precious time with the two of them.

I also thank Mr. Kanai, Research Assistant, Ms. Oya and Ms. Sato, secretaries, for their encouragements, and I am very thankful to Dr. Takeshi Takatoya, National Aerospace Laboratory, for his encouragements, cooperations and many technical advises, especially for giving know-hows for computer operations. I also want to thank to Mr. Takuro Suzuki, Shonan Institute of Technology, for making an offer of some valuable numerical results by CLEOPS/COMPOSIC Package.

Furthermore, I am deeply grateful to JSPS (the Japan Society for the Promotion of Science) for its financial support to my research activities as a JSPS Research Fellow.

Finally, I want to say "thank you" to my wife, Makiko. Without her patience, support and encouragement, it would have been impossible to complete this thesis work.

## Abstract

The main purpose of this thesis work is to formulate a proper and precise numerical model for laminated composite material structures (composite laminates), and then propose an efficient and flexible methodology for numerical analysis/design of composite materials.

According to the purpose, the first part of this thesis is focusing on numerical analysis models for composite laminates. The restrictions, limitations and deficiencies of the existing numerical models for conventional materials (i.e. commercially available finite element analysis packages in which designers must choose one of those of ESL-based first-order plate/shell elements, 2-D, 3-D continuum solid elements or their combinations) are revealed therein. After the drawbacks of the existing models for conventional materials are exposed, a new general theory for composite laminates based on the layerwise and higher-order displacement assumptions are proposed. The proposed general theory is capable of flexible modelings of composite laminates corresponding to any analysis demand. Further, by using the proposed theory, a flexible and versatile analysis/design methodology for composite laminates are established.

In the rest of this thesis, several finite element (FE) analysis programs are developed as specific approximations deduced from the proposed general theory. In each finite element development, several numerical applications are conducted and discussed, ranging from its accuracy and convergence checks to some practical problems. Through these actual finite element analysis examples, it is ensured that the proposed layerwise higher-order model certainly serves as a proper and efficient numerical model for the analysis and design of composite laminates.



# Contents

<b>1 Overview</b>	<b>1</b>
1.1 Introduction	2
1.1.1 Laminated composite material structures	2
1.1.2 Numerical modelings of composite materials	3
1.2 Objectives of this thesis	4
1.3 Layout of this thesis	5
<b>2 Case Studies by the Existing Numerical Models</b>	<b>7</b>
2.1 Introduction to this chapter	8
2.2 Anisotropic properties	9
2.2.1 Case 1 : trapezoid orthotropic plate bending	10
2.3 Weaker properties in the thickness direction	11
2.3.1 Case 2 : influence of thickness on global elastic responses	11
2.4 Laminate-like, through-the thickness inhomogeneity	13
2.4.1 Case 3 : NCF-coupling joint for composite drilling riser	14
2.4.2 Case 4 : composite sandwich motorboat	15
2.4.3 Case 5 : interlaminar stresses	16
2.5 Summary	17
<b>3 Numerical Models for Composite Laminates</b>	<b>42</b>
3.1 Introduction to this chapter	43
3.2 Theories and their finite elements for composite laminates	43
3.3 Formulation of the layerwise higher-order deformation theory	46
3.3.1 Multi-layer discretization scheme	46
3.3.2 Higher-order deformation theory for each layer	47
3.3.3 Assemblage of layers	51
3.3.4 Governing equations — in case of the penalty method	54
3.4 Numerical modeling methodology	57
3.5 Summary	58
<b>4 Selective Layerwise Sandwich Element</b>	<b>65</b>
4.1 Introduction to this chapter	66

4.2	Finite element approximation . . . . .	67
4.2.1	[[110](111)(110)] assumptions . . . . .	67
4.2.2	Finite element discretization . . . . .	73
4.3	Numerical examples . . . . .	74
4.3.1	Accuracy and convergence check . . . . .	74
4.3.2	Comparison with experimental results . . . . .	75
4.4	Discussion . . . . .	76
<b>5</b>	<b>Layerwise Laminated Plate Element</b>	<b>88</b>
5.1	Introduction to this chapter . . . . .	89
5.2	Finite element approximation . . . . .	89
5.2.1	[(332) <sup>NK</sup> ] assumption . . . . .	90
5.2.2	Finite element discretization . . . . .	94
5.2.3	Fracture mechanics consideration . . . . .	95
5.3	Numerical examples . . . . .	101
5.3.1	Accuracy and convergence check . . . . .	101
5.3.2	Interlaminar stress evaluations . . . . .	103
5.3.3	Strain energy release rate calculations . . . . .	106
5.4	Discussion . . . . .	108
<b>6</b>	<b>Applications to Practical Structural Analysis</b>	<b>139</b>
6.1	Introduction to this chapter . . . . .	140
6.2	Application to general shell laminates . . . . .	140
6.2.1	Layerwise laminated degenerated 3-D shell element . . . . .	141
6.2.2	Spherical shell under uniformly distributed pressure . . . . .	145
6.3	Application to structural joint in laminates . . . . .	147
6.3.1	Stress analysis of T-joint test specimen . . . . .	148
6.4	Discussion . . . . .	149
<b>7</b>	<b>Conclusion</b>	<b>168</b>
7.1	Conclusion to this thesis . . . . .	169
7.2	Future research proposals . . . . .	171
	Reference . . . . .	172

## List of Figures

2.1	A schematic of anisotropy in fiber-reinforced composite materials . . . .	18
2.2	A typical example of local variations of the material directions . . . . .	18
2.3	A schematic of a trapezoid plate under lateral bending pressure . . . . .	19
2.4	Convergence of deflections at the free end against mesh refinement . . . .	20
2.5	A schematic of a simply-supported square plate . . . . .	21
2.6	Asymptotic of the central deflections to CLT solution against $l/h$ . . . .	22
2.7	Asymptotic of the central flexural stresses to CLT solution against $l/h$ . .	22
2.8	Asymptotic of the first natural frequencies to CLT solution against $l/h$ .	23
2.9	Asymptotic of the bifurcation loads to CLT solution against $l/h$ . . . .	23
2.10	Typical laminated composite material structures . . . . .	24
2.11	Various inhomogeneities in composite materials . . . . .	25
2.12	3-D unitcell inhomogeneous model in a woven composite laminate . . . .	26
2.13	Comparison of composite materials and homogeneous materials with respect to inhomogeneity . . . . .	27
2.14	Through-the-thickness distributions of transverse shear stress $\tau_{zx}$ . . . .	29
2.15	Design particulars of NCF-coupling joint for composite riser . . . . .	30
2.16	Gridwork of finite element meshes and failure index margin contours within NCF-coupling joint for composite riser . . . . .	32
2.17	Stress contours within NCF-coupling joint for composite riser (1) . . . .	33
2.18	Stress contours within NCF-coupling joint for composite riser (2) . . . .	34
2.19	A schematic of mesh discretizations by 3-D continuum solid elements . .	35
2.20	Design draw for composite sandwich motorboat . . . . .	36
2.21	Gridwork of finite element meshes of composite sandwich motorboat . . .	37
2.22	Transverse displacement contours on composite sandwich motorboat . . .	38
2.23	Transverse shear stress $\tau_{zx}$ contours within the core part of composite sandwich motorboat . . . . .	38
2.24	Transverse shear stress $\tau_{yz}$ contours within the core part of composite sandwich motorboat . . . . .	39
2.25	Free-edge effect — an angle-ply symmetric laminated strip under uniform axial extension . . . . .	39
2.26	Free-edge effect — transverse stress contours obtained by 3-D continuum solid finite element analysis . . . . .	40



2.27	Free-edge effect — transverse stress contours obtained by 2-D stress-equilibrium finite element analysis . . . . .	41
3.1	Progressional history of numerical models for composite laminates . . . . .	59
3.2	Schematics of various multi-layer discretization schemes . . . . .	60
3.3	Coordinate system and geometry of a laminate, and higher-order deformation of the $k^{\text{th}}$ layer . . . . .	61
3.4	Physical meaning of the penalty number . . . . .	62
3.5	A schematic chart of possible combinations of deformation assumptions and layer discretizations . . . . .	63
4.1	A schematic of deformations in a sandwich construction . . . . .	77
4.2	Selective layerwise considerations for a sandwich . . . . .	78
4.3	Sandwich plate element — geometry and displacement assumptions . . . . .	80
4.4	Schematics of a simply-supported square sandwich plate subjected to uniform lateral pressure . . . . .	81
4.5	Deformed shape of the sandwich plate obtained by the detailed 3-D continuum solid element model . . . . .	82
4.6	Central deflections versus total degrees of freedom . . . . .	82
4.7	Distributions of deflection along the diagonal line . . . . .	83
4.8	In-plane normal stress $\sigma_x$ distributions through the thickness . . . . .	84
4.9	Transverse shear stress $\tau_{zx}$ distributions through the thickness . . . . .	85
4.10	Design perspective of the load-bearing sandwich panel test . . . . .	86
4.11	Clamped sandwich panel subjected to hydraulic pressure . . . . .	86
4.12	Variations of deflection along the diagonal line . . . . .	87
4.13	Variations of in-plane strain measure along the diagonal line . . . . .	87
5.1	General laminated plate element — geometry and displacement assumptions	110
5.2	Various failures and damages in composite laminates . . . . .	111
5.3	Concept of virtual crack closure integral (VCCI) . . . . .	112
5.4	Conventional modelings of delamination and crack extension in finite element analysis . . . . .	113
5.5	Schematics of geometry, boundary conditions and finite element meshes for cross-ply square laminate under sinusoidal lateral load . . . . .	114
5.6	Central deflections against the square mesh refinement for various penalty numbers . . . . .	115



5.7	Central in-plane normal stresses against the square mesh refinement for various penalty numbers . . . . .	115
5.8	Through-the-thickness distributions of the in-plane displacement $\bar{u}$ . . . . .	116
5.9	Through-the-thickness distributions of the in-plane normal stress $\bar{\sigma}_x$ . . . . .	117
5.10	Through-the-thickness distributions of the in-plane shear stress $\bar{\tau}_{xy}$ . . . . .	118
5.11	Through-the-thickness distributions of the transverse shear stress and the interlaminar shear stress $\bar{\tau}_{zx}$ . . . . .	119
5.12	Through-the-thickness distributions of the transverse normal stress and the interlaminar normal stress $\bar{\sigma}_z$ . . . . .	120
5.13	Problem definition for infinitely long laminated strip under uniform axial extension . . . . .	121
5.14	Variations of the in-plane stresses $\sigma_x$ and $\tau_{xy}$ at the layer interface along the width direction . . . . .	122
5.15	Variations of the interlaminar shear stress $\tau_{zx}$ at the layer interface along the width direction . . . . .	123
5.16	Variations of the interlaminar normal stress $\sigma_z$ at the layer interface along the width direction . . . . .	124
5.17	Variations of the interlaminar shear stress $\tau_{yz}$ at the layer interface along the width direction . . . . .	125
5.18	Schematics of through-the-thickness configurations of a laminated strip with resin films inserted . . . . .	126
5.19	Variations of the in-plane stresses $\sigma_x$ and $\tau_{xy}$ at the CFRP/resin-film interface along the width direction . . . . .	127
5.20	Variations of the interlaminar shear stress $\tau_{zx}$ at the CFRP/resin-film interface along the width direction . . . . .	128
5.21	Variations of the interlaminar normal stress $\sigma_z$ at the CFRP/resin-film interface along the width direction . . . . .	129
5.22	Variations of the interlaminar shear stress $\tau_{yz}$ at the CFRP/resin-film interface along the width direction . . . . .	130
5.23	Problem definition of a infinitely long laminated strip with edge delaminations . . . . .	131
5.24	Strain energy release rate $G$ versus delamination length $a$ for cross-ply laminate . . . . .	131
5.25	Strain energy release rate $G$ versus delamination length $a$ for angle-ply laminate . . . . .	132
5.26	Strain energy release rate $G$ versus delamination length $a$ for quasi-isotropic laminate . . . . .	132

5.27	Typical gridwork of finite element meshes for finite-length laminate coupon with edge delamination . . . . .	133
5.28	Distributions of the energy release rate $G_{\text{total}}$ along the delamination front for several cases of delamination length $a$ for angle-ply laminate . . . . .	134
5.29	Distributions of the energy release rate $G_{\text{II}}$ along the delamination front for several cases of delamination length $a$ for angle-ply laminate . . . . .	135
5.30	Distributions of the energy release rate $G_{\text{total}}$ along the delamination front for several cases of delamination length $a$ for quasi-isotropic laminate . . . . .	136
5.31	Distributions of the energy release rate $(G_{\text{II}} + G_{\text{III}})$ along the delamination front for several cases of delamination length $a$ for quasi-isotropic laminate . . . . .	137
5.32	Distributions of the energy release rate $G_I$ along the delamination front for several cases of delamination length $a$ for quasi-isotropic laminate . . . . .	138
6.1	Schematics of layerwise laminated degenerated 3-D shell element . . . . .	151
6.2	Schematics of geometry, boundary conditions and finite element meshes . . . . .	152
6.3	Deflections against the square mesh refinement for various penalty numbers . . . . .	153
6.4	In-plane normal stresses against the square mesh refinement for various penalty numbers . . . . .	154
6.5	Through-the-thickness distributions of the in-plane displacement $\bar{u}'$ . . . . .	155
6.6	Through-the-thickness distributions of the in-plane normal stress $\bar{\sigma}_{x'}$ . . . . .	156
6.7	Through-the-thickness distributions of the in-plane shear stress $\bar{\tau}_{x'y'}$ . . . . .	157
6.8	Through-the-thickness distributions of the transverse shear stress $\bar{\tau}_{x'z'}$ . . . . .	158
6.9	Through-the-thickness distributions of the transverse shear stress $\bar{\tau}_{y'z'}$ . . . . .	159
6.10	Through-the-thickness distributions of the transverse normal stress $\bar{\sigma}_{z'}$ . . . . .	160
6.11	Photographic view of Lap-Joint test . . . . .	161
6.12	Photographic view of T-Joint static strength test . . . . .	162
6.13	T-Joint construction . . . . .	163
6.14	Design details of T-Joint construction . . . . .	163
6.15	Thermoelastic stress analysis by SPATE . . . . .	164
6.16	Gridwork of finite element meshes and boundary conditions . . . . .	165
6.17	Thermoelastic stress distribution across the thickness along Line 1 . . . . .	166
6.18	Thermoelastic stress distribution across the thickness along Line 2 . . . . .	166
6.19	Thermoelastic stress distribution across the thickness along Line 3 . . . . .	167
6.20	Thermoelastic stress distribution across the thickness along Line 4 . . . . .	167

## List of Tables

2.1	Elastic moduli and thickness of the orthotropic trapezoid plate . . . . .	20
2.2	Elastic moduli, specific gravity and thickness of each lamina . . . . .	21
2.3	Possible combinations of different inhomogeneities in composite laminates	28
2.4	Elastic moduli and strength of materials in composite riser . . . . .	31
2.5	Typical material properties for composite sandwich motorboat . . . . .	36
3.1	Possible numerical models for various levels of inhomogeneity of composite laminates . . . . .	64
4.1	Characteristics of sandwich deformations . . . . .	78
4.2	Estimated accuracy of various numerical models for sandwiches . . . . .	79
6.1	Non-dimensionalized central deflections of the cross-ply spherical shell	154

## Notation

### *Superscripts and Subscripts*

$i, j$	indices, range from 1 to 3
$m, n$	indices, range from 1 to 3
$p, q$	indices, range from 1 to 6
$P, Q$	order of displacement assumption, range from 0 to $N_i^{(k)}$
$J$	index, range from 1 to 8
$(k)$	denotes $k^{\text{th}}$ layer
$(l, k)$	denotes $l^{\text{th}}$ lamina in $k^{\text{th}}$ layer
$CR$	denotes the core layer of a sandwich
$UF, LF$	denote the upper face and the lower face of a sandwich
$*F$	denotes the upper face or the lower face of a sandwich
$T$	transpose of a matrix
$-1$	inverse of a square matrix

### *Quantities*

$l, l_1, l_2$	span length of plates and panels, or half length of coupons, $l$ is also used for indentifying $l^{\text{th}}$ lamina in $k^{\text{th}}$ layer
$h$	total thickness of plates, panels, strips and coupons
$S$	span to thickness ratio, $S = l/h$
$h^{(k)}$	thickness of $k^{\text{th}}$ layer
$h_0$	thickness of each lamina of laminates
$t$	thickness of a resin film of laminates (in Chapter 5)
$b$	half width of laminated strips and coupons
$R$	radius of the middle plane of a spherical shell (in Chapter 5)
$q_0$	transversely distributed load intensity
$q$	transversely distributed load
$x, y, z$	Cartesian coordinates
$z^{(k)}$	the thickness coordinate measured from the middle plane of $k^{\text{th}}$ layer of laminates
$z, r, \theta$	Cylindrical coordinates, $z, r$ and $\theta$ denote axial, radial and circumferential directions, respectively (in Chapter 2)
$x_i$	Cartesian coordinates (index expression, in Chapter 3)
$x_3^{(k)}$	the thickness coordinate measured from the middle plane of $k^{\text{th}}$ layer of laminates (in Chapter 3)



$x', y', z'$	local orthogonal coordinates (in Chapter 6)
$L, T, n$	the reinforcing fiber direction, the perpendicular (transverse) direction to the fiber direction and the normal direction to $L$ - $T$ plane
$\xi, \eta, \zeta$	natural curvilinear coordinates (in Chapter 6)
$x_J, y_J, z_J$	nodal orthogonal coordinates (in Chapter 6)
$\hat{V}_L, \hat{V}_T, \hat{V}_n$	unit vectors along local orthogonal coordinates $L, T, n$ (in Chapter 6)
$\mu_J, \mu'$	nodal and local direction cosine matrix (in Chapter 6)
$E, \nu$	isotropic Young's modulus and Poisson's ratio
$G$	isotropic shear elastic modulus, or in Chapter 5 the strain energy release rate
$E_x, E_y$	orthotropic Young's moduli in Cartesian coordinate $x$ and $y$ directions
$E_z$	orthotropic Young's modulus in the out-of-plane direction or in Cartesian coordinate $z$ direction or in the axial $z$ direction of Cylindrical coordinates
$\nu_{xy}, \nu_{yz}, \nu_{zx}$	orthotropic Poisson's ratios in $y$ direction against $x$ , in $z$ direction against $y$ and in $x$ direction against $z$
$G_{xy}, G_{yz}, G_{zx}$	orthotropic shear elastic moduli in $x$ - $y$ plane, in $y$ - $z$ plane and in $z$ - $x$ plane of Cartesian coordinates
$E_L, E_T$	orthotropic Young's moduli in the fiber direction (denoted by $L$ ) and in the perpendicular direction to the fiber direction (denoted by $T$ )
$\nu_{LT}, \nu_{Tz}, \nu_{zL}$	orthotropic Poisson's ratios in $T$ direction against $L$ , in $z$ direction against $T$ and in $L$ direction against $z$
$G_{LT}, G_{Tz}, G_{zL}$	orthotropic shear elastic moduli in $L$ - $T$ plane, in $T$ - $z$ plane and in $z$ - $L$ plane
$E_r, E_\theta$	orthotropic Young's moduli in the radial $r$ direction and in the circumferential $\theta$ direction of Cylindrical coordinates
$\nu_{zr}, \nu_{r\theta}$	orthotropic Poisson's ratio in $r$ direction against $z$ and in $\theta$ direction against $r$ of Cylindrical coordinates
$G_{zr}$	orthotropic transverse shear elastic modulus in $z$ - $r$ plane of Cylindrical coordinates
$C_{ijmn}^{(k,l)}$	the reduced elastic coefficients for $l^{\text{th}}$ orthotropic lamina in $k^{\text{th}}$ layer of laminates (tensor form, index expression)
$A_{ijmn}^{(k)}$	the generalized rigidity coefficients for $k^{\text{th}}$ layer of laminates (tensor form, index expression)
$\bar{Q}_{pq}^{(k,l)}$	the components of the reduced elastic matrix (index expression) for $l^{\text{th}}$ orthotropic lamina in $k^{\text{th}}$ layer of laminates

$D_{mb}^{(k)}, D_s^{(k)}$	the membrane/flexure/transverse-normal rigidity matrix and the transverse-shear rigidity matrix for $k^{\text{th}}$ layer of laminates
$u, v, w$	displacement components
$U_P, V_P, W_P$	unknown displacement coefficients of the series expansion
$u^{(k)}, v^{(k)}, w^{(k)}$	displacement components for $k^{\text{th}}$ layer of laminates
$U_P^{(k)}, V_P^{(k)}, W_P^{(k)}$	unknown displacement coefficients of the series expansion for $k^{\text{th}}$ layer of laminates
$u_i^{(k)}$	displacement components for $k^{\text{th}}$ layer of laminates (index expression)
$U_i^{(k)}$	unknown displacement coefficients of the series expansion for $k^{\text{th}}$ layer of laminates (index expression)
$\delta$	generalized displacement vector
$\delta^{(k)}$	generalized displacement sub-vector for $k^{\text{th}}$ layer
$u', v', w'$	local displacement components (in Chapter 6)
$\varepsilon_{ij}$	strains (tensor form, index expression)
$\varepsilon_{ij}^{(k)}$	strains for $k^{\text{th}}$ layer of laminates (tensor form, index expression)
$E_{ij}^{(k)}$	general strain components for $k^{\text{th}}$ layer of laminates (tensor form, index expression)
$\varepsilon_x, \varepsilon_y, \varepsilon_z$	
$\gamma_{yz}, \gamma_{zx}, \gamma_{xy}$	strains (engineering form), that is, $\varepsilon_x = \varepsilon_{11}$ , $\varepsilon_y = \varepsilon_{22}$ , $\varepsilon_z = \varepsilon_{33}$ , $\gamma_{yz} = 2\varepsilon_{23}$ , $\gamma_{zx} = 2\varepsilon_{31}$ and $\gamma_{xy} = 2\varepsilon_{12}$ .
$E_x P, E_y P, E_z P$	
$E_{yz} P, E_{zx} P, E_{xy} P$	general strain components (engineering form)
$\epsilon_{mb}, \epsilon_s$	generalized strain vectors : membrane/flexure/transverse-normal portion and transverse-shear portion
$\sigma_{ij}^{(k,l)}$	stresses for $l^{\text{th}}$ lamina in $k^{\text{th}}$ layer (tensor form, index expression)
$M_{ij}^{(k)}$	layer stress resultants (index expression)
$M_{ij} P$	generalized stress resultants of the entire laminate (index expression)
$\sigma_x, \sigma_y, \sigma_z$	
$\tau_{yz}, \tau_{zx}, \tau_{xy}$	stresses (engineering form), that is, $\sigma_x = \sigma_{11}$ , $\sigma_y = \sigma_{22}$ , $\sigma_z = \sigma_{33}$ , $\tau_{yz} = \sigma_{23}$ , $\tau_{zx} = \sigma_{31}$ and $\tau_{xy} = \sigma_{12}$ .
$N, Q$	generalized stress resultant vectors : membrane/flexure/transverse-normal portion and transverse-shear portion
$\mathcal{U}^{(k)}$	strain energy density integrated through the layer thickness
$x_{3c}^{(k)}$	thickness coordinate of the middle point of $k^{\text{th}}$ layer ( $x_3 = x_3^{(k)} + x_{3c}^{(k)}$ )

$g_z^{(k)}$	relative displacements at the interface between $k^{\text{th}}$ and $(k+1)^{\text{th}}$ layers (index expression)
$g_x^{(k)}, g_y^{(k)}, g_z^{(k)}$	relative displacements at the interface between $k^{\text{th}}$ and $(k+1)^{\text{th}}$ layers in $x$ , $y$ and $z$ directions
$\alpha_i^{(k)}$	the penalty numbers (index expression)
$\alpha_x^{(k)}, \alpha_y^{(k)}, \alpha_z^{(k)}$	the penalty numbers in $x$ , $y$ and $z$ directions
$\lambda_j^{(k)}$	transverse stresses at the interface between $k^{\text{th}}$ and $(k+1)^{\text{th}}$ layers (index expression)
$\lambda_x^{(k)}, \lambda_y^{(k)}, \lambda_z^{(k)}$	transverse stresses in $x$ , $y$ and $z$ directions at the interface between $k^{\text{th}}$ and $(k+1)^{\text{th}}$ layers
$\Pi'_{mp}$	modified potential energy functional
$\Pi_p$	potential energy in the system obtained by summing the potential energy of all the layers
$\mathcal{H}$	the auxiliary energy term due to interfacial displacement constraints
$T_i$	mechanical boundary conditions on the upper and lower exterior surface of the laminate (index expression)
$T_x, T_y, T_z$	mechanical boundary conditions on the upper and lower exterior surface of the laminate in $x$ , $y$ and $z$ directions
$\bar{u}_i$	geometrical boundary conditions on the upper and lower exterior surface of the laminate (index expression)
$\bar{u}_x, \bar{u}_y, \bar{u}_z$	geometrical boundary conditions on the upper and lower exterior surface of the laminate in $x$ , $y$ and $z$ directions
$n_1, n_2$	direction cosines of a unit normal to the boundary of the middle plane $\Gamma$
$A$	delamination area of laminates
$a$	delamination length (depth) of laminated strips or coupons
$\mathcal{W}$	work by external forces
$\mathcal{U}$	total strain energy
$u_R$	the relative displacements after and prior to crack extension
$X$	interfacial tractions at any point in the virtual crack extension area $\Delta A$
$G_{\text{total}}$	total strain energy release rate
$G_I, G_{II}, G_{III}$	strain energy release rates regarding mode I, mode II and mode III of fracture

### Miscellaneous

$NK$	total number of layers
------	------------------------

$N$	total number of dissimilar material laminae in a laminate
$N_1^{(k)}, N_2^{(k)}, N_3^{(k)}$	the orders of termination of the displacement series expansions for $u_1^{(k)}$ , $u_2^{(k)}$ and $u_3^{(k)}$
$L^{(k)}$	total number of different material laminae the $k^{\text{th}}$ layer comprises
$\kappa^{(k,l)}, \kappa^{(k,l-1)}$	$x_3^{(k)}$ coordinate values at the upper and the lower surfaces of $l^{\text{th}}$ lamina in $k^{\text{th}}$ layer
$e$	each one of elements
$N_e$	total number of elements
$\Phi_J$	the shape functions ( $J = 1, 2, \dots, 8$ )
$B_{mb}, B_s$	strain matrices : membrane/flexure/transverse-normal portion and transverse-shear portion
$K, K_\alpha$	the global stiffness matrix without displacement constraints and the auxiliary energy portion including the penalty numbers
$d, f$	the assembled nodal displacement vector and the assembled nodal force vector
$C^{(k)}$	the operator that calculates small gaps $g^{(k)}$ at the interfaces from the nodal displacements $\delta_J^{(k+1)}$ and $\delta_J^{(k)}$
$p$	the magnitude of penalty number, $p = \log \left( \frac{\alpha}{h\sqrt{E_T E_T}} \right)$
$k_x, k_y$	shear correction factors



# Chapter 1

## Overview

## 1.1 Introduction

In this chapter, the background, motivation and objectives of this thesis research is presented.

### 1.1.1 Laminated composite material structures

Advanced composite material (ACM) is one of the most promising materials replacing and complementing the conventional metallic materials such as steel, aluminum alloy and so forth. Industrial fields in which recently ACM has been actively and increasingly used are, for example:

- Ocean/marine engineering — sailing and motor boats, drilling riser pipes for offshore oil;
- Aviation/aerospace industry — passenger planes, military use, artificial satellites;
- Civil engineering — reinforcing and rehabilitation of concrete structures;
- Leisure, sports equipment — tennis rackets, golf shafts, fishing rods.

And it is finding its further applications to various engineering and scientific fields day by day. ACMs' excellent potentials as a primary structural component are described as follows:

- They have high stiffness-to-weight and strength-to-weight ratios. This means that weight of structures can be substantially reduced. It is needless to say that weight reduction of structures will lead to improvement of their performance. For instance, a composite sandwich motorboat can run faster with a less power engine and less amount of fuel than wooden boats. A composite drilling riser pipe can reach and dig deeper ocean floors than steel pipes owing to its small specific gravity;
- During the forming and/or assembling processes, one can design and control their several physical and mechanical properties such as fiber volume fraction, weight, degree of anisotropy, orientation angle, load-bearing stiffness and so forth. This enables designers to carry out a flexible and optimum design;
- They are drapable. That is, one can fit them to arbitrarily shaped molds or buildings. One of the most successful applications which utilize this characteristic

is probably reinforcement and rehabilitation of concrete structures by composite sheets;

- Good thermal properties (thermal expansion coefficients are very small, sometimes even negative), good corrosion resistance and many other physical properties the existing materials do not possess.

Although ACMs have better engineering properties than conventional materials as described above, some obstacles to be gone over still exist. Among them, the most urgent are the following two issues:

- Reliability and durability have not been ensured. This is mainly because artificial composite materials are quite new materials compared to the conventional ones like steel, and therefore proper acquisition schemes and sufficient amounts of accumulations for material data have not been available yet;
- Material testings and numerical simulations are indispensable to assess the feasibility and estimate the limitation of composite material structures. However, the testing methods and numerical analysis tools available at present are not always applicable to composite materials. This problem is mainly due to the fact that *the existing numerical models were formulated for the conventional materials and hence they are not necessarily suited for these kinds of new materials*. Still worse, composite materials exhibit complicated, sometimes unfamiliar mechanical behaviors. This makes their appropriate numerical modelings more difficult and skillful.

Massive research attentions in the last decade have been gradually removing the first obstacle. On the other hand, studies on numerical modelings of composite materials have been stagnant for the last two or three decades. Reliable and accurate numerical models for composite materials are very important. That is what motivated the author to start this thesis research.

### 1.1.2 Numerical modelings of composite materials

As mentioned in the previous section, reliable and accurate numerical modelings of composite materials are very important. However, it is not so easy to propose their numerical models for the reasons listed as:

- Analytical modelings for composite materials require knowledge of anisotropic theories such as anisotropic elasticity/plasticity, anisotropic plate/shell theory,

anisotropic fracture mechanics and so forth. Accordingly, in numerical modelings of composite materials, first comes extension of isotropic theories to anisotropic ones. Furthermore, it is important to note that anisotropy of composite laminates is unbalancingly high in a specific in-plane direction, i.e., in the reinforcing fiber direction, and this characteristic greatly influences on numerical modelings accuracy;

- Composite materials and structural members made of them are inherently inhomogeneous. Unlike homogeneous materials, composite materials exhibit mechanical, geometrical and material inhomogeneities in every phase of analysis. Therefore, numerical models, e.g., geometrical configurations, constitutive relations, displacement/stress field assumptions and failure/damage criteria, should include inhomogeneities properly and efficiently. In particular, among various inhomogeneities of composite materials, laminate-like inhomogeneity through the thickness direction needs careful attentions. Historically, laminate-like, through-the-thickness inhomogeneity has been substantially simplified or totally neglected, and this often results in fatal discrepancies between the numerical model and the actual behavior;
- After all, a numerical model which is formulated by merely extending the existing models for isotropic, homogeneous materials is not applicable to composite materials, and a new model properly including anisotropy and inhomogeneities of composite materials is indispensable to their successful and satisfactory analysis/design.

## 1.2 Objectives of this thesis

Hence, the objectives of this thesis research are placed on a detailed investigation on proper and efficient numerical models for composite materials. In particular, the conventional single-layer plate/shell model, i.e., the classical lamination theory (CLT), need to be refined taking into account the unbalancingly high anisotropic properties and the laminate-like, through-the-thickness inhomogeneity.

The objectives of this thesis research thus can be summarized as follows:

1. To make clear what is lacking in the existing numerical models when they are applied to composite materials, through several case studies in which the author was actually involved;



2. In structural analysis and design, one of the most popular models are plate/shell models. Therefore, the next objective is to reveal the limitations of the classical lamination theory and then to propose an accurate and flexible model suitable for composite plate/shell structures;
3. To develop several refined plate/shell finite elements for the analysis of composite laminates, and to investigate their accuracies and validities through several numerical examples by using them.

### 1.3 Layout of this thesis

In accordance with the objectives mentioned in the previous section, the layout of this thesis work is as the following.

In this chapter, the background, the study motivations and the objective of this thesis research have been presented.

The next chapter presents several case studies of numerical analysis of composite materials by using the existing numerical models for conventional isotropic materials (in almost all cases by the commercially available finite element packages.) Through these case studies, the restrictions, limitations and deficiencies of the conventional numerical models, when they are applied to composite materials, are made clear.

In order to overcome the drawbacks of conventional numerical models, in Chapter 3, a new numerical modeling methodology for laminated composite material structures (composite laminates) are proposed. The main portion of this chapter is occupied with the formulation of a general and versatile lamination theory for composite laminates which is based on the layerwise higher-order displacement assumptions.

In Chapter 4 through Chapter 6, finite element approximations deduced from the proposed numerical modeling methodology will be developed.

In Chapter 4, development and numerical applications of a sandwich-type finite element are presented. After showing its accuracy/convergence and its comparative study to experimental results, the inherent restriction of the sandwich-type element are also discussed.

Chapter 5 is devoted to development of a generic laminated plate element model. In this chapter, several numerical results and discussions are also included concerning accuracy/convergence checks of the developed element, interlaminar stress evaluations and strain energy release rate calculations.

Chapter 6 is dedicated to a couple of applications of the proposed element models to practical structural analysis. To put it concretely, in this chapter, first the laminated plate element presented in Chapter 5 is extended to a degenerated 3-D shell element. Through its accuracy/convergence checks the validity of the extended shell element is also shown. The next example in this chapter is structural joint analysis by the developed element. By comparing the result obtained by the present element and the experimental results previously obtained in the literature, the applicability of the present numerical models to such a challenging problem in the analysis and design of composite laminates is demonstrated.

Finally, in Chapter 7, brief concluding remarks on this thesis work and some future proposals relevant to this thesis research are made.

## Chapter 2

### Case Studies by the Existing Numerical Models

## 2.1 Introduction to this chapter

As practical applications of ACM are increasing in number and scale, accurate and proper numerical analysis models for the structures composed of such advanced materials are becoming more and more important. Ironically, the unique and superior engineering properties of ACM compel studies of their numerical modelings more complicated and skillful than those of the conventional materials.

Thus far, designers have used one of the following numerical models and their finite element approximations for the analysis and design of laminated composite material structures (composite laminates).

**Equivalent-single-layer (ESL) first-order models** As well-known, in structural analysis and design for isotropic materials like steel, the classical plate theory (CPT) and its numerous incompatible finite elements (FEs) or first-order shear deformation theory (FOSDT) and its  $C^0$  continuity FEs are dominant. They are based on different kinds of constitutive assumptions in the thickness direction; CPT is based on Kirchhoff (Kirchhoff-Love for shells) hypothesis while FOSDT, on Reissner-Bollé-Mindlin assumption<sup>1,2,3</sup>. Although these two models are distinct from each other, they can be categorized into a specific model because both of them assume a linearly varying kinematic through the thickness (first-order model). In particular, for the last two or three decades, FOSDT and its FEs have been extensively used and then improved for isotropic structural analysis owing to the degenerated 3-D shell element developed by Ahmad, Irons and Zienkiewicz<sup>4</sup> in conjunction with the reduced integration technique<sup>5</sup>.

Hence, it is quite natural that these two first-order models for conventional isotropic materials were extended to composite laminates in the literature. The early attempts for extension of CPT to composite laminates were made by Ambartsumyan<sup>6</sup>, Reissner and Stavsky<sup>7</sup>, Dong *et al.*<sup>8</sup>, Whitney and Leissa<sup>9</sup>, Whitney<sup>10</sup>, and Ashton and Whitney<sup>11</sup>. Since CPT for composite laminates is formulated by using the lamination theory (LT), it is usually referred to as the classical lamination plate theory (CLPT or simply, CLT). On the other hand, FOSDT was extended to composite laminates by Yang, Norris and Stavsky<sup>12</sup>, Whitney<sup>13,14,15</sup>, Whitney and Pagano<sup>16</sup>, Pryor and Barker<sup>17</sup> and then Reddy<sup>18</sup> and Reddy and Chao<sup>19,20</sup>.

CLT and FOSDT consider the geometrical and material inhomogeneity over the thickness through the constitutive equations (i.e., through Hook's law) only. This simplification is called the lamination theory (LT). Displacement assumptions



over the thickness are similar to those of isotropic single-layer model. Therefore, these models can be referred to as equivalent-single-layer (ESL) models<sup>21</sup>.

**2-D, 3-D continuum solid models** For composite laminates, two-dimensional (2-D), three-dimensional (3-D) continuum solid models are also valid to some extent. There are several kinds of continuum models available. The most commonly used are continuum solid finite elements such as 3-D isoparametric brick elements, 2-D plane-strain or axisymmetric isoparametric solid elements, quasi-three-dimensional (quasi-3-D) generalized plane-strain isoparametric solid elements and so forth. Continuum solid models are capable of modeling the displacement field and the material inhomogeneity of composite laminates as precisely as one wishes if one does not mind any computational time and economy. Therefore these models are routinely used for local stress analysis of the critical regions of composite laminates.

Some have commented that "everything is done in finite element modelings for structural analysis and design because almost all structural problems can be solved by single-layer plate/shell elements and/or 2-D, 3-D continuum solid elements". However, for laminated composite material structures (composite laminates), that is not true at all.

In this chapter, the restrictions, limitations and deficiencies of the conventional numerical models will be revealed, through several case studies in which the author was actually involved during the early period of the thesis course.

## 2.2 Anisotropic properties

Composite material structures and composite materials themselves inherently possess anisotropic properties. Unlike isotropic materials, anisotropic materials are dependent on the direction. Besides, degree of anisotropy of composite materials is unbalancingly large in a specific direction, i.e., in the reinforcing fiber direction. Figure 2.1 illustrates this peculiar anisotropy originating from reinforcing fibers in composite materials.

Here, let  $E_L$ ,  $E_T$  and  $G_{LT}$ , respectively, be Young's moduli in the fiber direction (denoted by  $L$ ) and in the perpendicular direction to it ( $T$ ), and in-plane shear modulus. Among these elastic properties of fiber-reinforced composites,  $E_L$  is higher than the others by one or more orders of magnitude. For instance, in the case of ordinarily-used unidirectional CFRP,  $E_L/E_T$  and  $E_L/G_{LT}$  are approximately 10 and 20, respectively.

Thus these unbalancing anisotropy, say, " $E_L/E_T$ ,  $E_L/G_{LT}$  effects", should be considered in numerical modelings and their finite element approximations.

Furthermore, owing to the flexibility and drapability of reinforcing fibers, material reference axes in which the material properties are measured can vary along an arbitrary shaped object. A typical example is schematically illustrated in Figure 2.2. One will be aware that reinforcing fibers are aligned so that fibers avoid penetrating into the cutout. In order to model the complicated state of anisotropy around the cutout, the material coordinate system should be allowed to vary along the fibers. This unique characteristic, say, "drapability effect" should also be included in numerical modelings of composite materials, otherwise unexpected and disappointing results will be obtained.

### 2.2.1 Case 1 : trapezoid orthotropic plate bending – influence of locally varying material directions

In order to show the influence of strong degree of anisotropy ( $E_L/E_T$ ,  $E_L/G_{LT}$  effects) and the locally varying material direction (drapability effect) on the modeling accuracy, the author conducted a simple but persuasive example.

Consider an orthotropic trapezoid plate subjected to lateral bending load as shown in Figure 2.3. The fiber direction are aligned so that they get together toward the free edge. Material properties of the plate are given in Table 2.1.  $E_L/E_T$ ,  $E_L/G_{LT}$  are 14.03 and 27.42, respectively.

The author examined this problem by comparing the results obtained by the commercial shell finite element (thick shell element in MARC k-5<sup>22</sup>) and the in-house shell element developed by the author<sup>23</sup>. The commercial shell element does not consider any local variation of material directions inside the element, while the in-house shell element account for that by interpolating the nodal values at any point within the element. It is expected that the discrepancy between the results by the in-house element considering locally varying material direction and ones by the conventional one utilizing the averaged axes for representing anisotropic properties will not be negligible. Figure 2.4 shows convergence of deflections at the free end against total computational degrees of freedom. It is observed that the model considering varying material directions is almost independent of mesh refinement, while fairly fine mesh is necessary for the model not considering it to converge.

## 2.3 Weaker properties in the thickness direction

The unbalancing anisotropy of composite materials, i.e., the very high  $E_L$  compared to the other directions, influences the behaviors in the thickness direction as well. One might say that the high  $E_L$  has more severe influences on the thickness direction than on the in-plane directions.

For typical CFRP,  $E_L/G_{Tz}$  and  $E_L/G_{zL}$  are approximately 20 or larger, in which  $z$  denotes the thickness (out-of-plane or transverse) direction. These " $E_L/G_{Tz}$ ,  $E_L/G_{zL}$  effects" make composite laminates relatively thicker than isotropic plates ( $E/G = 2$  or 3), and consequently "thickness effect" becomes prominent in numerical modelings of composite materials.

### 2.3.1 Case 2 : influence of thickness on global elastic responses of composite laminated plates

A typical example was investigated by the author<sup>24</sup> and is shown here for quantitatively demonstrating the relation between " $E_L/G_{Tz}$ ,  $E_L/G_{zL}$  effects" and "thickness effect".

Consider numerical plate models for a simply-supported square plate as illustrated in Figure 2.5.

In accordance with Kirchhoff (Kirchhoff-Love for shells) hypothesis, CPT for isotropic single plates or CLT for composite laminates do not possess any degrees of freedom (DOF) in the thickness direction as described below:

$$u = U_0 - z \frac{\partial W_0}{\partial x}, \quad v = V_0 - z \frac{\partial W_0}{\partial y}, \quad w = W_0 \quad (2.1)$$

As well-known, it is proven that, when the plate thickness  $h$  is set infinitely small in comparison to span length  $l$ , then 3-D exact elasticity solution of the plate converges to the solution by CPT (or CLT for composite laminates)<sup>25, 26, 27</sup>. This means that, when the plate thickness  $h$  is very small (or span-to-thickness ratio  $l/h$  is very large), CLT serves as a proper numerical model of composite laminates as far as global elastic responses are concerned.

However, the problem is the vanishing point of "thickness effect", in other words, how small  $h$  is when "thickness effect" vanishes and CLT becomes the valid numerical model for composite laminates. As already mentioned, composite laminates exhibit " $E_L/G_{Tz}$ ,  $E_L/G_{zL}$  effects" and therefore the thickness can be relatively larger than that of the conventional isotropic materials.



In order to investigate this question, three different kinds of elastic properties and specific gravities are selected for the same plate dimension as listed in Table 2.2.  $E_L/G_{Tz}$  is 189.1, 6.02 and 2.68 for high-stiff CFRP, GFRP and Aluminum, respectively. Note that in the case of high-stiff CFRP and GFRP the plate is assumed to be a 8-layer symmetric cross-ply laminated plate  $[0/90]_{2s}$ , while in the case of Aluminum the plate is assumed to be a single-layer isotropic plate.

In addition to CLT (CPT for Aluminum) which neglects "thickness effect", the first-order shear deformation theory (FOSDT) and the higher-order shear deformation theory of Reddy (HOT of Reddy)<sup>28</sup> are adopted for evaluating elastic responses of the plate. Central deflections and flexural stresses under uniformly distributed lateral load, natural frequencies of free vibration and bifurcation (buckling) loads are examined for each of the three material cases. The displacement assumptions of these two models are:

for FOSDT;

$$u = U_0 + zU_1, \quad v = V_0 + zV_1, \quad w = W_0 \quad (2.2)$$

for HOT of Reddy;

$$u = U_0 + zU_1 - \frac{4}{3h^2}z^3(U_1 + \frac{\partial W_0}{\partial x}), \quad v = V_0 + zV_1 - \frac{4}{3h^2}z^3(V_1 + \frac{\partial W_0}{\partial y}), \quad w = W_0 \quad (2.3)$$

These equations imply that FOSDT and HOT of Reddy include two additional DOFs for describing shear deformations in the thickness direction.

Navier's analytical solution approach was employed for evaluating the elastic responses, and it was ensured that the termination order of sinusoidal series was sufficiently large to achieve the convergence. Figures 2.6 through 2.9 show, respectively, the asymptotic to CLT solutions of the central deflections, the central flexural stresses, the first natural frequencies and the bifurcation loads obtained by FOSDT and HOT of Reddy for each of the three material cases. All of these four results consistently indicate that, in the case of high-stiff CFRP,  $l/h = 100$  is required for solutions by FOSDT and HOT of Reddy to approach CLT solution. This means that when  $l/h$  is less than 100, "thickness effect" is not negligible and CLT is not applicable. On the other hand, in the case of GFRP  $l/h = 50$  is required to approach CLT solution and in the case of Aluminum,  $l/h = 50$  or a little bit less. As a consequence, it is concluded that although CPT (CLT for laminates) has been valid as a proper numerical model for isotropic plate/shell in a wide range of the span-to-thickness ratios  $l/h$ , for composite laminates its valid range is quite limited and higher-order models including "thickness effect" such as FOSDT, HOT of Reddy or further higher-order models are required.



Unfortunately, the commercial finite element packages has been focusing on isotropic plate/shell models only and hence they do not pay careful attentions to the relationships between "the vanishing point of thickness effect" and " $E_L/G_{Tz}$ ,  $E_L/G_{zL}$  effects".

## 2.4 Laminate-like, through-the-thickness inhomogeneity

Composite material applications are roughly classified into two types, that is, structural panels bearing lateral (transverse) loads and structural components carrying axial loads as respectively illustrated in Figure 2.10. The first one is plate/shell panels as in motorboats, while the latter is cylindric pipes like drilling risers, finite width strips like overlays (boundary angles) for T-joints. Although they appear to be quite different from each other, they have a similar characteristic. That is to say, they are made by piling vary thin sheet to form a certain thick laminated components; More strictly, cylindrical composite products are usually formed by filament winding process, but schematically saying they can be explained to be formed by piling process. This unique forming process gives rise to flexibility for material and structural designs of composite laminates. However, this causes some numerical modeling difficulty peculiar to composite materials, that is to say, "laminate-like, through-the-thickness inhomogeneity".

Composite materials possess various kinds of mechanical, geometrical and material inhomogeneities ranging from fiber/matrix interfaces to adhesive joints of structural components. Figure 2.11 illustrates various composite material inhomogeneities, and in Figure 2.12 a typical inhomogeneity model is shown. Recently, the author *et al.*<sup>29</sup> has categorized composite material inhomogeneities into five phases as presented in Figure 2.13, and in Table 2.3 possible combinations of these inhomogeneities in practical problems are tabulated.

In particular, in structural analysis and design, inhomogeneity in "Laminate-like Phase" must not be overlooked. Here is an example. Equivalent-single-layer (ESL) models coupled with the lamination theory (LT), e.g., CLT and FOSDT, provide satisfactory results only for global quantities such as deflections, flexural stresses. When one applies ESL models to local quantity evaluations such as through-the-thickness distributions of transverse stresses, then disappointing results will be obtained because of this "laminate-like, through-the-thickness inhomogeneity". For instance, Figure 2.14 shows through-the-thickness distributions of the transverse stress  $\tau_{xz}$  in a laminated plate evaluated by directly using FOSDT and HOT of Reddy. These plots indicate that

ESL models do not correctly represent the transverse stress distributions which are actually continuous at different material interfaces. This is because ESL models assume only a single set of displacement variations over the laminate thickness. This leads to continuous transverse strain variations through the thickness, and then discontinuous transverse stresses. As pointed out in the previous section, transverse stresses should be accurately evaluated because of the weak material properties of composite laminates in the thickness direction. In order to overcome this deficiency of ESL, transverse stress re-calculations via 3-D equilibrium equations

$$\sigma_{ij,j} = 0 \quad (2.4)$$

are proposed in the literature<sup>14, 17, 28, 30, 31</sup>. However, this does not give a solution to this defect of ESL itself.

In stead of ESL models, designers including the author have employed the other numerical models such as 2-D, 3-D continuum solids for evaluating such local quantities, some of which will be shown in the next and after.

#### 2.4.1 Case 3 : NCF-coupling joint for composite drilling riser — continuum solid models

Enthusiastic attempts to develop a brand-new drilling riser pipes are made in the world. Weight reduction of the riser pipe while preserving its service strength and life is very profitable. Thus development of a composite riser pipe is attracting much attention. Since the weakest part of a composite riser is the joint part, various types of joint are devised. Among them, no-cut-fiber (NCF) coupling joint<sup>32</sup> is the most efficient because this joint dose not require any adhesion and any mechanical joint, and hence is easy for maintenance.

The author carried out finite element analysis of NCF-coupling joint by using 2-D axisymmetric solid elements and special contact elements. The dimension, loading conditions and stacking sequences are presented in Figure 2.15, and material properties used are given in Table 2.4. The gridwork of finite element meshes is shown in Figure 2.16(a). The failure index margin contours obtained are shown in Figure 2.16(b). Figures 2.17(a), (b) and 2.18(a), (b) are contour plots of axial stress  $\sigma_z$ , radial stress  $\sigma_r$ , hoop stress  $\sigma_\theta$  and shear stress  $\tau_{zr}$ , respectively.

As demonstrated in this example, local stress analysis by continuum solid models alone is possibly conducted on condition that finite element meshes are sufficiently fine so that each different material lamina can be individually modeled.

However, continuum solid models have some difficulties. One of the most serious is computational cost. Figure 2.19 explains this economical deficiency. A continuum solid element can represent only one material region, so that the number of finite element discretizations over the thickness is required to be at least the same number of different material laminae. This requirement governs the number of discretizations in the in-plane directions as well, since width-to-height aspect ratio of each element must be kept under a certain upper limit, say, 5 or less. When one breaks this upper limit, ill-conditioning problems of the elements will become serious. Consequently, as the number of laminae is larger and the lamina thickness is smaller, finer meshes in the in-plane directions are also required. This results in a huge number of computational degrees of freedom if one attempts to model the overall laminated structure by continuum solid elements alone.

#### 2.4.2 Case 4 : composite sandwich motorboat — ESL/solid hybrid models

Continuum solid models are only applicable to local analysis of limited regions in a structure as pointed out in the previous section. Applications of continuum solid model to global structural analysis are not realistic from an economical point of view.

Designers including the author have avoided this economical difficulties by ambiguous and/or cumbersome schemes. Some use conventional ELS models by introducing some kinds of effective shear elastic moduli which are predicted from experimental estimations<sup>33</sup>. Another expedient is to combine ELS and continuum solid model<sup>34</sup>.

A typical example of the latter scheme is shown here. That is the case of the structural analysis of a sandwich composite structure. The author was involved in a research and development project for advanced material racing motorboats and was responsible for numerical stress analysis. The author was demanded to conduct global structural analysis of a composite motorboat while precisely evaluating transverse stress distributions in the core layer because the experimental observations warned that the structural strength was strongly governed by such local stresses in the core. A finite element modeling by 3-D continuum solid element only was out of the question, therefore the author adopted combination of ESL model and continuum solid.

Figure 2.20 is a schematic of the analysis model configuration, boundary and loading conditions. In the finite element modeling, 8-node thick shell elements (ESL-based FOSDT model) were used for representing the upper and lower skin faces, while 20-node 3-D continuum brick elements were used for the core layer. The gridwork of finite



element meshes used is shown in Figure 2.21. Material properties used are given in Table 2.5. In Figure 2.22, the contour plots of  $z$  direction displacement are shown. Figures 2.23 and 2.24, respectively, show the contour plots of transverse shear stresses  $\tau_{zx}$  and  $\tau_{yz}$  within the core.

This hybrid modeling of sandwich constructions was very cumbersome and time-consuming, but there was no choice at that time. Besides this modeling scheme is not always applicable.

Hence there is a strong demand for a new numerical model which is equipped with both simple two-dimensional geometry of ESL and precise three-dimensional and multi-layered displacement/stress state of continuum solid model.

### 2.4.3 Case 5 : interlaminar stresses

Finally, "Laminate-like, through-the-thickness inhomogeneity" gives rise to another kind of quantities at lamina interfaces. That is interlaminar stress. These kinds of stresses peculiar to this anisotropic and inhomogeneous materials sometimes play a dominant role in the overall strength of an entire laminated structure, even though they are quite localized quantities.

For example, Figures 2.25 is a schematics of an angle-ply symmetric laminated strip under uniform axial extension. This well-known problem exhibits interlaminar stress concentrations in the vicinity of the free edges (free-edge effect). Figures 2.26 and 2.27 are the results obtained by the author using 3-D continuum brick elements and 2-D stress-based boundary layer solution method (CLEOPS/COMPOSIC Package<sup>35</sup>), respectively. Both of the Figures show the interlaminar stress concentrations near the free edges.

In order to evaluate interlaminar stresses by ESL model, the pointwise re-calculations via the 3-D equilibrium equations are needed. On the other hand, 2-D, 3-D continuum solid models are also limited in a local region for interlaminar stress evaluations. Still worse, further finer meshes are needed because of their singular nature.

Consequently, there is also a strong demand for a new numerical model which has simple two-dimensional geometry of ESL and, at the same time, is capable of interlaminar stress evaluations.



## 2.5 Summary

In this chapter, three specific features of composite materials were shown, which are important for their numerical modelings, that is,

- anisotropic properties;
- weakness in the transverse direction;
- laminate-like, through-the-thickness inhomogeneity.

As shown herein, when one tries to numerically model laminated composite material structures (composite laminates) by using the existing model like ESL model, 2-D, 3-D continuum solid model and their combinations while taking into account these three specific aspects precisely, one experiences very cumbersome, skillful and uneconomical efforts.

Therefore, an efficient and rational modeling scheme is required, which properly account for these characteristics of composite laminates.

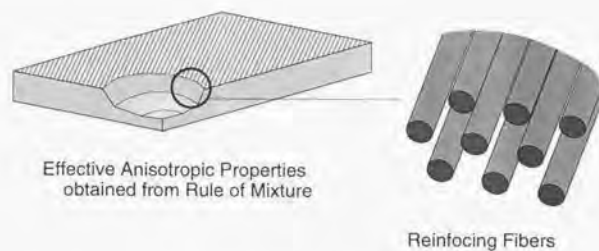


Figure 2.1 A schematic of anisotropy in fiber-reinforced composite materials

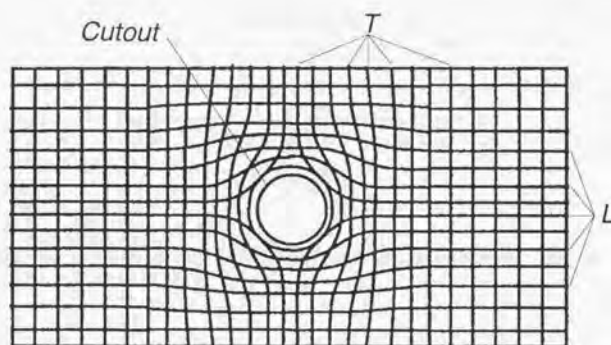


Figure 2.2 A typical example of local variations of the material directions  
— Solid curves denote fiber directions ( $L$  directions) and transverse directions perpendicular to them ( $T$  directions)

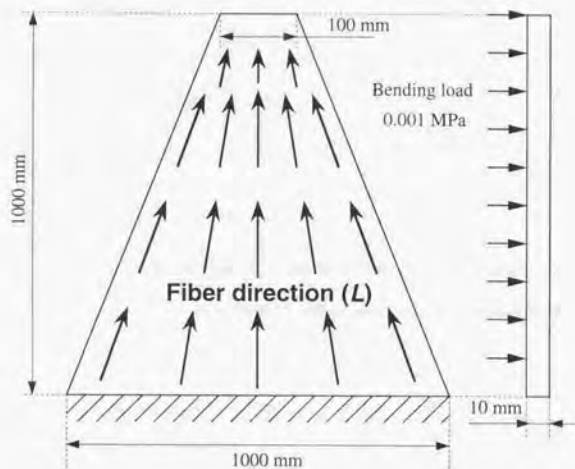


Figure 2.3 A schematic of a trapezoid plate under lateral bending pressure

Table 2.1 Elastic moduli and thickness of the orthotropic trapezoid plate

material		CFRP
Young's Moduli (GPa)	$E_L$	153
	$E_T$	10.9
Poisson's Ratios	$\nu_{LT}$	0.120
	$\nu_{Tz}$	0.121
Shear Elastic Moduli (GPa)	$G_{LT}$	5.58
	$G_{Tz}$	4.86
	$G_{zL}$	5.58

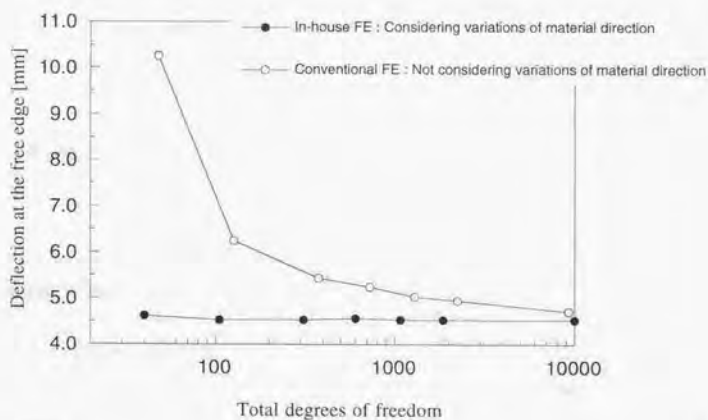
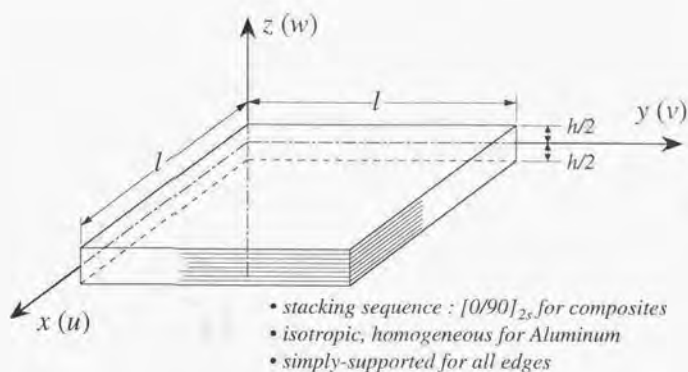


Figure 2.4 Convergence of deflections at the free end against mesh refinement (total degrees of freedom)





**Figure 2.5** A schematic of a simply-supported square plate;  
an eight-layup cross-ply symmetric laminate for FRPs and a homogeneous plate for Aluminum

**Table 2.2** Elastic moduli, specific gravity and thickness of each lamina

material		high-stiff CFRP	GFRP	Aluminum	
Young's Moduli (GPa)	$E_L$	450	60.7	$E$	71.0
	$E_T$	6.3	24.8		
Poisson's Ratio	$\nu_{LT}$	0.30	0.23	$\nu$	0.34
Shear Elastic Moduli (GPa)	$G_{LT}$	5.0	11.99	$G$	26.49
	$G_{Tz}$	2.38	10.08		
	$G_{zL}$	5.0	11.99		
$\frac{E_L}{G_{Tz}}$		189.1	6.02	2.68	
specific gravity		1.78	2.60	2.65	
total thickness (mm)		$8 \times 0.20$	$8 \times 0.20$	1.6	

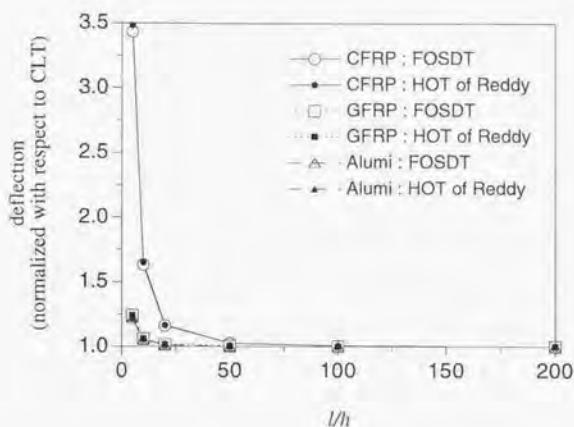


Figure 2.6 Asymptotic of the central deflections to CLT solution against  $l/h$

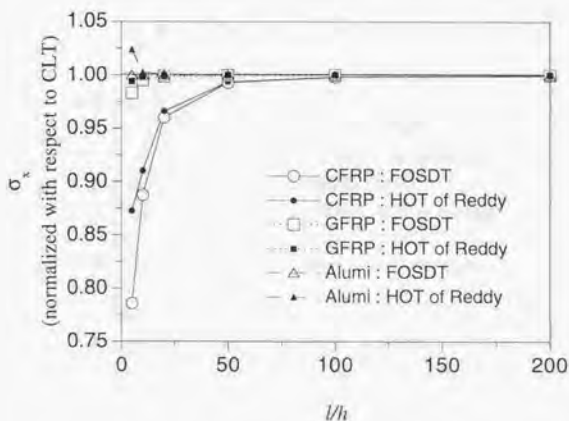


Figure 2.7 Asymptotic of the central flexural stresses to CLT solution against  $l/h$

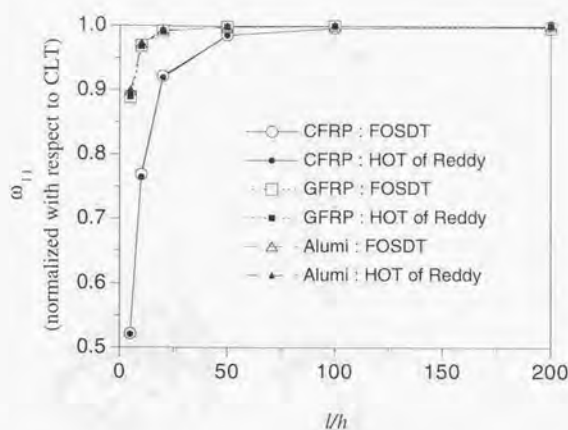


Figure 2.8 Asymptotic of the first natural frequencies to CLT solution against  $l/h$

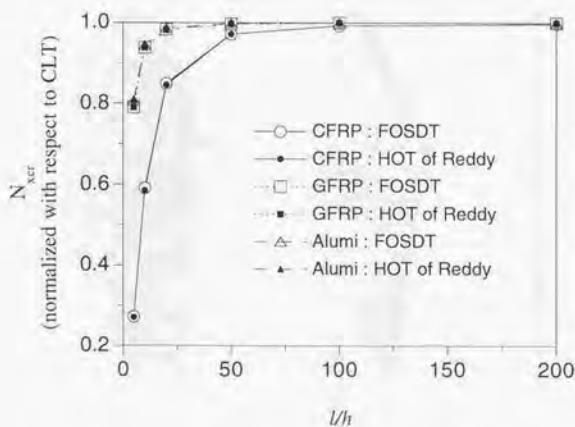


Figure 2.9 Asymptotic of the bifurcation loads to CLT solution against  $l/h$

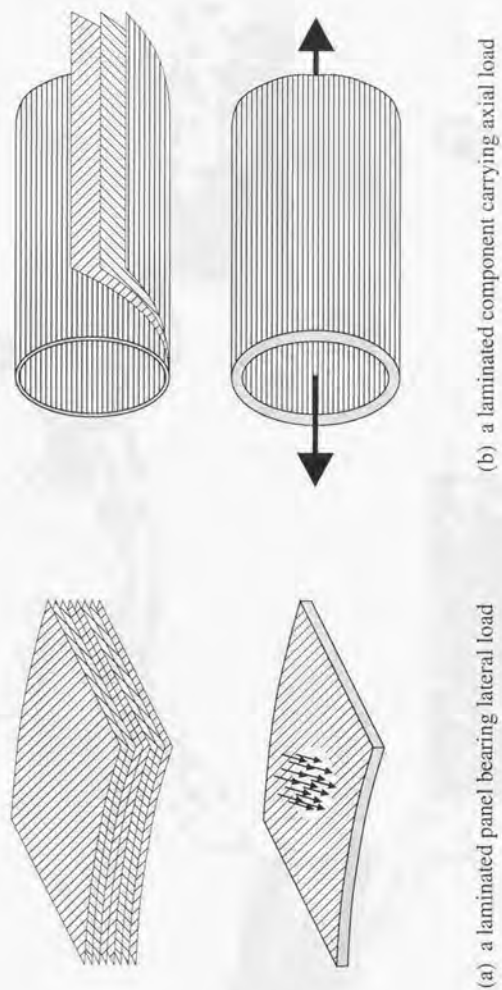


Figure 2.10 Typical laminated composite material structures



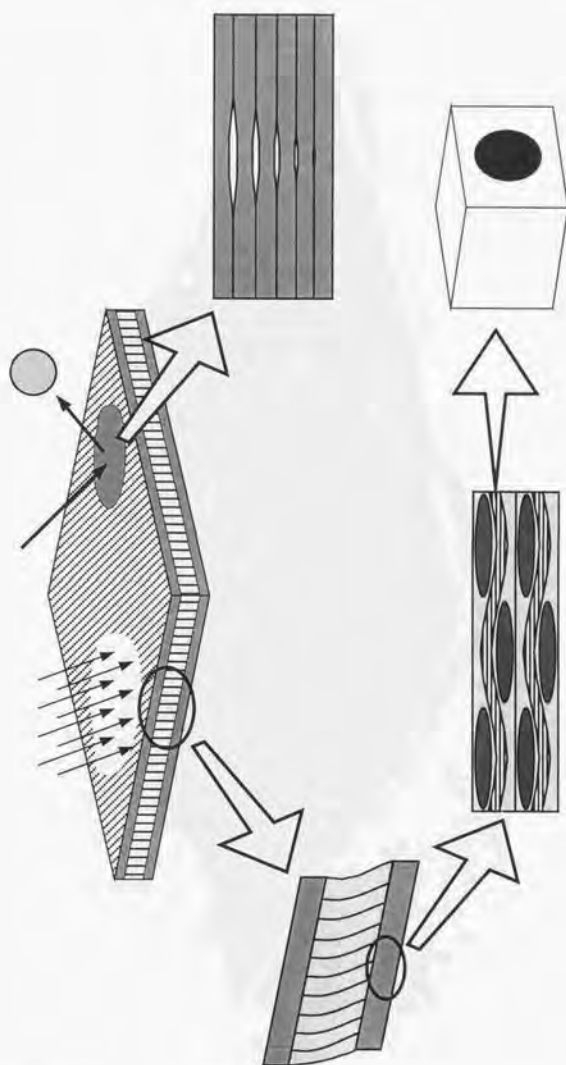


Figure 2.11 Various inhomogeneities in composite materials

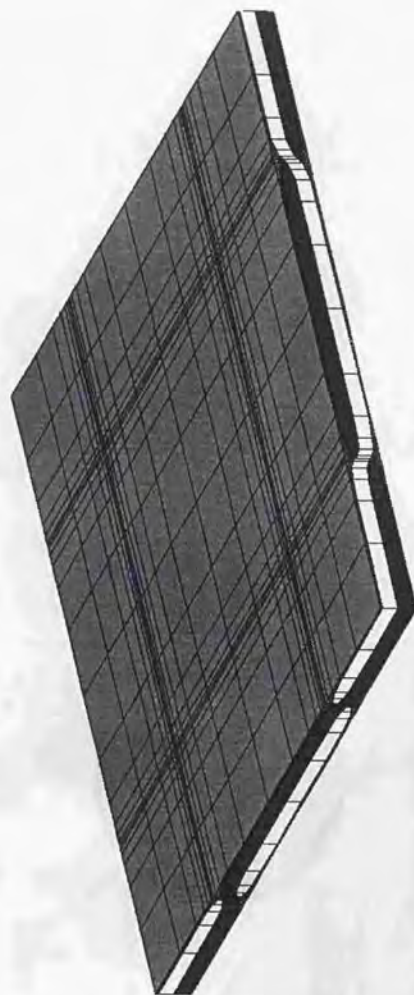


Figure 2.12 3-D unitcell inhomogeneous model in a woven composite laminate

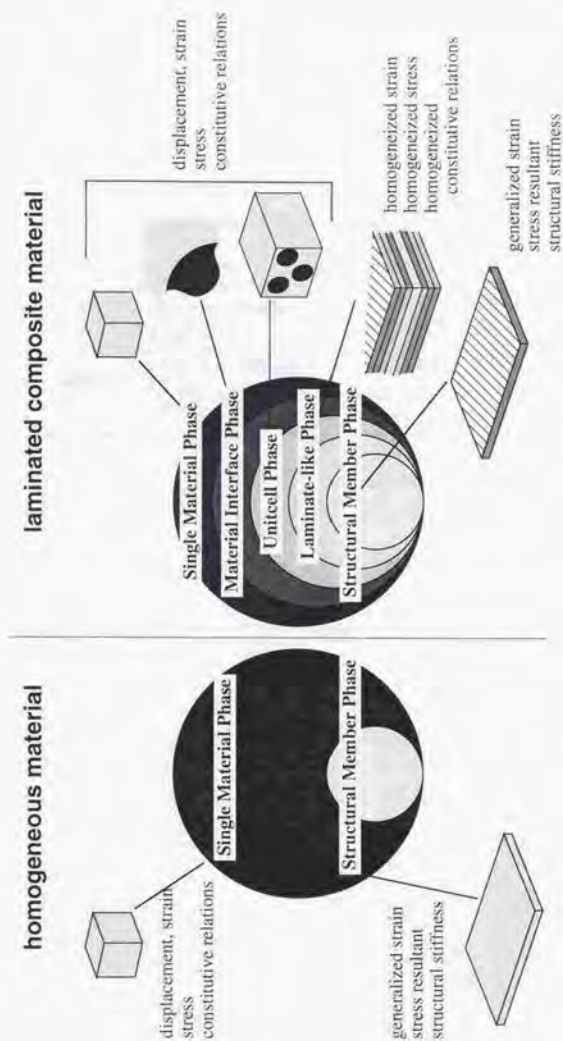


Figure 2.13 Comparison of composite materials and homogeneous materials with respect to inhomogeneity

Table 2.3 Possible combinations of different inhomogeneities in composite laminates

Combination of Phases	Examples
Structural Member + $\begin{cases} \text{Single Material} \\ \text{Material Interface} \\ \text{Unitcell} \end{cases}$	meso-mechanics homogenization method
Structural Member + Laminate-like	delamination CAI failure modes of sandwich
Laminate-like + $\begin{cases} \text{Single Material} \\ \text{Material Interface} \\ \text{Unitcell} \end{cases}$	interfacial stresses interlayer properties
Structural Member + Laminate-like + $\begin{cases} \text{Single Material} \\ \text{Material Interface} \\ \text{Unitcell} \end{cases}$	free-edge effects laminates with inserted films overlayed joints



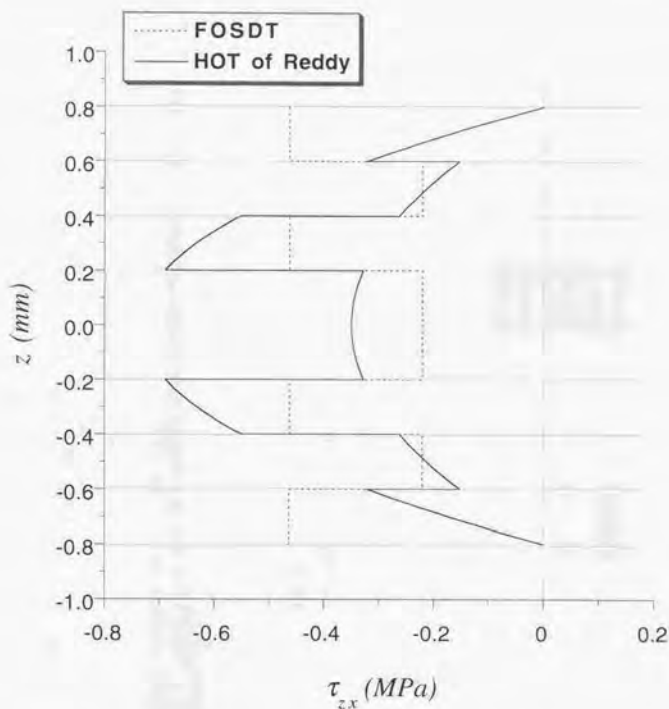


Figure 2.14 Through-the-thickness distributions of transverse shear stress  $\tau_{zx}$  directly evaluated from the lamination theory (LT)



Table 2.4 Elastic moduli and strength of materials in composite riser

materials		HOOP	HELICAL		STEEL
Young's Moduli $\dagger$ (kgf/mm <sup>2</sup> )	$E_z$	800	15500	$E$	21000
	$E_r$	800	800		
	$E_\theta$	29000	869		
Poisson's Ratios	$\nu_{zr}$	0.30	0.34	$\nu$	0.3
	$\nu_{\theta r}$	0.34	0.135		
	$\nu_{r\theta}$	0.0094	0.30		
Shear Modulus (kgf/mm <sup>2</sup> )	$G_{zr}$	308	500	$G$	8077
Strength $\ddagger$ (kgf/mm <sup>2</sup> )	$\sigma_{zT}^*$	3	141	$\sigma_T^*$	70
	$\sigma_{zC}^*$	20	19		
	$\sigma_{rT}^*$	3	3		
	$\sigma_{rC}^*$	20	20		
	$\sigma_{\theta T}^*$	180	3.7		
	$\sigma_{\theta C}^*$	45	21		
	$\tau_{zr}^*$	5	9		

$\dagger$  Cylindrical coordinate  $z$ - $r$ - $\theta$  is used.  $z$ ,  $r$  and  $\theta$  denote axial, radial and circumferential directions, respectively.

$\ddagger$   $T$  denotes "tension" and  $C$ , "compression".

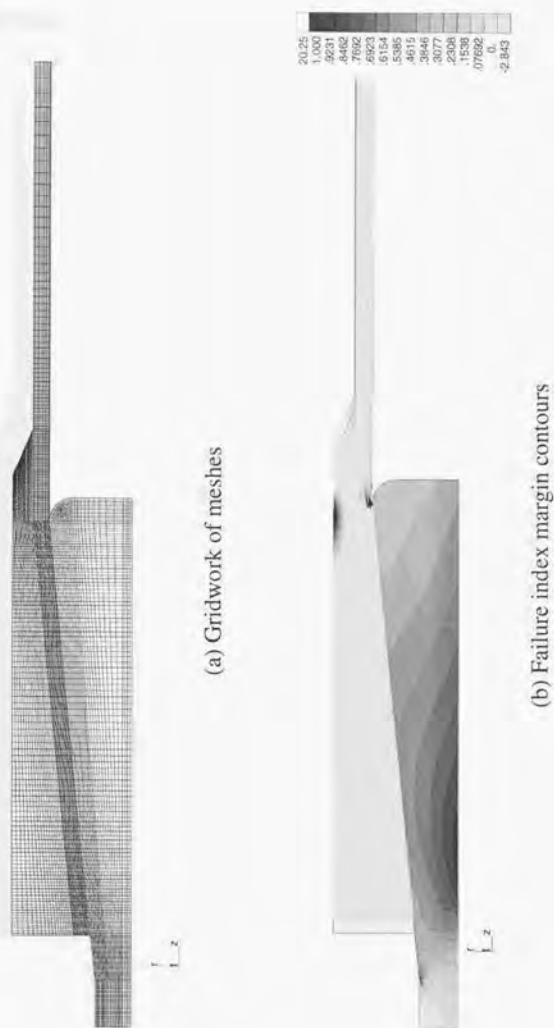


Figure 2.16 Gridwork of finite element meshes and failure index margin contours within NCF-coupling joint for composite riser





Figure 2.17 Stress contours within NCF-coupling joint for composite riser (1) (Unit in  $\text{kgf/mm}^2$ )



Figure 2.18 Stress contours within NCF-coupling joint for composite riser (2) (Unit in  $\text{kgf/mm}^2$ )

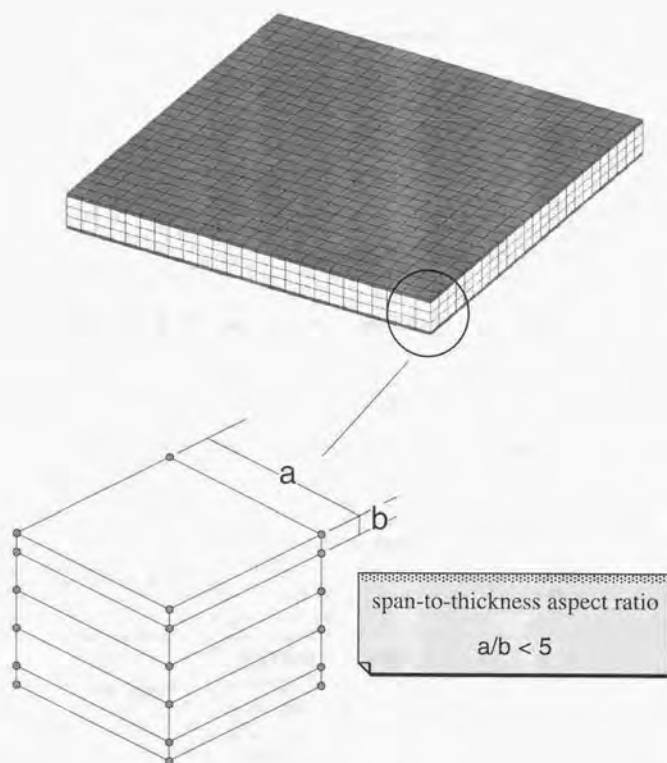


Figure 2.19 A schematic of mesh discretizations by 3-D continuum solid elements

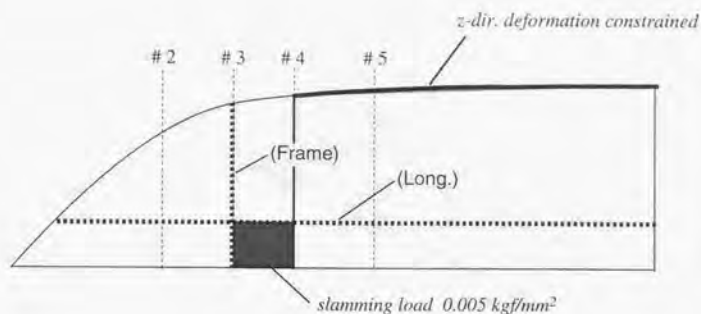


Figure 2.20 Design draw for composite sandwich motorboat

Table 2.5 Typical material properties for composite sandwich motorboat

CF-cloth †	$E_L = 4290, E_T = 4290 \text{ (kgf/mm}^2\text{)}$ $\nu_{LT} = 0.1$ $G_{LT} = 340, G_{Tz} = G_{zL} = 300 \text{ (kgf/mm}^2\text{)}$ $h = 0.116 \text{ (mm)}$
CF-UD ‡	$E_L = 11500, E_T = 798 \text{ (kgf/mm}^2\text{)}$ $\nu_{LT} = 0.302$ $G_{LT} = 400, G_{Tz} = G_{zL} = 300 \text{ (kgf/mm}^2\text{)}$ $h = 0.156 \text{ (mm)}$
Core §	$E = 16.1 \text{ (kgf/mm}^2\text{)}$ $\nu = 0.3$ $h = 5, 10, 20 \text{ (mm)}$

† Textile woven prepreg sheet for primary members.

‡ Unidirectional prepreg tape for adhesive joint area.

§ Devynycell foam.



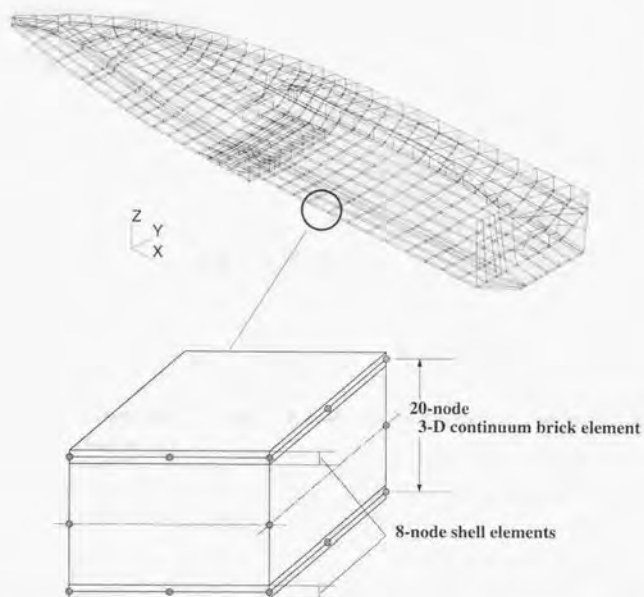


Figure 2.21 Gridwork of finite element meshes of composite sandwich motorboat — combination of ELS and continuum solid

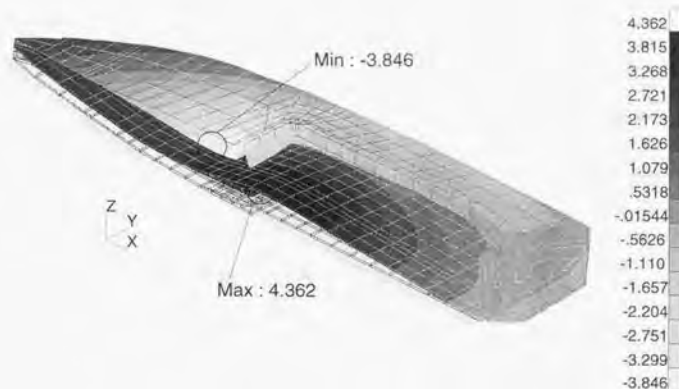


Figure 2.22 Transverse displacement contours on composite sandwich motorboat (Unit in mm)

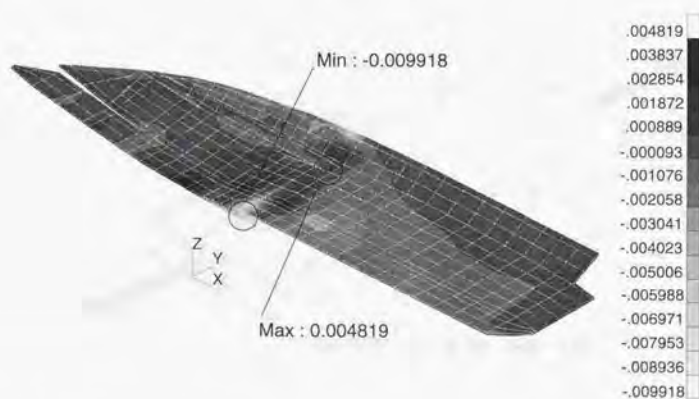


Figure 2.23 Transverse shear stress  $\tau_{zx}$  contours within the core part of composite sandwich motorboat (Unit in  $\text{kgf/mm}^2$ )

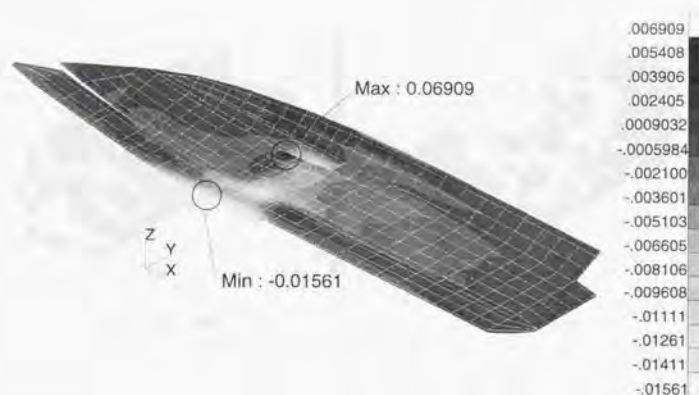


Figure 2.24 Transverse shear stress  $\tau_{yz}$  contours within the core part of composite sandwich motorboat (Unit in  $\text{kgf}/\text{mm}^2$ )

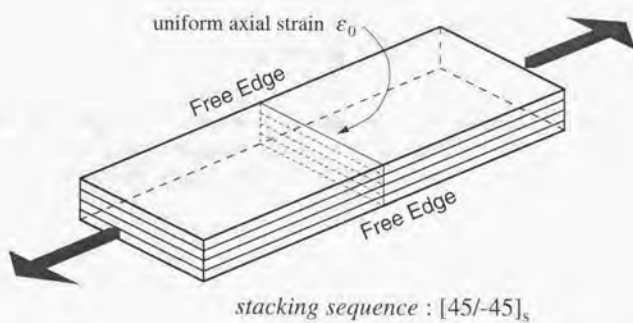


Figure 2.25 Free-edge effect — an angle-ply symmetric laminated strip under uniform axial extension

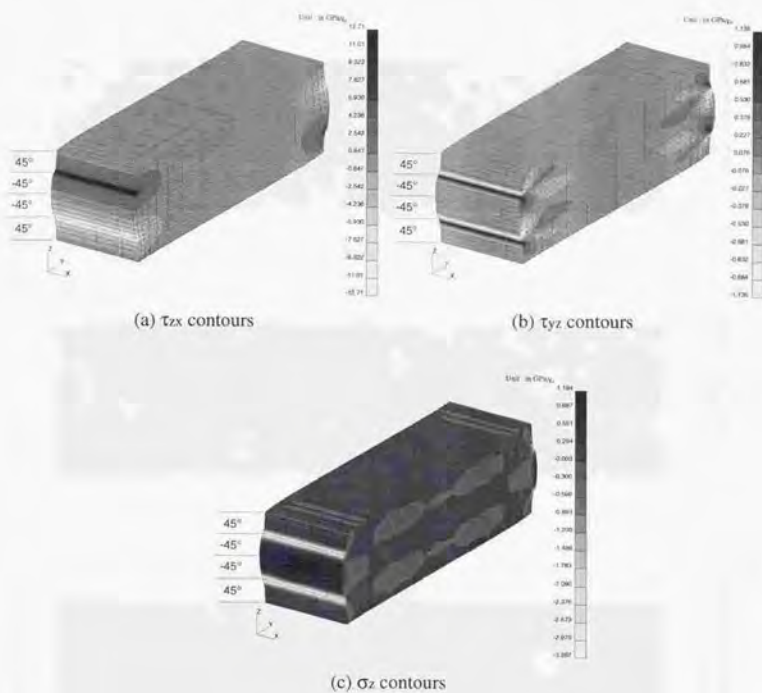


Figure 2.26 Free-edge effect — transverse stress contours obtained by 3-D continuum solid finite element analysis : MARC k52  
 (Unit in  $\times 10^6$  psi/ $\epsilon_0$  :  $10^6$  psi  $\doteq$  6.89 GPa)



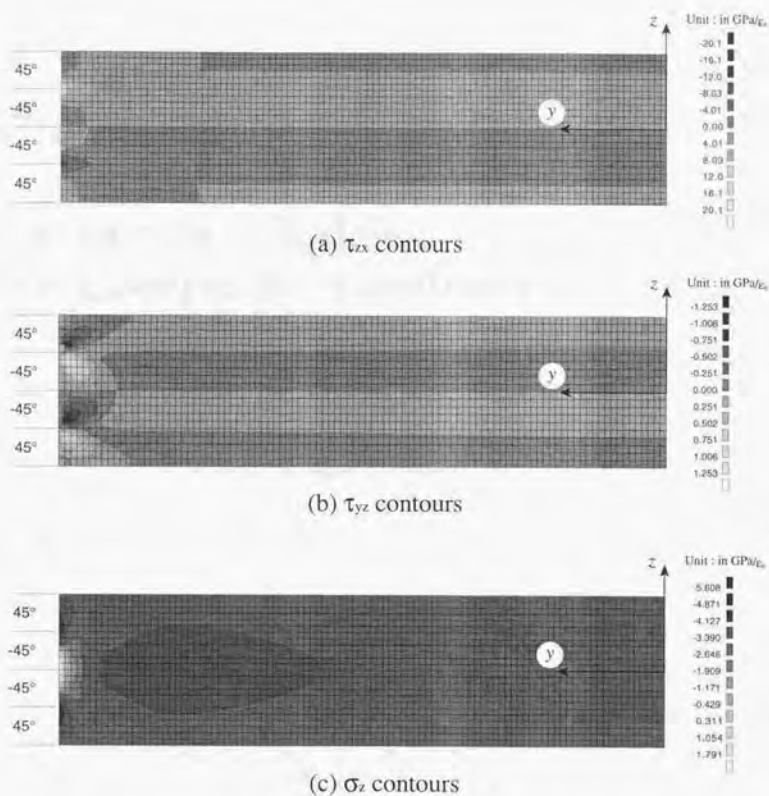


Figure 2.27 Free-edge effect — transverse stress contours obtained by 2-D stress-equilibrium finite element analysis : CLEOPS/COMPOSIC (Unit in  $\text{GPa}/\epsilon_0$ )

## Chapter 3

### Numerical Models for Composite Laminates

### 3.1 Introduction to this chapter

As demonstrated in the previous chapter, the existing models for isotropic materials, i.e., ESL-based first-order model, 2-D, 3-D continuum solid models and their combinations are not necessarily suited for analysis and design of laminated composite material structures (composite laminates), because composite materials possess peculiar characteristics, i.e., "anisotropic properties", "weaker properties over the thickness" and "laminar-like, through-the-thickness inhomogeneity".

In this chapter, a proper numerical model for composite laminates is sought for.

### 3.2 Theories and their finite elements for composite laminates

As an alternative numerical model for composite laminates, which replaces the conventional models, two different kinds of models have been proposed in the literature, that is,

- ESL-based higher-order theories (HOTs) and their FEs
- Multi-layer (ML) theories and their FEs

Progressional history of numerical model proposals for composite laminates is roughly charted in Figure 3.1. As a detailed reviews on the progress of refinements of theories and FEs for composite laminates, one can refer to the works, for example, by Reissner<sup>36</sup>, Reddy<sup>37, 38</sup>, Noor and Burton<sup>39</sup>, and Narita<sup>40</sup>.

#### ESL-based higher-order models

The family of equivalent-single-layer (ESL) theories and FEs is probably the most dominant mainly because they have been well tested, robust and have been proven to produce satisfactory predictions of global responses of thin to moderately thick composite laminates (e.g. deflections and flexural stresses). Another reason for their popularity is that degrees of freedom (DOF) in ESL-based theories and FEs, whether classical or refined, are independent of the number of laminae (which means drastically decreased DOF in number), and at the time of inferior computational circumstances, only such a small scale calculation was acceptable. However, as demonstrated in the previous chapter, first-order models like CLT and FOSDT are restricted to some extent.

In stead of the ELS-based first-order models, higher-order deformation theories (HODT or simply, HOT) and their  $C^0$  continuity FEs which account for further higher-order deformations such as warping of the cross-section, elongation of the transverse-normal were studied by Naghdi <sup>41</sup>, Librescu <sup>42</sup>, Whitney and Sun <sup>43</sup>, Nelson and Lorch <sup>44</sup>, Reissner <sup>45</sup>, Krishna Murty <sup>46</sup> and then Lo, Christensen and Wu <sup>47, 48</sup>.

More lately, Bhimaraddi and Stevens <sup>49</sup>, Di Sciuva <sup>50</sup> and Kant *et al.* <sup>51, 52, 53</sup> extensively studied ELS-based HOTs and developed several FEs based on them. One of the most successful ESL-based HOTs is perhaps Reddy's third-order theory (HOT of Reddy) <sup>28, 54, 55, 56, 57, 58</sup>. This theory assumes cubic variations of in-plane displacement components over the thickness while suppressing excessive DOFs via the traction-free conditions on the exterior surfaces of laminates.

In the early time, the primary purpose of HOTs was placed on eliminating the shear correction factors of FOSDT. In addition to that, HOTs have several advantages over CLT and FOSDT such as

- HOTs are capable of evaluating six non-zero strain and hence stress components in the laminates.
- HOTs are especially effective for evaluating higher-order vibration modes.
- HOTs are generalization or unification of ESL-based models precedent to them <sup>57</sup>.

However, ESL-based HOTs do not precisely model multi-layered kinematical configurations of the actual laminates just the same as CLT and FOSDT. Besides they don't provide meaningful predictions of transverse stress (and hence interlaminar stresses) unless pointwise re-calculations by means of the 3-D equilibrium equations are carried out.

### Multi-layer (ML) models

In order to improve these drawbacks of ESL, the family of multi-layer (ML) theories and their FEs have been proposed in the literature. Roughly three different types of ML are listed in accordance with variational considerations they adopt,

**Pian's assumed stress hybrid method** Since Mau, Tong and Pian <sup>59</sup> developed stress-based multi-layer FEs based on Pian's assumed stress hybrid method <sup>60</sup>, these types of stress-based hybrid FEs have been extensively studied and refined by many researchers <sup>61, 62, 63</sup>. In particular, Spilker's works <sup>64, 65, 66, 67</sup> are



prominent. This type of element assumes stress distributions for each layer by introducing stress parameters so that equilibriums of stresses at the interlayers and the surfaces are satisfied *a priori*.

**Other mixed variational method** Another type of ML theories and their FEs were proposed by several researchers. Pagano<sup>68</sup> and then Yeom and Lee<sup>69</sup> employed Hellinger-Reissner's variational principle<sup>70</sup> for their finite element formulations in the stress analysis of composite laminates (assumed strain mixed model). Moriya<sup>71</sup> used Hu-Washizu's variational principle<sup>72</sup> in the formulation of his multi-layer degenerated 3-D shell element. On the other hand, Murakami<sup>73</sup> and Toledano and Murakami<sup>74,75</sup> formulated a new multi-layer theory and its plate FE, as a response to Reissner's new variational principle<sup>76,77</sup>. Bhaskar and Varadan<sup>78</sup> also used Reissner's new variational principle for derivation of their multi-layer cylindrical shell theory.

**Displacement-based layerwise theories** On the other hand, various displacement-based multi-layer theories have also been proposed. Sun and Whitney<sup>79</sup>, Mau<sup>80</sup> and Srinivas<sup>81</sup> were the early ones who proposed this type of displacement-based ML plate theories. After that, displacement-based ML FEs were developed by Epstein and Huttelmaier<sup>82</sup>, Owen and Li<sup>83</sup>, Chaudhuri and Seide<sup>84,85</sup> and many others. Recently, refinements and unifications of these displacement-based ML theories have been made by Soldatos<sup>86</sup>, Wu *et al.*<sup>87,88,89,90</sup>, Verijenko<sup>91,92</sup> and others. Reddy<sup>93</sup>, Reddy and Barbero<sup>94,95</sup> and Robbins, Jr. and Reddy<sup>96</sup> also extensively studied on analytical (closed-form) solutions and finite elements based on Reddy's generalized multi-layer theory<sup>97</sup>.

In this study, the displacement-based ML models will be called "Layerwise" models for distinguishing it from the other ML models.

These multi-layer theories and their FEs will make a mainstream in the numerical analysis and design for composite laminates, because they can provide sufficiently good results for both global values (e.g. deflections and flexural stresses) and local values (e.g. transverse stresses and interlaminar stresses) of thin-to-thick laminates.

Stress-based and mixed multi-layer models are, if anything, appropriate for local stress analysis, not for structural analysis and design, of composite laminates. Displacement-based layerwise models on the other hand match the aim of the present study very well because they model laminate-like inhomogeneity through the thickness in the most natural manner. Besides, they are easy to integrate into the existing systems and extend to dynamic problems or non-linear problems such as Von-Kármán

strains and modeling of delaminations. Increasing DOFs proportional to the numbers of discrete layers will not be so serious in near future due to the recent accelerating advancements of computational facilities symbolized by massive parallel computers equipped with vary large extensional core storages. Furthermore, one will witness less amount of total DOFs in the layerwise models than those discretized by 3-D continuum solid elements which is necessary to be meshed obeying a proper aspect ratio.

### Layerwise higher-order models

Hence, in this study, it is concluded that, as a proper numerical model for analysis and design of composite laminates, a "Layerwise" and "Higher-order" model will be appropriate, because this model is equipped with both simple two-dimensional geometry of ESL and three-dimensional/multi-layer state of displacements and stresses. It should be emphasized that such a numerical model that accounts for both of the layerwise and the higher-order concepts is still rare.

## 3.3 Formulation of the layerwise higher-order deformation theory

The layerwise higher-order deformation theory newly proposed by the author will be formulated herein.

For preserving its generality, summation conventions are implied for repeated subscripts in the mathematical formulae.

### 3.3.1 Multi-layer discretization scheme

In the present theory, a laminate is divided into a certain number of layers in the laminate thickness direction. There are several possible schemes and their combinations considered for dividing a laminate into layers as depicted in Figure 3.2.

It should be noted that layers can be defined independently of physical laminae. The most natural manner of layer division is probably to divide a laminate according to the individual dissimilar material lamina (natural ML). However, in the present formulation, a laminate can be divided into sub-laminates which include several dissimilar material lamina in themselves (coarse ML). On the contrary, in some cases, an individual lamina should be divided into several layers so that complicated displacement fields can be modeled (fine ML). For clarifying this ML discretization scheme,

the number of layers is denoted by  $NK$ , while the number of laminae is denoted by  $N$ .

### 3.3.2 Higher-order deformation theory for each layer

#### Kinematics

The present theory is categorized into the displacement-based theories, therefore, formulation begins by kinematical assumptions. This theory assumes the three displacement components in each discrete layer in the form of the power series expansions in terms of the thickness coordinates ' $x_3^{(k)}$ ', as follows:

$$\begin{aligned} u_i^{(k)}(x_1, x_2, x_3^{(k)}) \\ = U_{i0}^{(k)}(x_1, x_2) + x_3^{(k)} U_{i1}^{(k)}(x_1, x_2) + (x_3^{(k)})^2 U_{i2}^{(k)}(x_1, x_2) + \cdots + (x_3^{(k)})^{N_i^{(k)}} U_{iN_i^{(k)}}^{(k)}(x_1, x_2) \\ = (x_3^{(k)})^P U_{iP}^{(k)}(x_1, x_2) \quad (i = 1, 2, 3 \text{ and } P = 0, 1, 2, \dots, N_i^{(k)}) \end{aligned} \quad (3.1)$$

where the superscript ' $k$ ' denotes each one of layers of a laminate, numbered from the bottom layer to the top, and  $U_{iP}^{(k)}$  are the unknown coefficients of the series expansion, and  $x_3^{(k)}$  is the thickness coordinate measured from the middle plane of the considered layer. The geometric configuration of a laminate and the deformation of the typical layer ' $k$ ' are schematically illustrated in Figure 3.3.

Geometrically,  $U_{10}^{(k)}$ ,  $U_{20}^{(k)}$  and  $U_{30}^{(k)}$  are the translational components along  $x_1$ ,  $x_2$  and  $x_3$  axes, respectively, and  $U_{11}^{(k)}$  and  $U_{21}^{(k)}$  denote small rotations about  $x_2$  and  $-x_1$  axes, respectively. The rest of coefficients of power series expansions are higher-order influences such as parabolic stretching, cubic warping of the cross-section, the elongation of a transverse normal and so forth. It will be necessary to discuss whether or not these polynomial series assumptions can be sufficiently correct representations for displacement variations through the layer thickness. However at least it can be said that this polynomial approximation will be adequate except certain "unusual" local regions such as the vicinity of concentrated loads or the free edges. Besides, even in that cases, one can employ a further fine ML scheme for representing such a complicated displacement field.

The series in Equation (3.1) will be terminated at a proper order of expansion, however, at this moment, the orders of termination is not determined yet for preserving the flexibility of the present theory. For conceptual sake, when the orders of the series for  $k^{\text{th}}$  layer are  $N_1^{(k)}$ ,  $N_2^{(k)}$  and  $N_3^{(k)}$  for  $u_1^{(k)}$ ,  $u_2^{(k)}$  and  $u_3^{(k)}$ , respectively, the notation  $(N_1^{(k)} N_2^{(k)} N_3^{(k)})$  will be used to express the order of displacement assumptions, and the



notation

$$\left[ \left( N_1^{(1)} N_2^{(1)} N_3^{(1)} \right) \left( N_1^{(2)} N_2^{(2)} N_3^{(2)} \right) \dots \left( N_1^{(NK)} N_2^{(NK)} N_3^{(NK)} \right) \right]$$

will also be used for the entire laminate made up of  $NK$  layers. Note that the parentheses denote layers and the brackets denote entire laminates.

### Strain-displacement relations

Based on small deformation elasticity, the strain-displacement relations are expressed in the following expansion forms:

$$\varepsilon_{ij}^{(k)} = \frac{1}{2} \left( \frac{\partial u_i^{(k)}}{\partial x_j} + \frac{\partial u_j^{(k)}}{\partial x_i} \right) = \left( x_3^{(k)} \right)^P E_{ijP}^{(k)}(x_1, x_2) \quad (i, j = 1, 2, 3; i \leq j \text{ and } P = 0, 1, 2, \dots, \max(N_i^{(k)}, N_j^{(k)})) \quad (3.2)$$

here,  $E_{ijP}^{(k)}$  are general strain components and taking into account the following relations with regard to displacement gradients,

$$\begin{aligned} \frac{\partial u_i^{(k)}}{\partial x_j} &= \left( x_3^{(k)} \right)^P \frac{\partial U_{iP}^{(k)}}{\partial x_j} \quad (i = 1, 2, 3; j = 1, 2 \text{ and } P = 0, 1, 2, \dots, N_i^{(k)}) \\ \frac{\partial u_i^{(k)}}{\partial x_3} &= P \left( x_3^{(k)} \right)^{P-1} U_{iP}^{(k)} \quad (i = 1, 2, 3 \text{ and } P = 1, 2, \dots, N_i^{(k)}) \end{aligned} \quad (3.3)$$

$E_{ijP}^{(k)}$  can be explicitly expressed as follows:

For in-plane general strains,

$$E_{ijP}^{(k)} = \frac{1}{2} \left( \frac{\partial U_{iP}^{(k)}}{\partial x_j} + \frac{\partial U_{jP}^{(k)}}{\partial x_i} \right) \quad (i, j = 1, 2; i \leq j \text{ and } 0 \leq P \leq \max(N_i^{(k)}, N_j^{(k)})) \quad (3.4)$$

in which, except for the case that  $N_1^{(k)}$  and  $N_2^{(k)}$  are identical, any term with respect to  $\min(N_i^{(k)}, N_j^{(k)})$  is set equal to zero through its undefined range,

$$\min(N_i^{(k)}, N_j^{(k)}) < P \leq \max(N_i^{(k)}, N_j^{(k)})$$

For transverse normal general strains,

$$\left. \begin{aligned} E_{330}^{(k)} &= 0 \\ E_{33P}^{(k)} &= P U_{3P}^{(k)} \quad (1 \leq P \leq N_3^{(k)}) \end{aligned} \right\} \quad (3.5)$$



For transverse shear general strains,

$$E_{i3P}^{(k)} = \frac{1}{2} \left( \frac{\partial U_{3P}^{(k)}}{\partial x_i} + (P+1)U_{iP+1}^{(k)} \right) \quad (i = 1, 2 \text{ and } 0 \leq P \leq \max(N_i^{(k)}, N_3^{(k)} - 1)) \quad (3.6)$$

where, except for the case that  $N_i^{(k)}$  ( $i = 1, 2$ ) and  $N_3^{(k)} - 1$  are identical, any term with respect to  $\min(N_i^{(k)}, N_3^{(k)} - 1)$  is set equal to zero through its undefined range,

$$\min(N_i^{(k)}, N_3^{(k)} - 1) < P \leq \max(N_i^{(k)}, N_3^{(k)} - 1)$$

Physically,  $E_{ij0}^{(k)}$  ( $i \leq j$ ) are pointwise strains at the middle plane of the considered layer, and  $E_{ij1}^{(k)}$  ( $i, j = 1, 2; i \leq j$ ) are curvatures of the layer.  $E_{i30}^{(k)}$  ( $i = 1, 2$ ) stand for the first approximations of transverse shear strains. When  $E_{i30}^{(k)}$  ( $i = 1, 2$ ) are set equal to zero, then the same displacement/strain assumptions as the classical plate theory (CPT) are implied in the  $k^{\text{th}}$  layer (not in the entire laminate), which provides exact representations of the plate in the infinitely-small-thickness state. On the other hand, when these terms are set non-zero, then the first-order shear deformation theory (FOSDT), i.e., Reissner-Bollé-Mindlin assumption, are implied in this layer. The rest of the general strains are higher-order components which arise corresponding to the higher-order displacement coefficients.

Obviously, the orders of through-the-thickness variations of strains depend upon the displacement orders  $(N_1^{(k)}, N_2^{(k)}, N_3^{(k)})$ . For instance, in order to assume the six non-zero strain components, at least the displacement assumption (111) is required, and when displacement assumption (332) is adopted, then cubic variations of in-plane strains, parabolic variations of transverse shear strains and linear variations of transverse normal strain are accommodated.

The aim of the higher-order deformation theory is placed on a precise modeling of displacement and strain variations over the thickness as close to the actual as possible. Appropriate orders of displacements should be determined in accordance with the actual laminate to be modeled and then the analysis demands.

### Constitutive equations

For  $l^{\text{th}}$  orthotropic arbitrarily oriented lamina in the considered layer (note that there is a possibility that layers include several laminae in themselves), the stress-strain relations (the constitutive equations) can be written as follows:

$$\sigma_{ij}^{(k,l)} = C_{ijmn}^{(k,l)} \varepsilon_{mn}^{(k)} \quad \left( \begin{array}{l} i, j = 1, 2; i \leq j \text{ or } i = j = 3 \\ m, n = 1, 2; m \leq n \text{ or } m = n = 3 \end{array} \right)$$

$$\sigma_{i3}^{(k,l)} = C_{i3mn}^{(k,l)} \varepsilon_{mn}^{(k)} \quad (i = 1, 2 \text{ and } m = 1, 2) \quad (3.7)$$

where the material constants  $C_{ijmn}^{(k,l)}$  are referred to as the reduced elastic coefficients and can be obtained by using the transformation relations with the elastic coefficients in the material principal axes and the orientation angle<sup>98</sup>. Note that there exist no coupling terms between transverse shear and the other components in orthotropic laminae.

In the present theory, the lamination theory (LT) is applied to an individual layer, not to the entire laminate. Hence the present theory can be referred to as the generalized lamination theory.

Consider the strain energy density integrated through the layer thickness:

$$U^{(k)} = \int_{-h^{(k)}/2}^{h^{(k)}/2} \frac{1}{2} \sigma_{ij}^{(k,l)} \varepsilon_{ij}^{(k)} dx_3^{(k)} \quad (i, j = 1, 2, 3; i \leq j) \quad (3.8)$$

Substituting Equation (3.2) into Equation (3.8) leads to the definition of the layer stress resultants  $M_{ijP}^{(k)}$  as follows:

$$\begin{aligned} U^{(k)} &= \int_{-h^{(k)}/2}^{h^{(k)}/2} \frac{1}{2} \sigma_{ij}^{(k,l)} \left\{ (x_3^{(k)})^P E_{ijP}^{(k)} \right\} dx_3^{(k)} \\ &= \frac{1}{2} \left\{ \int_{-h^{(k)}/2}^{h^{(k)}/2} (x_3^{(k)})^P \sigma_{ij}^{(k,l)} dx_3^{(k)} \right\} E_{ijP}^{(k)} = \frac{1}{2} M_{ijP}^{(k)} E_{ijP}^{(k)} \end{aligned} \quad (3.9)$$

in which

$$M_{ijP}^{(k)} = \int_{-h^{(k)}/2}^{h^{(k)}/2} (x_3^{(k)})^P \sigma_{ij}^{(k,l)} dx_3^{(k)} = \sum_{l=1}^{L^{(k)}} \left\{ \int_{\kappa^{(k,l-1)}}^{\kappa^{(k,l)}} (x_3^{(k)})^P \sigma_{ij}^{(k,l)} dx_3^{(k)} \right\} \quad (3.10)$$

where  $L^{(k)}$  is the total number of different material laminae the  $k^{\text{th}}$  layer comprises.  $\kappa^{(k,l)}$  and  $\kappa^{(k,l-1)}$ , respectively, denote  $x_3^{(k)}$  coordinate values at the upper and the lower surfaces of the  $l^{\text{th}}$  lamina in the  $k^{\text{th}}$  layer. Note that  $\kappa^{(k,L^{(k)})} = h^{(k)}/2$  and  $\kappa^{(k,0)} = -h^{(k)}/2$ .

Physically,  $M_{ij0}^{(k)}$  and  $M_{ij1}^{(k)}$  ( $i, j = 1, 2; i \leq j$ ) are the conventional force and moment resultants acted in the  $k^{\text{th}}$  layer, respectively. On the other hand,  $M_{i30}^{(k)}$  ( $i = 1, 2$ ) are the conventional transverse shear force resultants. Other quantities are higher-order resultants arising from the higher-order displacement series expansions.

Introducing Equation (3.7) into Equation (3.10), the following layer constitutive equations are obtained:

$$M_{ijP}^{(k)} = \sum_{l=1}^{L^{(k)}} \left\{ \int_{\kappa^{(k,l-1)}}^{\kappa^{(k,l)}} (x_3^{(k)})^P C_{ijmn}^{(k,l)} \varepsilon_{mn}^{(k)} dx_3^{(k)} \right\}$$

$$\begin{aligned}
&= \sum_{l=1}^{L^{(k)}} \left[ \int_{\kappa^{(k,l-1)}}^{\kappa^{(k,l)}} (x_3^{(k)})^P C_{ijmn}^{(k,l)} \left\{ (x_3^{(k)})^Q E_{mnQ}^{(k)} \right\} dx_3^{(k)} \right] \\
&= \sum_{l=1}^{L^{(k)}} \left\{ \int_{\kappa^{(k,l-1)}}^{\kappa^{(k,l)}} (x_3^{(k)})^{P+Q} C_{ijmn}^{(k,l)} dx_3^{(k)} \right\} E_{mnQ}^{(k)} = A_{ijmn PQ}^{(k)} E_{mnQ}^{(k)} \quad (3.11)
\end{aligned}$$

where the generalized rigidity coefficients  $A_{ijmn PQ}^{(k)}$  for the  $k^{\text{th}}$  layer can be explicitly calculated from the upper and the lower coordinate values and the reduced elastic coefficients of each lamina as the following:

$$\begin{aligned}
A_{ijmn PQ}^{(k)} &= \sum_{l=1}^{L^{(k)}} \left\{ \int_{\kappa^{(k,l-1)}}^{\kappa^{(k,l)}} (x_3^{(k)})^{P+Q} C_{ijmn}^{(k,l)} dx_3^{(k)} \right\} \\
&= \sum_{l=1}^{L^{(k)}} \left[ \frac{1}{P+Q+1} \left\{ (\kappa^{(k,l)})^{P+Q+1} - (\kappa^{(k,l-1)})^{P+Q+1} \right\} C_{ijmn}^{(k,l)} \right] \quad (3.12)
\end{aligned}$$

$A_{ijmn 00}^{(k)}$  and  $A_{ijmn 11}^{(k)}$  ( $i, j, m, n = 1, 2; i \leq j, m \leq n$ ) are, respectively, the membrane and the flexure rigidities of the  $k^{\text{th}}$  layer, while  $A_{ijmn 10}^{(k)}$ ,  $A_{ijmn 01}^{(k)}$  ( $i, j, m, n = 1, 2; i \leq j, m \leq n$ ) are the membrane-flexure coupling rigidities. On the other hand,  $A_{i3m3 00}^{(k)}$  ( $i, m = 1, 2$ ) are the transverse shear rigidities. Further higher-order rigidity coefficients are due to the higher-order displacement terms.

### 3.3.3 Assemblage of layers

After assuming the higher-order displacements in each layer, next comes assemblage of layers to form the entire laminate.

#### Generalized stress resultants of the entire laminate

The generalized stress resultants of the entire laminate  $M_{ij P}$  can be defined as follows:

$$\begin{aligned}
M_{ij P} &= \int_{-h/2}^{h/2} (x_3)^P \sigma_{ij} dx_3 \\
&= \sum_{k=1}^{NK} \int_{x_{3c}^{(k)} - h^{(k)}/2}^{x_{3c}^{(k)} + h^{(k)}/2} (x_3)^P \sigma_{ij} dx_3 \\
&= \sum_{k=1}^{NK} \int_{-h^{(k)}/2}^{h^{(k)}/2} (x_3^{(k)} + x_{3c}^{(k)})^P \sigma_{ij}^{(k)} dx_3^{(k)} \quad (3.13)
\end{aligned}$$

where  $x_3$  is the global coordinate measured from the middle plane of the laminate and  $h$  denotes the total thickness of the laminate.  $x_{3c}^{(k)}$  is the coordinate of the middle point of the  $k^{\text{th}}$  layer and  $x_3 = x_3^{(k)} + x_{3c}^{(k)}$ .

The relations between the stress resultants of the entire laminate in Equation (3.13) and those of each layer given in Equation (3.10) are, for instance,

$$\begin{aligned}
 P = 0 : M_{ij0} &= \sum_{k=1}^{NK} \int_{-h^{(k)}/2}^{h^{(k)}/2} \sigma_{ij}^{(k)} dx_3^{(k)} = \sum_{k=1}^{NK} M_{ij0}^{(k)} \\
 P = 1 : M_{ij1} &= \sum_{k=1}^{NK} \int_{-h^{(k)}/2}^{h^{(k)}/2} (x_3^{(k)} + x_{3c}^{(k)}) \sigma_{ij}^{(k)} dx_3^{(k)} \\
 &= \sum_{k=1}^{NK} (M_{ij1}^{(k)} + x_{3c}^{(k)} M_{ij0}^{(k)}) \\
 P = 2 : M_{ij2} &= \sum_{k=1}^{NK} \int_{-h^{(k)}/2}^{h^{(k)}/2} (x_3^{(k)} + x_{3c}^{(k)})^2 \sigma_{ij}^{(k)} dx_3^{(k)} \\
 &= \sum_{k=1}^{NK} (M_{ij2}^{(k)} + 2x_{3c}^{(k)} M_{ij1}^{(k)} + (x_{3c}^{(k)})^2 M_{ij0}^{(k)})
 \end{aligned} \tag{3.14}$$

and so forth.

### Constraint conditions at layer interfaces

Constraint conditions to be taken into account at the interfaces between the adjacent layers are as the followings,

- (a) Displacement continuities. The displacement continuity constraints at the perfectly adhered interfaces between the  $k^{\text{th}}$  and the  $(k+1)^{\text{th}}$  layers are given as follows:

$$\begin{aligned}
 g_i^{(k)}(x_1, x_2) &= u_i^{(k+1)}\left(x_1, x_2, \frac{-h^{(k+1)}}{2}\right) - u_i^{(k)}\left(x_1, x_2, \frac{h^{(k+1)}}{2}\right) \\
 &= \left(\frac{-h^{(k+1)}}{2}\right)^P U_{iP}^{(k+1)}(x_1, x_2) - \left(\frac{h^{(k)}}{2}\right)^P U_{iP}^{(k)}(x_1, x_2) = 0 \\
 &\quad (i = 1, 2, 3 \text{ and } P = 0, 1, 2, \dots, \max(N_i^{(k)}, N_i^{(k+1)})) \tag{3.15}
 \end{aligned}$$

- (b) Transverse stress continuities and/or transverse strain discontinuities at the interfaces between the adjacent dissimilar material laminae.
- (c) As special cases of interface constraints, traction-free and equilibrium conditions on the exterior surfaces.



In particular, the displacement continuities are indispensable for the present layerwise theory. The three different approaches for introducing the displacement continuities into the formulation are considered herein,

- **Direct elimination method** — In this method, the displacement assumptions described in Equation (3.1) are revised by introducing Equation (3.15) so as to enforce the displacement continuities at the layer interfaces *a priori*. This is the most straightforward and robust method and quite effective for a certain case, e.g., sandwich composites. Kimpura *et al.*<sup>99</sup> proposed sandwich-type finite elements which assume the classical plate displacements for the upper and the lower skin layers and the higher-order displacements for the core layer with the aid of this direct elimination method.

This method is efficient in computational expense because displacement unknowns are decreased in number during the elimination process. Besides the governing equations are derived from the standard displacement-based energy principle, and hence this method is free from such spurious energy modes as sometimes become a problem in stress-based or mixed hybrid energy principles.

On the other hand, revised displacement assumptions become meaninglessly complicated as the number of layers and the order of displacements increase. Therefore, this method can be only applicable to at most three-layered laminates like sandwich composites. It should be noted that this method does not consider the transverse stress continuities at the layer interfaces and hence stress recalculations via the 3-D equilibrium equations are required for transverse and interlaminar stress evaluations.

- **Lagrange multiplier** — This is a more general method than the elimination method for enforcing the displacement continuities. As well-known, in this method the displacement continuity constraints in Equation (3.15) are introduced into the formulation via additional non-displacement unknowns, Lagrange multipliers. Man<sup>80</sup> used the Lagrange multipliers for his layerwise FOSDT theory. Wu *et al.*<sup>87, 88</sup> also proposed a layerwise higher-order theory and its finite element approximation with the displacement continuities at the layer interfaces satisfied via Lagrange multipliers. Furthermore, Wu *et al.*<sup>90</sup> also developed a finite element which includes the transverse stress continuities at the interfaces and the traction-free conditions on the surfaces by similarly using the multipliers. It should be noted that physically the multipliers stand for pointwise transverse stresses at the interface, i.e., interlaminar stresses, when they are used for achieving the displacement continuities. This is one of the most profitable advantages

of the multipliers because, even in the case that intralaminar stresses are poorly evaluated, there is a possibility that interlaminar stresses are precisely predicted as a result of the layer equilibriums of force resultants.

On the other hand, the multiplier method gives rise to additional unknowns to be solved for each layer, which leads to computational difficulty as the number of layers increases.

- **The penalty method** — This method is a specific approximation of Lagrange multiplier. Ascione and Fraternali<sup>100</sup> constructed their curved composite beam model in which the displacement continuities at the layer interfaces are approximated via the penalty method. Soon after that, Fraternali and Reddy<sup>101</sup> proposed a layerwise curved shell theory and its finite element approximation similarly using the penalty method for achieving the displacement continuity at the interfaces. As pointed out in some precedent studies, adopting the penalty method has several advantage over Lagrange multipliers, and one of them is that there are no extra, non-displacement unknown variables adding to the formulation like the multipliers.

The other interface constraints than that of displacement can be certainly introduced in the formulations in such a way as Lagrange multipliers or the penalty method. However, in a practical point of view, they can be neglected because they do not play a significant role in structural responses and strength even though they might become important in numerical models for localized regions of a structure.

### 3.3.4 Governing equations — in case of the penalty method

Finally, the governing equations for a laminate are derived herein. The governing equations for elimination-type theories can not be described in a general form because the displacement unknowns can vary in each case. However, they can be easily obtained from the standard displacement-based energy principle. Therefore, only the governing equations via the penalty method is presented herein.

The modified potential energy functional with displacement continuities relaxed at layer interfaces is expressed as the following form:

$$\Pi'_{mp} = \Pi_p + \mathcal{H} \quad (3.16)$$

where  $\Pi_p$  is the potential energy in the system obtained by summing the potential

energy of all of the layers with no constraints at the layer interfaces as the following:

$$\begin{aligned}\Pi_p &= \sum_{k=1}^{NK} \iint_{\Omega} \int_{-h^{(k)}/2}^{h^{(k)}/2} \frac{\sigma_{ij}^{(k,l)} \varepsilon_{ij}^{(k)}}{2} dx_3^{(k)} d\Omega - \iint_{\Omega} T_i \bar{u}_i d\Omega \\ &= \sum_{k=1}^{NK} \iint_{\Omega} \frac{M_{ij}^{(k)} E_{ij}^{(k)}}{2} d\Omega - \iint_{\Omega} T_i \bar{u}_i d\Omega\end{aligned}\quad (3.17)$$

where  $T_i$  and  $\bar{u}_i$  ( $i = 1, 2, 3$ ), respectively, denote mechanical and geometrical boundary conditions on the upper and lower exterior surface of the laminate.

On the other hand,  $\mathcal{H}$  is the auxiliary energy term due to interfacial displacement constrains, and it can be described as follows:

$$\mathcal{H} = \sum_{k=1}^{NK-1} \iint_{\Omega} \frac{\lambda_i^{(k)} g_i^{(k)}}{2} d\Omega \quad (3.18)$$

In Lagrange-multiplier formulation,  $\lambda_i^{(k)}$  and  $g_i^{(k)}$  are independent of each other and  $\lambda_i^{(k)}$  also stand for unknown primary variables. In the penalty method, on the other hand,  $\lambda_i^{(k)}$  are described such that

$$\lambda_i^{(k)} = \alpha_i^{(k)} g_i^{(k)} \quad (3.19)$$

$\alpha_i^{(k)}$  are positive and called the penalty numbers<sup>102, 103, 104</sup>. Reciprocals of  $\alpha_i^{(k)}$  are also called the penalty parameters. When each  $\alpha_i^{(k)}$  is set infinite, then the displacement continuity conditions in Equation (3.15) are strictly satisfied and the auxiliary energy term  $\mathcal{H}$  vanishes.

$$\alpha_i^{(k)} \rightarrow \infty \Rightarrow g_i^{(k)} \rightarrow 0, \quad \mathcal{H} \rightarrow 0 \quad (3.20)$$

Furthermore, the penalty numbers are also explained as very stiff spring constants in the normal and tangential directions which are scattered on the interfaces between layers. This physical meaning of the penalty numbers is schematically illustrated in Figure 3.4. Note that transverse stresses  $\lambda_i^{(k)}$  at the interface between the  $k^{\text{th}}$  and the  $(k+1)^{\text{th}}$  layers (interlaminar stresses) can be directly evaluated as the reactions of these springs from Equation (3.19). It is also noted that when  $\alpha_i^{(k)}$  is set infinitely large then  $\lambda_i^{(k)}$  become identical to Lagrange multipliers.

Finally, the governing equations in the system are obtained by taking the first variation of the present modified potential functional with penalty numbers as the following:

$$\delta \Pi'_{mp} = 0 \quad (3.21)$$



Considering Equations (3.4) through (3.6) and (3.15),

$$\begin{aligned}
 \delta \Pi'_{mp} &= \sum_{k=1}^{NK} \iint_{\Omega} M_{ij}^{(k)} \delta E_{ij}^{(k)} d\Omega - \iint_{\Omega} T_i \delta \bar{u}_i d\Omega + \sum_{k=1}^{NK-1} \iint_{\Omega} \lambda_i^{(k)} \delta g_i^{(k)} d\Omega \\
 &= \sum_{k=1}^{NK} \iint_{\Omega} \left\{ M_{11P}^{(k)} \frac{\partial \delta U_{1P}^{(k)}}{\partial x_1} + M_{12P}^{(k)} \frac{\partial \delta U_{1P}^{(k)}}{\partial x_2} + (P+1) M_{13P}^{(k)} \delta U_{1P+1}^{(k)} + \right. \\
 &\quad M_{22P}^{(k)} \frac{\partial \delta U_{2P}^{(k)}}{\partial x_2} + M_{12P}^{(k)} \frac{\partial \delta U_{2P}^{(k)}}{\partial x_1} + (P+1) M_{23P}^{(k)} \delta U_{2P+1}^{(k)} + \\
 &\quad M_{13P}^{(k)} \frac{\partial \delta U_{3P}^{(k)}}{\partial x_1} + M_{23P}^{(k)} \frac{\partial \delta U_{3P}^{(k)}}{\partial x_2} + P M_{33P}^{(k)} \delta U_{3P}^{(k)} \left. \right\} d\Omega \\
 &\quad - \sum_{k=1}^{NK} \iint_{\Omega} \left\{ \lambda_1^{(k)} \left( \frac{h^{(k)}}{2} \right)^P \delta U_{1P}^{(k)} - \lambda_1^{(k-1)} \left( -\frac{h^{(k)}}{2} \right)^P \delta U_{1P}^{(k)} + \right. \\
 &\quad \lambda_2^{(k)} \left( \frac{h^{(k)}}{2} \right)^P \delta U_{2P}^{(k)} - \lambda_2^{(k-1)} \left( -\frac{h^{(k)}}{2} \right)^P \delta U_{2P}^{(k)} + \\
 &\quad \left. \lambda_3^{(k)} \left( \frac{h^{(k)}}{2} \right)^P \delta U_{3P}^{(k)} - \lambda_3^{(k-1)} \left( -\frac{h^{(k)}}{2} \right)^P \delta U_{3P}^{(k)} \right\} d\Omega \\
 &= 0
 \end{aligned} \tag{3.22}$$

in which

$$\lambda_i^{(k)} = \alpha_i^{(k)} g_i^{(k)} \quad (k = 1, 2, \dots, NK-1)$$

$$\lambda_i^{(0)} = T_i^{(0)}, \quad \lambda_i^{(NK)} = T_i^{(NK)}$$

where  $T_i^{(0)}$  and  $T_i^{(NK)}$  are the tractions applied to the lower and upper surfaces of the laminate, respectively.

Taking the integral by parts and collecting the terms with respect to primary displacement variables, the following Euler-Lagrange equations are deduced.

$$\left. \begin{aligned}
 \delta U_{1P}^{(k)} : \quad & \frac{\partial M_{11P}^{(k)}}{\partial x_1} + \frac{\partial M_{12P}^{(k)}}{\partial x_2} - P M_{13P}^{(k)} - \left( \frac{-h^{(k)}}{2} \right)^P \lambda_1^{(k-1)} + \left( \frac{h^{(k)}}{2} \right)^P \lambda_1^{(k)} = 0 \\
 \delta U_{2P}^{(k)} : \quad & \frac{\partial M_{22P}^{(k)}}{\partial x_2} + \frac{\partial M_{12P}^{(k)}}{\partial x_1} - P M_{23P}^{(k)} - \left( \frac{-h^{(k)}}{2} \right)^P \lambda_2^{(k-1)} + \left( \frac{h^{(k)}}{2} \right)^P \lambda_2^{(k)} = 0 \\
 \delta U_{3P}^{(k)} : \quad & \frac{\partial M_{13P}^{(k)}}{\partial x_1} + \frac{\partial M_{23P}^{(k)}}{\partial x_2} - P M_{33P}^{(k)} - \left( \frac{-h^{(k)}}{2} \right)^P \lambda_3^{(k-1)} + \left( \frac{h^{(k)}}{2} \right)^P \lambda_3^{(k)} = 0
 \end{aligned} \right\} \tag{3.23}$$



and the admissible boundary conditions are

$$\text{essential : } \begin{cases} U_{1P}^{(k)} \\ U_{2P}^{(k)} \\ U_{3P}^{(k)} \end{cases} \quad \text{natural : } \begin{cases} M_{11P}^{(k)} n_1 + M_{12P}^{(k)} n_2 \\ M_{12P}^{(k)} n_1 + M_{22P}^{(k)} n_2 \\ M_{13P}^{(k)} n_1 + M_{23P}^{(k)} n_2 \end{cases}$$

where  $n_1$  and  $n_2$  are the direction cosines of a unit normal to the boundary of the middle plane  $\Gamma$ .

### 3.4 Numerical modeling methodology

In the previous section, a general theory for composite laminates are proposed based on the layerwise higher-order displacement assumptions and a few possible ways for introducing interfacial displacement continuity conditions.

In the present general theory, there are three possible choices undetermined, that is,

- layer discretization scheme — coarse ML, natural ML or fine ML;
- orders of terminations of higher-order displacement assumptions — lower like FOSDT or higher such as (332);
- interfacial displacement continuity constraints representations — the direct elimination method or the penalty method.

In Figure 3.5, possible numerical models are charted with respect to the order of deformation assumptions and the order of layer discretization. As for the interfacial constraints, as the number of layers is small and order of displacement assumptions is low, the direct elimination method becomes more applicable and attracting.

In the conventional numerical models, all of these have been determined *a priori*, but in the present modeling, these are individually determined corresponding to the actual analysis demand. In some cases, ESL-based first-order terminations will be enough, while in other cases such as evaluations of interlaminar stress singularity, extremely fine layer discretizations and higher-order terminations might be required.

In order to establish an efficient numerical analysis and design for composite laminates, the most important task is to arrange an appropriate specific model to each individual problem. Hence in the present study, the numerical modeling methodology are proposed in Table 3.1.

The spirit of the proposed methodology is that, since the laminate-like, through-the-thickness inhomogeneity of composite laminates plays a dominant role in numerical modeling accuracy, the numerical model is supposed to be determined in accordance with the inhomogeneity levels of the problem.

For instance, when global responses of the entire laminated structure are of primary interest, ESL models like  $[(110)]$  or  $[(330)]$  serve as the most appropriate model. In the case that Laminate-like Phase can not be neglected, such as in sandwich structures and delaminated plates, coarse ML models like  $[(110)(110)]^{(Direct)}$ ,  $[(110)(111)(110)]^{(Direct)}$  or  $[(331)(332)(331)]^{(Direct)}$  will be required. On the other hand, when one wishes to evaluate localized quantities such as interlaminar stresses, fine ML and higher-order models like  $[(332)^{NK}]^{(Penalty)}$  will be available.

### 3.5 Summary

In this chapter, a general and versatile displacement-based theory which is based on the layerwise higher-order displacement assumptions were proposed. The present theory identifies itself from the previous similar theories by the following features:

1. the number of discretized layers is independent of the number of the actual laminae.
2. the orders of polynomial series of displacements assumed for each layer can be different from each other.
3. displacement continuity requirements at the layer interfaces are included by using either the direct elimination method or the penalty method as a specific approximation of Lagrange multiplier.

After the formulation of the general theory for composite laminates were given, a flexible and versatile numerical modeling methodology for composite laminates were proposed in accordance with the level of inhomogeneity.

The proposed methodology is inherently inductive and hence its validity should be confirmed through actual numerical applications step by step. Hence in the next chapter and after, some typical cases of finite element approximations deduced from the proposed theory will be presented for the purpose of showing the validity of the proposed general theory and methodology.



Figure 3.1 Progressional history of numerical models for composite laminates

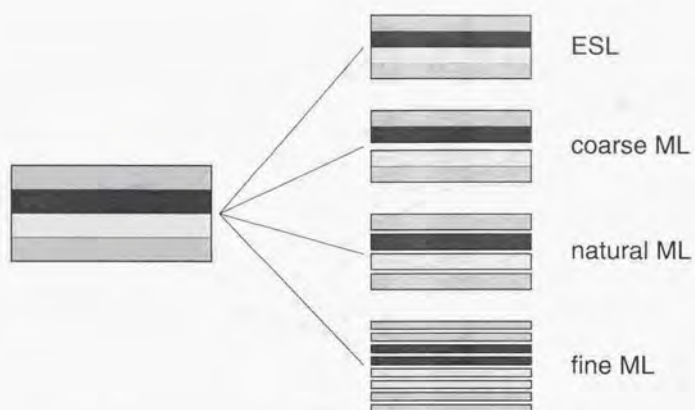
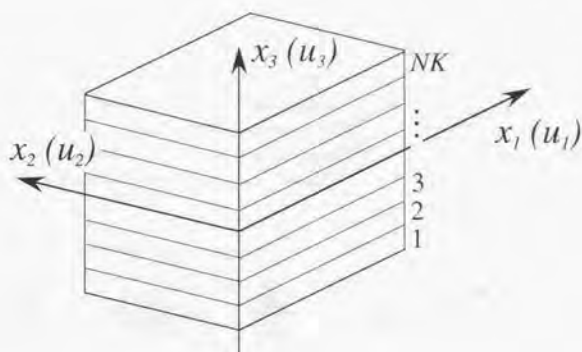
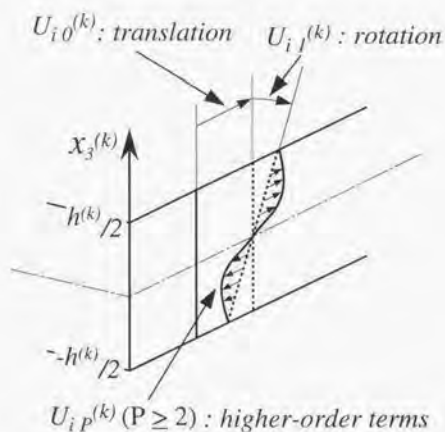


Figure 3.2 Schematics of various multi-layer discretization schemes





(a) Geometry and coordinate system



(b) Deformation of the layer 'k'

**Figure 3.3** Coordinate system and geometry of a laminate, and higher-order deformation of the  $k^{\text{th}}$  layer

- (a) coordinate system and geometry of a laminate;  
 (b) higher-order deformations in the  $k^{\text{th}}$  layer

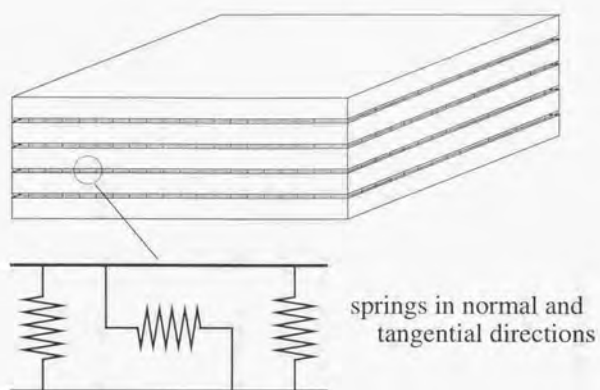


**Figure 3.4** Physical meaning of the penalty number — springs attached on the layer interfaces



**Figure 3.5** A schematic chart of possible combinations of deformation assumptions and layer discretizations

**Table 3.1** Possible numerical models for various levels of inhomogeneity of composite laminates

inhomogeneity levels	possible numerical models	examples
Structural Member	$[(110)], [(330)], [(332)]$	general laminates
	$[(110)(111)(110)]^{(D)}$ $[(331)(332)(331)]^{(D)}$	sandwiches
	$[(110)(111) \dots (110)]^{(D)}$ $[(330)(221) \dots (330)]^{(D)}$	hybrid laminates
Laminate-like	$[(110)(110)]^{(P)}$ $[(332)(332)]^{(P)}$	delamination
	$[(110)^{NK}]^{(P)}$ $[(332)^{NK}]^{(P)}$	CAI
Continuum	$[(332)^{NK}]^{(P)}$	interlaminar stress
Structural+Laminate-like	$[(110)^{NK}]^{(P)}, [(332)^{NK}]^{(P)}$	joint with overlays



## Chapter 4

### Selective Layerwise Sandwich Element

## 4.1 Introduction to this chapter

In this chapter, as the first example of the layerwise higher-order model of the author, [(110)(111)(110)] selective layerwise sandwich element is to be presented.

High-performance sandwich structures are becoming a primary structural component in a variety of industrial fields such as aviation, aerospace, marine engineering like America's Cup yacht, leisure and sports like skiing and so forth. A sandwich-type plate is composed of three layers, i.e., the upper and lower skins and the core. The upper and lower skin layers usually very thin but very stiff compared to the core layer. This fact leads to a suspicion of multi-layer (ML) deformations through the thickness as illustrated in Figure 4.1 and then tabulated in Table 4.1. Apparently ESL-based models like CLT and FOSDT are not applicable to thick and soft-core sandwich structures, as the author *et al.*<sup>105</sup> reported, and hence a numerical model considering inhomogeneity through the laminate thickness, that is, a layerwise model is indispensable for the analysis of sandwich structures. The conventional layerwise theories and their FEs, however, assume the same displacement field in each layer, in spite of the fact that the mechanical properties of the faces and the core are quite different from each other, and accordingly they are not necessarily of practical use for the actual sandwich constructions, even though they are very refined. On the other hand, since the work of Reissner<sup>106</sup>, various field equations are derived from energy principles with appropriate restrictive assumptions on the constitutions of faces and a core in the sandwich constructions in the literature. They treat a sandwich construction in a selective layerwise manner as shown in Figure 4.2, because they knew such a treatment of sandwiches is essential. For instance, Kimpara *et al.*<sup>99</sup> had proposed a selective layerwise sandwich FE in which CLT and HOT of order 1 (111) are assumed for the skin surfaces and the core, respectively. In Table 4.2, estimated accuracy of numerical models mentioned above is summarized.

The present finite element can be regarded as an extension of Kimpara's selective layerwise sandwich model; That is, the first-order shear deformation theory (FOSDT) is adopted for the faces, while HOT1 (111) is adopted for the core. The displacement continuity requirements at the face/core interfaces are included via "the direct elimination method", and then the displacements of the core are expressed in terms of those of the faces. In finite element approximation, an eight-node quadratical  $C^0$  isoparametric element is employed. The accuracy and then the superiority over the conventional theories of the developed element are ensured by comparing the present and the other analytical results to the detailed 3-D continuum solid FE solution in the case of bending of simply-supported square sandwich plate. Furthermore, by com-

paring the present results with the experiments in the case of a clamped sandwich panel subjected to hydraulic pressure, the practicability of the developed element is also validated.

## 4.2 Finite element approximation

In this section, [(110)(111)(110)] selective layerwise sandwich element will be formulated.

### 4.2.1 [(110)(111)(110)] assumptions

The geometric configuration of a sandwich plate construction is illustrated in Figure 4.3.

**Deformation series termination** The present theory uses displacement assumptions of a kind of the layerwise HOTs. However, the different degrees of freedom are selected for the faces and the core, respectively, because the material properties and the thickness of them are totally different from each other. The displacement power series in Equation (3.1) are truncated as follows:

For the core, the displacement assumption of order 1 (HOT1; (111)) is adopted such that,

$$\left. \begin{aligned} u^{CR}(x, y, z^{CR}) &= U_0^{CR}(x, y) + z^{CR} U_1^{CR}(x, y) \\ v^{CR}(x, y, z^{CR}) &= V_0^{CR}(x, y) + z^{CR} V_1^{CR}(x, y) \\ w^{CR}(x, y, z^{CR}) &= W_0^{CR}(x, y) + z^{CR} W_1^{CR}(x, y) \end{aligned} \right\} \text{ for } -\frac{h^{CR}}{2} \leq z^{CR} \leq \frac{h^{CR}}{2} \quad (4.1)$$

where the superscript 'CR' denotes the core. Note that  $W_1^{CR}$  represents the elongation of a transverse normal.

For the upper and lower faces, because of their thinner thickness than that of the core, the displacement assumption of the first-order shear deformation theory (FOSDT; (110)) is adopted as,

$$\left. \begin{aligned} u^{*F}(x, y, z^{*F}) &= U_0^{*F}(x, y) + z^{*F} U_1^{*F}(x, y) \\ v^{*F}(x, y, z^{*F}) &= V_0^{*F}(x, y) + z^{*F} V_1^{*F}(x, y) \\ w^{*F}(x, y, z^{*F}) &= W_0^{*F}(x, y) \end{aligned} \right\} \text{ for } -\frac{h^{*F}}{2} \leq z^{*F} \leq \frac{h^{*F}}{2} \quad (4.2)$$

in which the superscript '\*F' implies the upper face 'UF' or the lower face 'LF'.

Displacement continuities — via the direct elimination method The displacement continuity constraints in Equation (3.15) between the faces and the core are given as

$$\left. \begin{aligned} g_x^{UF/CR}(x, y) &= u^{UF}\left(x, y, -\frac{h^{UF}}{2}\right) - u^{CR}\left(x, y, \frac{h^{CR}}{2}\right) \\ &= U_0^{UF} - \frac{h^{UF}}{2}U_1^{UF} - U_0^{CR} - \frac{h^{CR}}{2}U_1^{CR} = 0 \\ g_y^{UF/CR}(x, y) &= v^{UF}\left(x, y, -\frac{h^{UF}}{2}\right) - v^{CR}\left(x, y, \frac{h^{CR}}{2}\right) \\ &= V_0^{UF} - \frac{h^{UF}}{2}V_1^{UF} - V_0^{CR} - \frac{h^{CR}}{2}V_1^{CR} = 0 \\ g_z^{UF/CR}(x, y) &= w^{UF}\left(x, y, -\frac{h^{UF}}{2}\right) - w^{CR}\left(x, y, \frac{h^{CR}}{2}\right) \\ &= W_0^{UF} - W_0^{CR} - \frac{h^{CR}}{2}W_1^{CR} = 0 \end{aligned} \right\} \quad (4.3)$$

$$\left. \begin{aligned} g_x^{CR/LF}(x, y) &= u^{CR}\left(x, y, -\frac{h^{CR}}{2}\right) - u^{LF}\left(x, y, \frac{h^{LF}}{2}\right) \\ &= U_0^{CR} - \frac{h^{CR}}{2}U_1^{CR} - U_0^{LF} - \frac{h^{LF}}{2}U_1^{LF} = 0 \\ g_y^{CR/LF}(x, y) &= v^{CR}\left(x, y, -\frac{h^{CR}}{2}\right) - v^{LF}\left(x, y, \frac{h^{LF}}{2}\right) \\ &= V_0^{CR} - \frac{h^{CR}}{2}V_1^{CR} - V_0^{LF} - \frac{h^{LF}}{2}V_1^{LF} = 0 \\ g_z^{CR/LF}(x, y) &= w^{CR}\left(x, y, -\frac{h^{CR}}{2}\right) - w^{LF}\left(x, y, \frac{h^{LF}}{2}\right) \\ &= W_0^{CR} - \frac{h^{CR}}{2}W_1^{CR} - W_0^{LF} = 0 \end{aligned} \right\} \quad (4.4)$$

From Equations (4.3) and (4.4), the core displacement unknowns are found to be



completely expressed in terms of those of the faces as follows,

$$\left. \begin{aligned} U_0^{CR} &= \frac{U_0^{UF} + U_0^{LF}}{2} - \frac{h^{UF} U_1^{UF} - h^{LF} U_1^{LF}}{4} \\ U_1^{CR} &= \frac{1}{h^{CR}} \left\{ \left( U_0^{UF} - U_0^{LF} \right) - \frac{h^{UF} U_1^{UF} + h^{LF} U_1^{LF}}{2} \right\} \\ V_0^{CR} &= \frac{V_0^{UF} + V_0^{LF}}{2} - \frac{h^{UF} V_1^{UF} - h^{LF} V_1^{LF}}{4} \\ V_1^{CR} &= \frac{1}{h^{CR}} \left\{ \left( V_0^{UF} - V_0^{LF} \right) - \frac{h^{UF} V_1^{UF} + h^{LF} V_1^{LF}}{2} \right\} \\ W_0^{CR} &= \frac{W_0^{UF} + W_0^{LF}}{2}, \quad W_1^{CR} = \frac{W_0^{UF} - W_0^{LF}}{h^{CR}} \end{aligned} \right\} \quad (4.5)$$

and the number of the unknown displacement variables is reduced to 10.

Thus, the generalized displacement vector is defined as follows,

$$[\delta]^T = \{U_0^{UF} \ V_0^{UF} \ W_0^{UF} \ U_1^{UF} \ V_1^{UF} \ U_0^{LF} \ V_0^{LF} \ W_0^{LF} \ U_1^{LF} \ V_1^{LF}\} \quad (4.6)$$

**Strain-displacement relations** Based on small deformation elasticity, the strain-displacement relations are then given as:

For the core;

$$\left. \begin{aligned} \varepsilon_x^{CR} &= E_{x0}^{CR} + z^{CR} E_{x1}^{CR} \\ \varepsilon_y^{CR} &= E_{y0}^{CR} + z^{CR} E_{y1}^{CR} \\ \varepsilon_z^{CR} &= E_{z0}^{CR} \\ \gamma_{yz}^{CR} &= E_{yz0}^{CR} + z^{CR} E_{yz1}^{CR} \\ \gamma_{zx}^{CR} &= E_{zx0}^{CR} + z^{CR} E_{zx1}^{CR} \\ \gamma_{xy}^{CR} &= E_{xy0}^{CR} + z^{CR} E_{xy1}^{CR} \end{aligned} \right\} \quad (4.7)$$

in which

$$\left. \begin{aligned}
 E_{x0}^{CR} &= \frac{\partial}{\partial x} \left( \frac{U_0^{UF} + U_0^{LF}}{2} - \frac{h^{UF} U_1^{UF} - h^{LF} U_1^{LF}}{4} \right) \\
 E_{x1}^{CR} &= \frac{\partial}{\partial x} \left( \frac{U_0^{UF} - U_0^{LF}}{h^{CR}} - \frac{h^{UF} U_1^{UF} + h^{LF} U_1^{LF}}{2h^{CR}} \right) \\
 E_{y0}^{CR} &= \frac{\partial}{\partial y} \left( \frac{V_0^{UF} + V_0^{LF}}{2} - \frac{h^{UF} V_1^{UF} - h^{LF} V_1^{LF}}{4} \right) \\
 E_{y1}^{CR} &= \frac{\partial}{\partial y} \left( \frac{V_0^{UF} - V_0^{LF}}{h^{CR}} - \frac{h^{UF} V_1^{UF} + h^{LF} V_1^{LF}}{2h^{CR}} \right) \\
 E_{z0}^{CR} &= \frac{W_0^{UF} - W_0^{LF}}{h^{CR}} \\
 E_{yz0}^{CR} &= \frac{V_0^{UF} - V_0^{LF}}{h^{CR}} - \frac{h^{UF} V_1^{UF} + h^{LF} V_1^{LF}}{2h^{CR}} + \frac{\partial}{\partial y} \left( \frac{W_0^{UF} + W_0^{LF}}{2} \right) \\
 E_{yz1}^{CR} &= \frac{\partial}{\partial y} \left( \frac{W_0^{UF} - W_0^{LF}}{h^{CR}} \right) \\
 E_{zx0}^{CR} &= \frac{U_0^{UF} - U_0^{LF}}{h^{CR}} - \frac{h^{UF} U_1^{UF} + h^{LF} U_1^{LF}}{2h^{CR}} + \frac{\partial}{\partial x} \left( \frac{W_0^{UF} + W_0^{LF}}{2} \right) \\
 E_{zx1}^{CR} &= \frac{\partial}{\partial x} \left( \frac{W_0^{UF} - W_0^{LF}}{h^{CR}} \right) \\
 E_{xy0}^{CR} &= \frac{\partial}{\partial x} \left( \frac{V_0^{UF} + V_0^{LF}}{2} - \frac{h^{UF} V_1^{UF} - h^{LF} V_1^{LF}}{4} \right) \\
 &\quad + \frac{\partial}{\partial y} \left( \frac{U_0^{UF} + U_0^{LF}}{2} - \frac{h^{UF} U_1^{UF} - h^{LF} U_1^{LF}}{4} \right) \\
 E_{xy1}^{CR} &= \frac{\partial}{\partial x} \left( \frac{V_0^{UF} - V_0^{LF}}{h^{CR}} - \frac{h^{UF} V_1^{UF} + h^{LF} V_1^{LF}}{2h^{CR}} \right) \\
 &\quad + \frac{\partial}{\partial y} \left( \frac{U_0^{UF} - U_0^{LF}}{h^{CR}} - \frac{h^{UF} U_1^{UF} + h^{LF} U_1^{LF}}{2h^{CR}} \right)
 \end{aligned} \right\} \quad (4.8)$$

For the upper or lower face;

$$\left. \begin{aligned} \varepsilon_x^{*F} &= E_{x0}^{*F} + z^{*F} E_{x1}^{*F} \\ \varepsilon_y^{*F} &= E_{y0}^{*F} + z^{*F} E_{y1}^{*F} \\ \varepsilon_z^{*F} &= 0 \\ \gamma_{yz}^{*F} &= E_{yz0}^{*F} \\ \gamma_{zx}^{*F} &= E_{zx0}^{*F} \\ \gamma_{xy}^{*F} &= E_{xy0}^{*F} + z^{*F} E_{xy1}^{*F} \end{aligned} \right\} \quad (4.9)$$

in which

$$\left. \begin{aligned} E_{x0}^{*F} &= \frac{\partial U_0^{*F}}{\partial x}, \quad E_{x1}^{*F} = \frac{\partial U_1^{*F}}{\partial x} \\ E_{y0}^{*F} &= \frac{\partial V_0^{*F}}{\partial y}, \quad E_{y1}^{*F} = \frac{\partial V_1^{*F}}{\partial y} \\ E_{xy0}^{*F} &= \frac{\partial U_0^{*F}}{\partial y} + \frac{\partial V_0^{*F}}{\partial x}, \quad E_{xy1}^{*F} = \frac{\partial U_1^{*F}}{\partial y} + \frac{\partial V_1^{*F}}{\partial x} \\ E_{yz0}^{*F} &= V_1^{*F} + \frac{\partial W_0^{*F}}{\partial y} \\ E_{zx0}^{*F} &= U_1^{*F} + \frac{\partial W_0^{*F}}{\partial x} \end{aligned} \right\} \quad (4.10)$$

The generalized strain vectors are defined as follows:

For the core;

$$\left. \begin{aligned} [\epsilon_{mb}^{CR}]^T &= \{E_{x0} \ E_{y0} \ E_{xy0} \ E_{x1} \ E_{y1} \ E_{xy1} \ E_{z0}\}^{CR} \\ [\epsilon_s^{CR}]^T &= \{E_{zx0} \ E_{yz0} \ E_{zx1} \ E_{yz1}\}^{CR} \end{aligned} \right\} \quad (4.11)$$

and for the faces;

$$\left. \begin{aligned} [\epsilon_{mb}^{*F}]^T &= \{E_{x0} \ E_{y0} \ E_{xy0} \ E_{x1} \ E_{y1} \ E_{xy1}\}^{*F} \\ [\epsilon_s^{*F}]^T &= \{E_{zx0} \ E_{yz0}\}^{*F} \end{aligned} \right\} \quad (4.12)$$

**Constitutive equations** The stress-strain relations can be written as follows:

For the core;

$$\begin{Bmatrix} \sigma_x \\ \sigma_y \\ \sigma_z \\ \tau_{yz} \\ \tau_{zx} \\ \tau_{xy} \end{Bmatrix}^{CR} = \begin{bmatrix} \bar{Q}_{11} & \bar{Q}_{12} & \bar{Q}_{13} & 0 & 0 & \bar{Q}_{16} \\ \bar{Q}_{12} & \bar{Q}_{22} & \bar{Q}_{23} & 0 & 0 & \bar{Q}_{26} \\ \bar{Q}_{13} & \bar{Q}_{23} & \bar{Q}_{33} & 0 & 0 & \bar{Q}_{36} \\ 0 & 0 & 0 & \bar{Q}_{44} & \bar{Q}_{45} & 0 \\ 0 & 0 & 0 & \bar{Q}_{45} & \bar{Q}_{55} & 0 \\ \bar{Q}_{16} & \bar{Q}_{26} & \bar{Q}_{36} & 0 & 0 & \bar{Q}_{66} \end{bmatrix}^{CR} \begin{Bmatrix} \varepsilon_x \\ \varepsilon_y \\ \varepsilon_z \\ \gamma_{yz} \\ \gamma_{zx} \\ \gamma_{xy} \end{Bmatrix}^{CR} \quad (4.13)$$

For  $l^{\text{th}}$  lamina in the upper or lower face (it should be noted that face layers themselves are usually laminates);

$$\begin{Bmatrix} \sigma_x \\ \sigma_y \\ \tau_{xy} \\ \tau_{zx} \\ \tau_{yz} \end{Bmatrix}^{(*F,l)} = \begin{bmatrix} \bar{Q}_{11} & \bar{Q}_{12} & \bar{Q}_{16} & 0 & 0 \\ \bar{Q}_{12} & \bar{Q}_{22} & \bar{Q}_{26} & 0 & 0 \\ \bar{Q}_{16} & \bar{Q}_{26} & \bar{Q}_{66} & 0 & 0 \\ 0 & 0 & 0 & k_x k_x \cdot \bar{Q}_{55} & k_x k_y \cdot \bar{Q}_{45} \\ 0 & 0 & 0 & k_x k_y \cdot \bar{Q}_{45} & k_y k_y \cdot \bar{Q}_{44} \end{bmatrix}^{(*F,l)} \begin{Bmatrix} \varepsilon_x \\ \varepsilon_y \\ \gamma_{xy} \\ \gamma_{zx} \\ \gamma_{yz} \end{Bmatrix}^{*F} \quad (4.14)$$

where  $\bar{Q}_{pq}^K$  ( $K = CR, (UF, l)$  or  $(LF, l)$ ;  $p, q = 1, 2, \dots, 6$ ) are the elastic coefficients of the stiffness matrix in the laminate geometrical axes and can be determined by using the transformation relation with the elastic coefficients of stiffness matrix  $Q_{pq}^K$  in the material principal axes.  $k_x, k_y$  are the shear correction factors and  $k_x k_x = k_y k_y = k_x k_y = 5/6$  is adopted in this study.

By integrating the stresses through the thickness of each of the three layers, the generalized stress resultant-generalized strain relations are obtained as:

$$\begin{Bmatrix} \mathbf{N} \\ \mathbf{Q} \end{Bmatrix}^K = \begin{bmatrix} \mathbf{D}_{mb} & \mathbf{0} \\ \mathbf{0} & \mathbf{D}_s \end{bmatrix}^K \begin{Bmatrix} \boldsymbol{\epsilon}_{mb} \\ \boldsymbol{\epsilon}_s \end{Bmatrix}^K \quad (4.15)$$

in which submatrices  $\mathbf{D}_{mb}^K$  and  $\mathbf{D}_s^K$  are, respectively, the membrane/flexure/transverse-normal rigidity matrix (the membrane/flexure rigidity matrix for the faces) and the transverse-shear rigidity matrix, and the generalized stress resultants are defined as follows:

For the core ( $K = CR$ ),

$$\left. \begin{aligned} [\mathbf{N}^{CR}]^T &= \int_{-h^{CR}/2}^{h^{CR}/2} \{ \sigma_x \sigma_y \tau_{xy} z \sigma_x z \sigma_y z \tau_{xy} \sigma_z \}^{CR} dz^{CR} \\ [\mathbf{Q}^{CR}]^T &= \int_{-h^{CR}/2}^{h^{CR}/2} \{ \tau_{zx} \tau_{yz} z \tau_{zx} z \tau_{yz} \}^{CR} dz^{CR} \end{aligned} \right\} \quad (4.16)$$

For the upper or lower face ( $K = *F$ ),

$$\left. \begin{aligned} [\mathbf{N}^{*F}]^T &= \int_{-h^{*F}/2}^{h^{*F}/2} \{ \sigma_x \sigma_y \tau_{xy} z \sigma_x z \sigma_y z \tau_{xy} \}^{*F} dz^{*F} \\ [\mathbf{Q}^{*F}]^T &= \int_{-h^{*F}/2}^{h^{*F}/2} \{ \tau_{zx} \tau_{yz} \}^{*F} dz^{*F} \end{aligned} \right\} \quad (4.17)$$



**Governing equation** The total potential energy is obtained by summing the contributions from the three layers as follows:

$$\Pi_p(\delta) = \Pi_p^{CR}(\delta) + \Pi_p^{UF}(\delta) + \Pi_p^{LF}(\delta) \quad (4.18)$$

where

$$\Pi_p^{CR}(\delta) = \iint_{\Omega} \frac{1}{2} ([N]^T \cdot \epsilon_{mb} + [Q]^T \cdot \epsilon_s)^{CR} d\Omega \quad (4.19)$$

and

$$\Pi_p^{*F}(\delta) = \iint_{\Omega} \frac{1}{2} ([N]^T \cdot \epsilon_{mb} + [Q]^T \cdot \epsilon_s)^{*F} d\Omega - \iint_{\Omega} ([T]^T \cdot \bar{u})^{*F} d\Omega \quad (4.20)$$

Finally, the governing equations can be obtained by taking the first order variation of the present potential energy functional with respect to the unknown displacement variables.

#### 4.2.2 Finite element discretization

In the present finite element formulation, the total domain of the considered sandwich plate is discretized into  $N_e$  elements such that:

$$\Pi_p(\delta) = \sum_{e=1}^{N_e} \Pi_p^{(e)}(\delta) = \sum_{e=1}^{N_e} [\Pi_p^{CR}(\delta) + \Pi_p^{UF}(\delta) + \Pi_p^{LF}(\delta)]^{(e)} \quad (4.21)$$

where  $\Pi_p^{(e)}(\delta) = [\Pi_p^{CR}(\delta) + \Pi_p^{UF}(\delta) + \Pi_p^{LF}(\delta)]^{(e)}$  are the total potential energy of the element.

Eight-node quadratical  $C^0$  isoparametric element is introduced in the present formulation. The nodal values of the two-dimensional geometry and the primary displacement variables are interpolated into the element as follows:

$$x = \sum_{J=1}^8 \Phi_J x_J, \quad y = \sum_{J=1}^8 \Phi_J y_J \quad (4.22)$$

$$\delta = \sum_{J=1}^8 \Phi_J \delta_J \quad (4.23)$$

whereas  $\Phi_J$ ;  $J = 1, 2, \dots, 8$  are the shape functions.

The generalized strain vectors  $\epsilon_{mb}^K$  and  $\epsilon_s^K$  ( $K = CR, UF, LF$ ) can be obtained by

$$\epsilon_{mb}^K = \sum_{J=1}^8 [B_{mb}^K]_J \delta_J, \quad \epsilon_s^K = \sum_{J=1}^8 [B_s^K]_J \delta_J \quad (4.24)$$

where  $[B_{mb}^K]_J$  and  $[B_s^K]_J$  are the so-called strain matrices, containing the shape functions and their derivatives.

Similarly the generalized stress resultant vectors can be obtained as

$$\mathbf{N}^K = \sum_{J=1}^8 [\mathbf{D}_{mb}^K \mathbf{B}_{mb}^K]_J \delta_J, \quad \mathbf{Q}^K = \sum_{J=1}^8 [\mathbf{D}_s^K \mathbf{B}_s^K]_J \delta_J \quad (4.25)$$

The element stiffness matrix is obtained by the minimization of the internal strain energy and is evaluated by summing up the contribution of the three layers as

$$\frac{\partial \Pi_p^{(e)}}{\partial \delta} = 0 \quad (4.26)$$

### 4.3 Numerical examples

Finite element calculations is conducted on DEC alpha 3000 model 800 with 128MB main core storage and double precision arithmetic is used. In order to avoid the so-called "shear locking", the reduced integration technique<sup>5</sup>, which means the  $2 \times 2$  Gauss rule is used for evaluating the stiffness matrix, in stead of the  $3 \times 3$  Gauss rule, is adopted for the portion of the faces. For the portion of the core, the normal integration (i.e. the  $3 \times 3$  Gauss rule) is adopted.

#### 4.3.1 Accuracy and convergence check

In order to assess the accuracy and convergence property of the developed element, comparative results are presented in the case of a simply-supported CFRP/honeycomb-core sandwich plate subjected to an uniformly distributed load over the whole area of the upper face surface as shown in Figure 4.4. The geometry and material data and applied load intensity for the numerical simulation are listed as follows:

for the entire sandwich plate;

$$l = 200 \text{ mm}, \quad h = 9.6 \text{ mm}, \quad q_0 = 1.0 \text{ MPa}$$

for the faces;

$$h^{UF} = h^{LF} = 0.8 \text{ mm}$$

$$E_x = 560 \text{ GPa}, \quad E_y = 560 \text{ GPa}, \quad \nu_{xy} = 0.0813$$

$$G_{xy} = 259 \text{ GPa}, \quad G_{yz} = 29.5 \text{ GPa}, \quad G_{zx} = 29.5 \text{ GPa}$$

and the core is assumed aluminum honeycomb characterized by the following properties,

$$h^{CR} = 8.0 \text{ mm}$$

$$\begin{aligned}E_x &= 0.51 \text{ GPa}, & E_y &= 0.63 \text{ GPa}, & E_z &= 14.1 \text{ GPa} \\ \nu_{xy} &= 0.830, & \nu_{yz} &= 0.0150, & \nu_{zx} &= 0.340 \\ G_{xy} &= 0.49 \text{ GPa}, & G_{yz} &= 2.46 \text{ GPa}, & G_{zx} &= 3.03 \text{ GPa}\end{aligned}$$

As a baseline for numerical accuracy, a detailed 3-D continuum solid model is also generated using the general purpose finite element package MARC (version k-5) with the use of 20-node isoparametric 3-D continuum solid elements with three translational degrees of freedom in each node, and due to the symmetry of the problem only one quadrant of the sandwich plate is considered. One layer of elements are used for modeling the faces, and three layers of elements are used for modeling the core layer of the sandwich plate. The total number of nodes in the 3-D solid FEM model is 15236, and the number of elements is 3125. Figure 4.5 shows wire-framed deformations of the sandwich plate obtained by the 3-D solid FE. At the same time, analytical solutions by CLT, FOSDT<sup>110</sup>, HOT of Reddy<sup>28</sup>, and the sandwich model of Allen<sup>111</sup> are also reproduced for comparison.

The variation of the central deflection against square mesh refinement is shown in Figure 4.6. It is observed that, as the degrees of freedom are increased in number, the present FE solutions are converging to the constant value 2 or 3% below the result by the detailed 3-D continuum solid FE. On the other hand, the other analytical models provide poor (too stiff) results.

Figure 4.7 illustrates the variations of deflection along the diagonal line. The very good agreements of the present FE solutions with those of the detailed 3-D continuum solid FE are observed again.

Finally, Figures 4.8 and 4.9 illustrate the through-the-thickness variations of the in-plane normal stresses  $\sigma_x$  and the transverse shear stresses  $\tau_{xz}$ , respectively. In Figure 4.8, the present FE solution is observed to be in good agreement with the 3-D continuum solid FE results. On the other hand, because FOSDT assumption was adopted for the upper and lower faces, the transverse shear stresses in Figure 4.9 are constant through the thickness in the faces and discontinuous at the interfaces.

#### 4.3.2 Comparison with experimental results

In order to illustrate the applicability of the developed element, next, a comparative study with experimental results is presented. The example is the case of a fully-clamped CFRP/Rohacell sandwich plate subjected to hydraulic pressure over the whole area of one side of surface as shown in Figures 4.10 and 4.11. The geometry and material

data for the numerical simulation are listed as follows:

for the faces;

$$h^{UF} = h^{LF} = 0.48 \text{ mm}$$

$$E_x = 4500 \text{ kgf/mm}^2, \quad E_y = 4300 \text{ kgf/mm}^2, \quad \nu_{xy} = 0.05$$

$$G_{xy} = 400 \text{ kgf/mm}^2, \quad G_{yz} = 400 \text{ kgf/mm}^2, \quad G_{zx} = 400 \text{ kgf/mm}^2$$

and for the core;

$$h^{CR} = 7.20 \text{ mm}$$

$$E_x = E_y = 10 \text{ kgf/mm}^2, \quad \nu_{xy} = 0.8, \quad E_z = 140 \text{ kgf/mm}^2$$

$$G_{xy} = 5 \text{ kgf/mm}^2, \quad G_{yz} = 21 \text{ kgf/mm}^2, \quad G_{zx} = 12 \text{ kgf/mm}^2$$

Figures 4.12 and 4.13 illustrate the variations of deflection and strain measures along the diagonal line, respectively. It is observed that the difference of the present FE solution from the experimental results is below 5%. It is important to note that, although FOSDT model also provides as much accurate results as the present FE, it is possible for the present FE to evaluate, if required, the quantities which FOSDT can not give, such as transverse stresses within the core.

## 4.4 Discussion

A very accurate FE model for sandwich plates is presented, based on the selective layerwise assumptions [(110)(111)(110)]. This model is more accurate than the ESL-based theories such as CLT, FOSDT. Both deflections and in-plane stresses are precisely predicted, while transverse shear stresses are also predicted to some extent in the middle-plane of each layer, without employing 3-D equilibrium equations. The developed FE has less degrees of freedom than those of the customary layerwise HOTs., therefore, is more applicable to global stress analysis for actual sandwich structures.

On the other hand, the present sandwich-type plate element employs the direct elimination method for introducing interfacial displacement continuities. This makes the finite element formulation complicated and skillful. Still more, transverse stresses can only be evaluated as a mean value of the actual distributions.



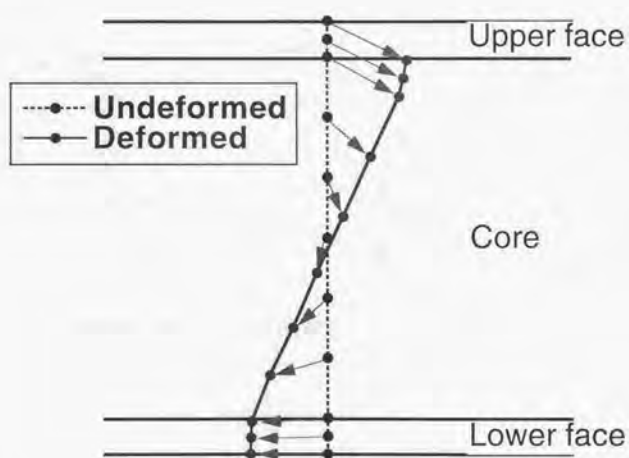
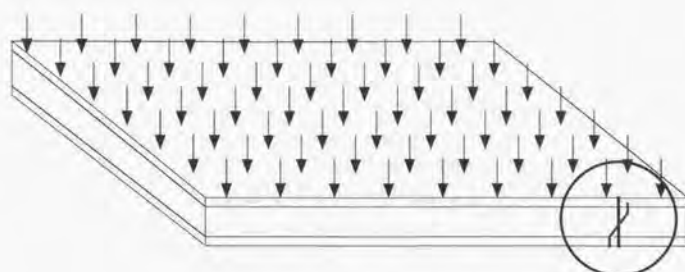


Figure 4.1 A schematic of deformations in a sandwich construction

Table 4.1 Characteristics of sandwich deformations

	Characteristics
common for both	Layerwise deformation Transverse normals before deformation remain straight
skin layers	Transverse normals are nearly inextensible Thin compared to core layer
core layer	Transverse normals are extensible Thick and soft compared to skin layers

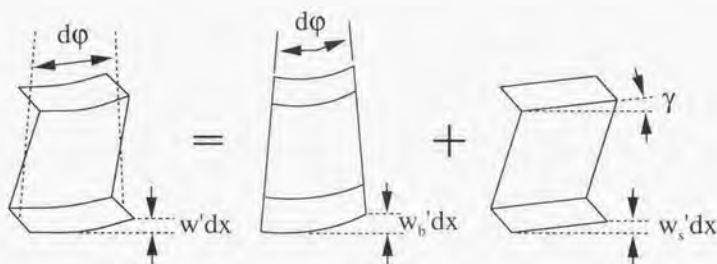
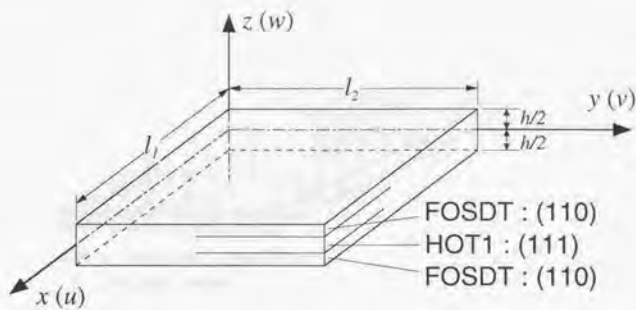


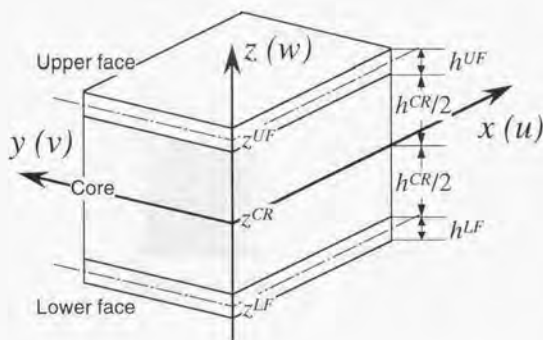
Figure 4.2 Selective layerwise considerations for a sandwich

Table 4.2 Estimated accuracy of various numerical models for sandwiches

Numerical models			accuracy	comments
ELS	CLT	—	×	inaccurate
	FOSDT	Yang <i>et al.</i>	△	
	HOT	Kant <i>et al.</i>	△	
Layerwise	[(FOSDT) <sup>3</sup> ]	Ferreira	△	excessive DOF
	[(HOT) <sup>3</sup> ]	Wu <i>et al.</i>	○	
Selective layerwise	[CLT/HOT <sub>1</sub> /CLT]	Kimpara	△	incompatible
	[FOSDT/HOT <sub>1</sub> /FOSDT]	<b>present</b>	?	



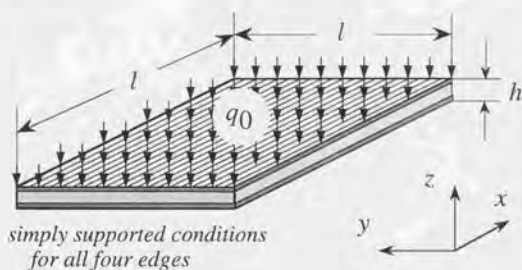
(a) geometry, coordinate and deformations



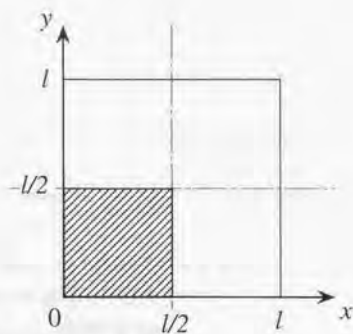
(b) through-the-thickness configurations

Figure 4.3 Sandwich plate element - geometry and displacement assumptions





(a) perspective of the problem

(b) top view of the plate  
- shaded quadrant was modeled**Figure 4.4** Schematics of a simply-supported square sandwich plate subjected to uniform lateral pressure

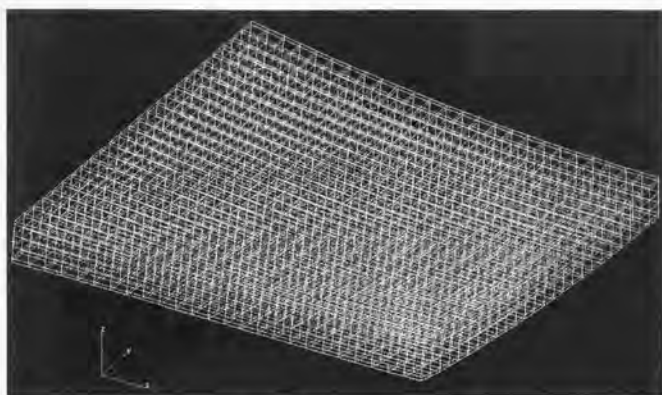


Figure 4.5 Deformed shape of the sandwich plate obtained by the detailed 3-D continuum solid element model

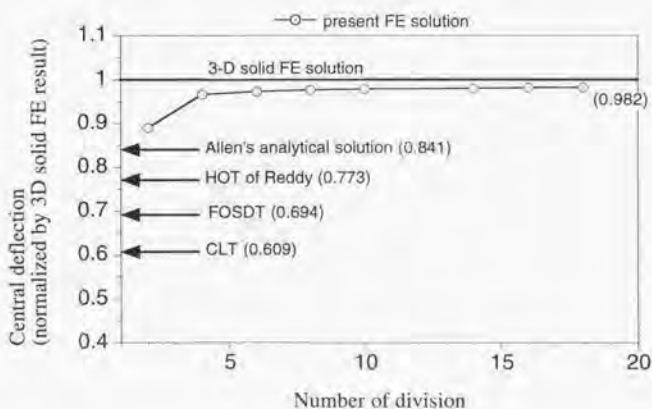


Figure 4.6 Central deflections versus total degrees of freedom (number of division for square mesh)

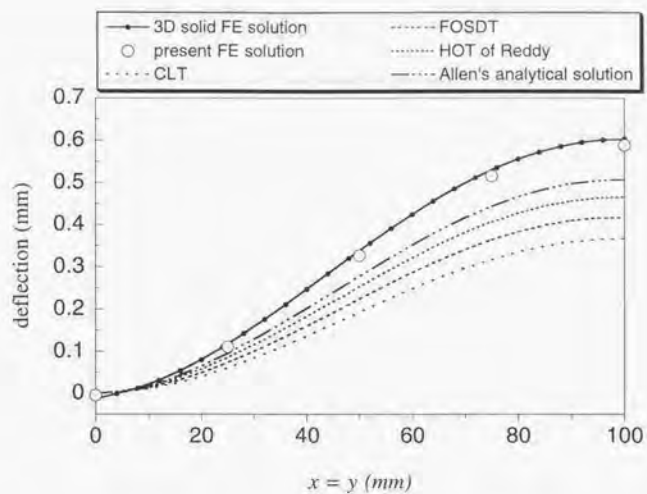


Figure 4.7 Distributions of deflection along the diagonal line

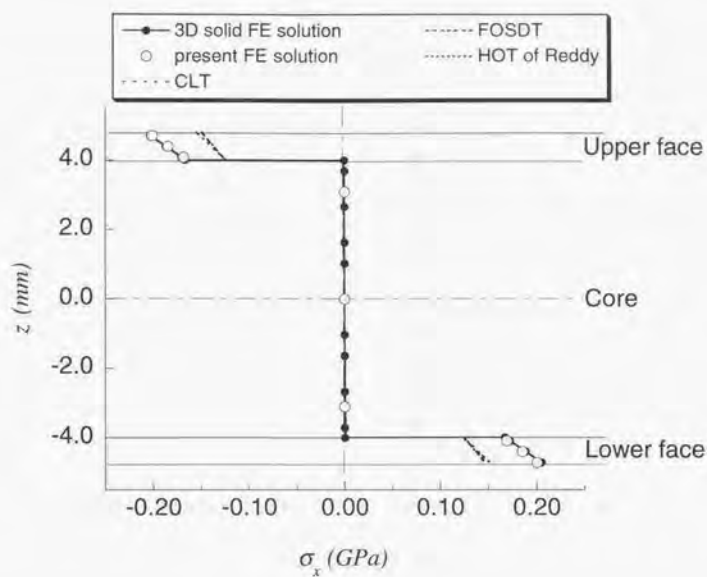


Figure 4.8 In-plane normal stress  $\sigma_x$  distributions through the thickness at  $(l/4, l/4)$



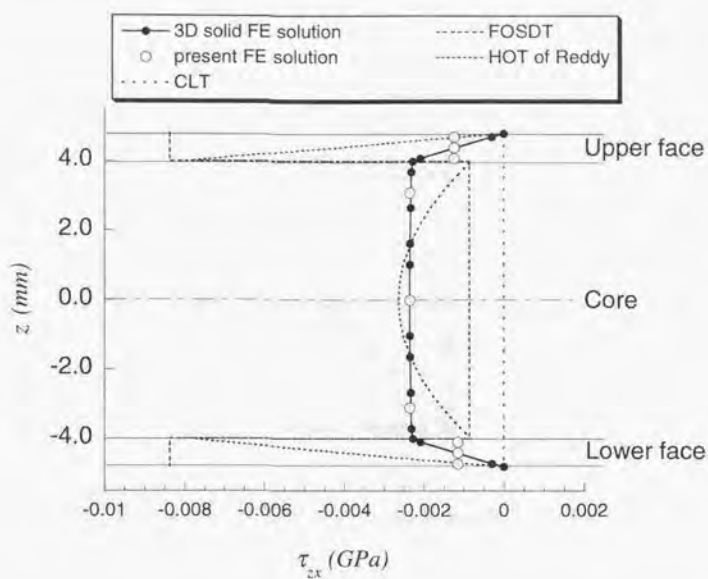


Figure 4.9 Transverse shear stress  $\tau_{zx}$  distributions through the thickness at  $(l/4, l/4)$

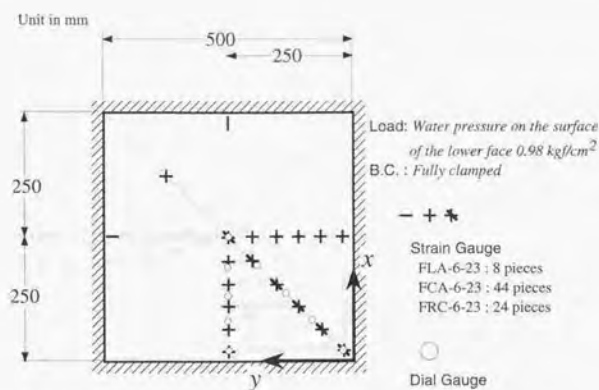


Figure 4.10 Design perspective of the load-bearing sandwich panel test



Figure 4.11 Clamped sandwich panel subjected to hydraulic pressure

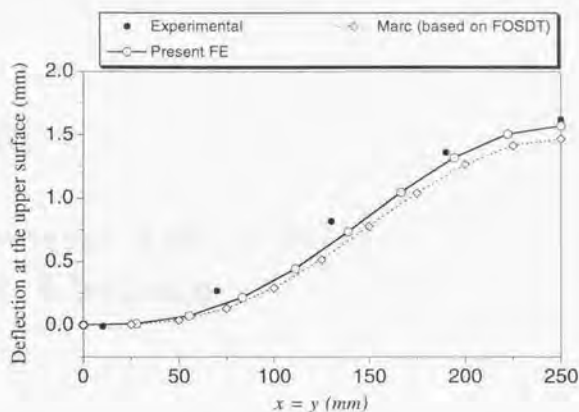


Figure 4.12 Variations of deflection along the diagonal line on the upper surface of the sandwich panel

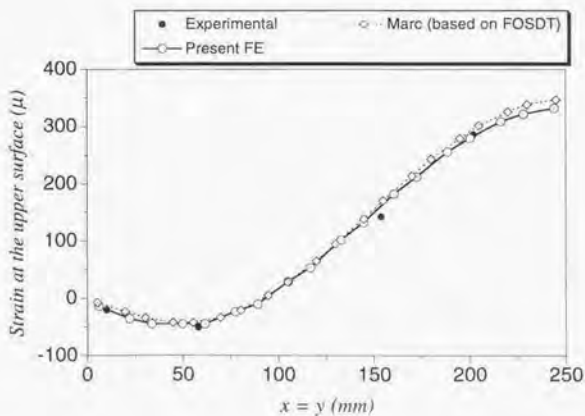


Figure 4.13 Variations of in-plane strain measure along the diagonal line on the upper surface of the sandwich panel

## Chapter 5

### Layerwise Laminated Plate Element



## 5.1 Introduction to this chapter

In this chapter, as the second example deduced from the layerwise higher-order model of the author, a general laminated plate finite element (FE) is to be presented for achieving a satisfactory analysis and design of composite laminates. The present FE identifies itself from the preceding similar FEs in that,

- The present FE can exactly model a laminated plate composed of the unlimited number of different material layups (N-layered FE model). As layer discretization schemes, natural ML or fine ML is supposed;
- The displacement assumption  $[(332)^{NK}]$  are employed. The higher-order displacement assumption (332) was first studied by Lo, Christensen and Wu<sup>47</sup> for ESL models. More recently, Wu *et al.*<sup>87</sup> have employed this (332) assumption for each layer in their layerwise theory and FEs. This displacement assumption leads to the cubic variations of the in-plane strains, the parabolic of the transverse-shear strains and the linear of the transverse-normal strain in the thickness direction for each layer, and hence six non-zero stress components can be directly evaluated from the constitutive equations without the aid of post-processing by 3-D equilibrium equations;
- In the  $[(332)^{NK}]$  models of Wu *et al.*, the displacement continuity constraints at layer-interfaces is introduced by Lagrange multipliers. On the other hand, in the present model, this interfacial constraints are approximated by the penalty method, and thus the present model is more efficient than the Wu's model in computational aspect without loss of accuracy;
- The interlaminar stresses are directly evaluated from the penalty numbers and the small gaps between the adjacent layers as previously given in Equation (3.19). These pointwise quantities also enable, more or less, fracture mechanics approaches such as free-edge effect examinations and delamination modelings.

By using the developed layerwise higher-order plate FE, several numerical applications and discussions are also included, ranging from its accuracy and convergence checks to interlaminar stress evaluations and strain energy release rate calculations.

## 5.2 Finite element approximation

In this section,  $[(332)^{NK}]$  layerwise laminated plate element will be formulated.

### 5.2.1 [(332)<sup>NK</sup>] assumption

The geometric configuration of the present element is illustrated in Figure 5.1. Although it is possible to divide a laminate into sub-laminates (i.e. coarse ML scheme), in this formulation, natural ML or fine ML scheme for layer discretization is supposed.

**Deformation series termination** The orders of displacements are (332) for each of the unlimited numbers of layers, such that,

$$\left. \begin{aligned} u^{(k)}(x, y, z^{(k)}) &= U_0^{(k)}(x, y) + z^{(k)} U_1^{(k)}(x, y) + (z^{(k)})^2 U_2^{(k)}(x, y) + (z^{(k)})^3 U_3^{(k)}(x, y) \\ v^{(k)}(x, y, z^{(k)}) &= V_0^{(k)}(x, y) + z^{(k)} V_1^{(k)}(x, y) + (z^{(k)})^2 V_2^{(k)}(x, y) + (z^{(k)})^3 V_3^{(k)}(x, y) \\ w^{(k)}(x, y, z^{(k)}) &= W_0^{(k)}(x, y) + z^{(k)} W_1^{(k)}(x, y) + (z^{(k)})^2 W_2^{(k)}(x, y) \end{aligned} \right\} \quad (5.1)$$

where the superscript '(k)' denotes each one of layers of a laminated plate, numbered from the bottom layer to the top, and  $z^{(k)}$  is the thickness coordinate measured from the middle plane of the considered layer.

The generalized displacement vector  $\delta$  are defined such that,

$$[\delta]^T = \left\{ [\delta^{(1)}]^T \dots [\delta^{(k)}]^T \dots [\delta^{(NK)}]^T \right\} \quad (5.2)$$

in which the  $k^{\text{th}}$  sub-vector in  $\delta$  are

$$[\delta^{(k)}]^T = \{U_0 \ V_0 \ W_0 \ U_1 \ V_1 \ W_1 \ U_2 \ V_2 \ W_2 \ U_3 \ V_3\}^{(k)} \quad (5.3)$$

The number of components of  $\delta^{(k)}$  is 11, hence, the total number of components of  $\delta$  amounts to  $11 \times NK$ .

**Strain-displacement relations** The strain-displacement relations in each layer are obtained as follows:

$$\left. \begin{aligned} \varepsilon_x^{(k)} &= E_{x0}^{(k)} + z^{(k)} E_{x1}^{(k)} + (z^{(k)})^2 E_{x2}^{(k)} + (z^{(k)})^3 E_{x3}^{(k)} \\ \varepsilon_y^{(k)} &= E_{y0}^{(k)} + z^{(k)} E_{y1}^{(k)} + (z^{(k)})^2 E_{y2}^{(k)} + (z^{(k)})^3 E_{y3}^{(k)} \\ \varepsilon_z^{(k)} &= E_{z0}^{(k)} + z^{(k)} E_{z1}^{(k)} \\ \gamma_{yz}^{(k)} &= E_{yz0}^{(k)} + z^{(k)} E_{yz1}^{(k)} + (z^{(k)})^2 E_{yz2}^{(k)} \\ \gamma_{zx}^{(k)} &= E_{zx0}^{(k)} + z^{(k)} E_{zx1}^{(k)} + (z^{(k)})^2 E_{zx2}^{(k)} \\ \gamma_{xy}^{(k)} &= E_{xy0}^{(k)} + z^{(k)} E_{xy1}^{(k)} + (z^{(k)})^2 E_{xy2}^{(k)} + (z^{(k)})^3 E_{xy3}^{(k)} \end{aligned} \right\} \quad (5.4)$$

in which

$$\left. \begin{aligned} E_{x0}^{(k)} &= \frac{\partial U_0^{(k)}}{\partial x}, E_{x1}^{(k)} = \frac{\partial U_1^{(k)}}{\partial x}, E_{x2}^{(k)} = \frac{\partial U_2^{(k)}}{\partial x}, E_{x3}^{(k)} = \frac{\partial U_3^{(k)}}{\partial x} \\ E_{y0}^{(k)} &= \frac{\partial V_0^{(k)}}{\partial y}, E_{y1}^{(k)} = \frac{\partial V_1^{(k)}}{\partial y}, E_{y2}^{(k)} = \frac{\partial V_2^{(k)}}{\partial y}, E_{y3}^{(k)} = \frac{\partial V_3^{(k)}}{\partial y} \\ E_{z0}^{(k)} &= W_1^{(k)}, E_{z1}^{(k)} = 2W_2^{(k)} \\ E_{yz0}^{(k)} &= V_1^{(k)} + \frac{\partial W_0^{(k)}}{\partial y}, E_{yz1}^{(k)} = 2V_2^{(k)} + \frac{\partial W_1^{(k)}}{\partial y}, E_{yz2}^{(k)} = 3V_3^{(k)} + \frac{\partial W_2^{(k)}}{\partial y} \\ E_{zx0}^{(k)} &= U_1^{(k)} + \frac{\partial W_0^{(k)}}{\partial x}, E_{zx1}^{(k)} = 2U_2^{(k)} + \frac{\partial W_1^{(k)}}{\partial x}, E_{zx2}^{(k)} = 3U_3^{(k)} + \frac{\partial W_2^{(k)}}{\partial x} \\ E_{xy0}^{(k)} &= \frac{\partial U_0^{(k)}}{\partial y} + \frac{\partial V_0^{(k)}}{\partial x}, E_{xy1}^{(k)} = \frac{\partial U_1^{(k)}}{\partial y} + \frac{\partial V_1^{(k)}}{\partial x} \\ E_{xy2}^{(k)} &= \frac{\partial U_2^{(k)}}{\partial y} + \frac{\partial V_2^{(k)}}{\partial x}, E_{xy3}^{(k)} = \frac{\partial U_3^{(k)}}{\partial y} + \frac{\partial V_3^{(k)}}{\partial x} \end{aligned} \right\} \quad (5.5)$$

Physically,  $E_{x0}^{(k)}, E_{y0}^{(k)}, E_{z0}^{(k)}, E_{yz0}^{(k)}, E_{zx0}^{(k)}$  and  $E_{xy0}^{(k)}$  are pointwise strains at the middle plane of the layer in consideration, and  $E_{x1}^{(k)}, E_{y1}^{(k)}$  and  $E_{xy1}^{(k)}$  are curvatures of the layer. The other components represent higher-order influences of the cross-section in the considered layer. Equation (5.4) also shows that the orders of through-the-thickness variation are the cubic for the in-plane strains, the parabolic for the transverse shear strains and the linear for the transverse normal strain, respectively.

The generalized strain vectors for the  $k^{\text{th}}$  layer are as follows:

For the membrane/flexure/transverse-normal portion,

$$[\epsilon_{mb}^{(k)}]^T = \{E_{x0} E_{y0} E_{xy0} E_{x1} E_{y1} E_{xy1} E_{x2} E_{y2} E_{xy2} E_{x3} E_{y3} E_{xy3} E_{x0} E_{y0} E_{x1}\}^{(k)} \quad (5.6)$$

For the transverse-shear portion,

$$[\epsilon_s^{(k)}]^T = \{E_{zx0} E_{yz0} E_{zx1} E_{yz1} E_{zx2} E_{yz2}\}^{(k)} \quad (5.7)$$

**Constitutive equations** For  $l^{\text{th}}$  orthotropic arbitrarily oriented lamina in the  $k^{\text{th}}$  layer (note that there is a possibility that layers include several laminae in themselves if any coarse ML scheme is taken for the layer discretizations), the stress-strain relations can be written in the following matrix form:

$$\begin{Bmatrix} \sigma_x \\ \sigma_y \\ \sigma_z \\ \tau_{yz} \\ \tau_{zx} \\ \tau_{xy} \end{Bmatrix}^{(k,l)} = \begin{bmatrix} \bar{Q}_{11} & \bar{Q}_{12} & \bar{Q}_{13} & 0 & 0 & \bar{Q}_{16} \\ \bar{Q}_{12} & \bar{Q}_{22} & \bar{Q}_{23} & 0 & 0 & \bar{Q}_{26} \\ \bar{Q}_{13} & \bar{Q}_{23} & \bar{Q}_{33} & 0 & 0 & \bar{Q}_{36} \\ 0 & 0 & 0 & \bar{Q}_{44} & \bar{Q}_{45} & 0 \\ 0 & 0 & 0 & \bar{Q}_{45} & \bar{Q}_{55} & 0 \\ \bar{Q}_{16} & \bar{Q}_{26} & \bar{Q}_{36} & 0 & 0 & \bar{Q}_{66} \end{bmatrix}^{(k,l)} \begin{Bmatrix} \epsilon_x \\ \epsilon_y \\ \epsilon_z \\ \gamma_{yz} \\ \gamma_{zx} \\ \gamma_{xy} \end{Bmatrix}^{(k)} \quad (5.8)$$

where  $\bar{Q}_{pq}^{(k,l)}$  ( $p, q = 1, 2, 3, 6, p \leq q$  or  $p, q = 4, 5, p \leq q$ ) are reduced elastic coefficients.

By integrating the stresses through the layer thickness, the generalized resultant-generalized strain relations can be expressed in the matrix form as follows:

$$\begin{Bmatrix} N \\ Q \end{Bmatrix}^{(k)} = \begin{bmatrix} D_{mb} & 0 \\ 0 & D_s \end{bmatrix}^{(k)} \begin{Bmatrix} \epsilon_{mb} \\ \epsilon_s \end{Bmatrix}^{(k)} \quad (5.9)$$

in which

$$[N^{(k)}]^T = \int_{-h^{(k)}/2}^{h^{(k)}/2} \{\sigma_x \sigma_y \tau_{xy} z \sigma_x z \sigma_y z \tau_{xy} z^2 \sigma_x z^2 \sigma_y z^2 \tau_{xy} z^3 \sigma_x z^3 \sigma_y z^3 \tau_{xy} \sigma_z z \sigma_z\}^{(k)} dz^{(k)} \quad (5.10)$$

and

$$[Q^{(k)}]^T = \int_{-h^{(k)}/2}^{h^{(k)}/2} \{\tau_{xz} \tau_{yz} z \tau_{xz} z^2 \tau_{yz} z^2 \tau_{yz}\}^{(k)} dz^{(k)} \quad (5.11)$$

Submatrices  $D_{mb}^{(k)}$  and  $D_s^{(k)}$  are, respectively, the membrane/flexure/transverse-normal rigidity matrix and the transverse-shear rigidity matrix.

**Interface continuity constraints** The displacement continuity constraints at the perfectly adhered interfaces between the  $k^{\text{th}}$  and the  $(k+1)^{\text{th}}$  layers are given as follows:

$$[g^{(k)}]^T = \{g_x g_y g_z\}^{(k)} = \{0 \ 0 \ 0\} \quad (5.12)$$



in which  $g_x$ ,  $g_y$  and  $g_z$  are, respectively, relative displacement differences in  $x$ ,  $y$  and  $z$  directions at the layer interface between the  $k^{\text{th}}$  and the  $(k+1)^{\text{th}}$  layers (that is, "gaps" at the interface of adjacent layers), and in this case,

$$\left. \begin{aligned} g_x^{(k)} &= U_0^{(k+1)} - \frac{h^{(k+1)}}{2} U_1^{(k+1)} + \frac{(h^{(k+1)})^2}{4} U_2^{(k+1)} - \frac{(h^{(k+1)})^3}{8} U_3^{(k+1)} \\ &\quad - U_0^{(k)} + \frac{h^{(k)}}{2} U_1^{(k)} - \frac{(h^{(k)})^2}{4} U_2^{(k)} + \frac{(h^{(k)})^3}{8} U_3^{(k)} \\ g_y^{(k)} &= V_0^{(k+1)} - \frac{h^{(k+1)}}{2} V_1^{(k+1)} + \frac{(h^{(k+1)})^2}{4} V_2^{(k+1)} - \frac{(h^{(k+1)})^3}{8} V_3^{(k+1)} \\ &\quad - V_0^{(k)} + \frac{h^{(k)}}{2} V_1^{(k)} - \frac{(h^{(k)})^2}{4} V_2^{(k)} + \frac{(h^{(k)})^3}{8} V_3^{(k)} \\ g_z^{(k)} &= W_0^{(k+1)} - \frac{h^{(k+1)}}{2} W_1^{(k+1)} + \frac{(h^{(k+1)})^2}{4} W_2^{(k+1)} \\ &\quad - W_0^{(k)} + \frac{h^{(k)}}{2} W_1^{(k)} - \frac{(h^{(k)})^2}{4} W_2^{(k)} \end{aligned} \right\} \quad (5.13)$$

Corresponding to  $g^{(k)}$ , the reaction forces  $\lambda^{(k)}$  which adhere these adjacent layers (i.e. interlaminar stresses) arise as follows,

$$[\lambda^{(k)}]^T = \{\lambda_x \lambda_y \lambda_z\}^{(k)} = \{\alpha_x g_x \alpha_y g_y \alpha_z g_z\}^{(k)} \quad (5.14)$$

where  $\alpha_x$ ,  $\alpha_y$  and  $\alpha_z$  are the penalty numbers which are set in  $x$ ,  $y$  and  $z$  directions, respectively, at the layer interface.

**Governing equation** Finally, the modified potential energy functional with the penalty numbers is described below:

$$\Pi'_{mp}(\delta) = \Pi_p(\delta) + \mathcal{H}(\delta) \quad (5.15)$$

in which

$$\Pi_p(\delta) = \sum_{k=1}^{NK} \iint_{\Omega} \frac{1}{2} ([N]^T \cdot \epsilon_{mb} + [Q]^T \cdot \epsilon_s)^{(k)} d\Omega - \iint_{\Omega} ([T]^T \cdot \bar{u}) d\Omega \quad (5.16)$$

where  $T$  and  $\bar{u}$  are the tractions and the prescribed displacements on the upper and the lower surfaces of the laminate, respectively.

$$[T]^T = \{T_x \ T_y \ T_z\}, \quad [\bar{u}]^T = \{\bar{u} \ \bar{v} \ \bar{w}\} \quad (5.17)$$

and the auxiliary energy term,

$$\mathcal{H} = \sum_{k=1}^{NK} \iint_{\Omega} \frac{1}{2} ([\lambda]^T \cdot \mathbf{g})^{(k)} d\Omega \quad (5.18)$$

The governing equations can be obtained by taking the extremum (not minimum) of the present modified potential energy functional with respect to the unknown displacement variables  $\delta$ .

### 5.2.2 Finite element discretization

In the present finite element formulation, an entire laminated plate in the problem is discretized into  $N_e$  elements such that:

$$\Pi'_{mp}(\delta) = \sum_{e=1}^{N_e} \Pi'^{(e)}_{mp}(\delta) \quad (5.19)$$

where  $\Pi'^{(e)}_{mp}$  is the modified potential energy functional of each element.

Eight-node  $C^0$  two-dimensional shape functions  $\Phi_J$ ;  $J = 1, 2, \dots, 8$  is adopted for interpolating both the geometry and generalized displacements such that:

$$x = \sum_{J=1}^8 \Phi_J x_J, \quad y = \sum_{J=1}^8 \Phi_J y_J \quad (5.20)$$

$$\delta^{(k)} = \sum_{J=1}^8 \Phi_J \delta_J^{(k)} \quad (5.21)$$

where  $x_J$ ,  $y_J$  and  $\delta_J^{(k)}$ ;  $J = 1, 2, \dots, 8$  are the nodal values.

Taking the first variation of the functional,

$$\frac{\partial \Pi'^{(e)}_{mp}}{\partial \delta} = 0 \quad (5.22)$$

and assembling the contributions from all elements yields the equilibrium equation system as follows:

$$[\mathbf{K} + \mathbf{K}_\alpha] \mathbf{d} = \mathbf{f} \quad (5.23)$$

in which  $\mathbf{K}$  is the global stiffness matrix without displacement constraints and  $\mathbf{K}_\alpha$  is the auxiliary energy portion including the penalty numbers.  $\mathbf{d}$  and  $\mathbf{f}$  are the assembled nodal displacement vector and the assembled nodal force vector, respectively.

After solving the linear algebraic equations in Equation (5.23), the generalized strain and the generalized resultant vectors can then be obtained, respectively, as follows:

$$\epsilon_{mb}^{(k)} = \sum_{J=1}^8 [\mathbf{B}_{mb}^{(k)}]_J \delta_J^{(k)}, \quad \epsilon_s^{(k)} = \sum_{J=1}^8 [\mathbf{B}_s^{(k)}]_J \delta_J^{(k)} \quad (5.24)$$

$$\mathbf{N}^{(k)} = \sum_{j=1}^8 [\mathbf{D}_{mb}^{(k)} \mathbf{B}_{mb}^{(k)}]_j \delta_j^{(k)}, \quad \mathbf{Q}^{(k)} = \sum_{j=1}^8 [\mathbf{D}_s^{(k)} \mathbf{B}_s^{(k)}]_j \delta_j^{(k)} \quad (5.25)$$

where  $[\mathbf{B}_{mb}^{(k)}]_j$  and  $[\mathbf{B}_s^{(k)}]_j$  are the strain matrices, containing the shape functions and their derivatives.

Once the generalized strains are obtained from Equation (5.24), six strain components and then six stress components are evaluated from Equation (5.4) and then from Equation (5.8) (the constitutive equations).

Furthermore, small gaps  $\mathbf{g}^{(k)}$  between adjacent layers are calculated from the obtained nodal displacements such that:

$$\mathbf{g}^{(k)} = \sum_{j=1}^8 [\mathbf{C}^{(k)} \left\{ \begin{matrix} \delta_j^{(k+1)} \\ \delta_j^{(k)} \end{matrix} \right\}]_j \quad (5.26)$$

in which  $[\mathbf{C}^{(k)}]_j$  is the operator that calculates small gaps at the interfaces from the nodal displacements  $\delta_j^{(k+1)}$  and  $\delta_j^{(k)}$ . After small gaps  $\mathbf{g}^{(k)}$  are calculated, interlaminar stresses  $\lambda^{(k)}$  can be obtained from Equation (5.14).

### 5.2.3 Fracture mechanics consideration

Insofar, the basic formulation of the present FE has been shown. By using the present FE, very accurate displacement and stress analysis of composite laminates can be carried out. In particular, it is notable that interlaminar stresses can be accurately evaluated in the fully three-dimensional (3-D) sense.

The primary purpose of the present FE is satisfactory analysis and design of composite laminates. However, this model has further potentials, and one of them is that this FE model is capable of evaluating some quantities of the linear fracture mechanics. Today, an absolute majority of the researches on composite materials use the concept of the fracture mechanics. Thus a numerical model which considers, more or less, the fractures mechanics will be quite beneficial. As excellent reviews on the fracture mechanics for composite materials, one can refer to Kageyama's works<sup>112, 113, 114</sup>.

#### Free-edge effect problem

Since Hayashi<sup>115</sup>, Sierakowski *et al.*<sup>116</sup> and then Puppo and Evensen<sup>118</sup> reported interlaminar shear stress concentrations in the vicinity of free edges in a laminated strip, the free-edge effect problem has been attracting massive research attentions to date. As an informative review on the early progress of numerical investigations of the free-edge effect, one can look up Salamon's paper<sup>117</sup>.



The dawn of the investigations was broken by Pipes and Pagano<sup>119, 120, 121, 122</sup>. Pipes and Pagano mainly examined infinitely-long laminated strip with straight free edges under uniform axial extension, and they assumed quasi-three-dimensional (quasi-3-D) strain and stress state. The numerical approach they mainly employed was finite-difference scheme. There were numerous researches which followed them. Rybicki<sup>123</sup> used stress-function based equilibrium finite element analysis for tracing the results by Pipes and Pagano. On the other hand, Wang and Crossman<sup>124, 125</sup> developed a displacement-based quasi-3-D finite element for this Pipes-Pagano problem. Since then, this displacement-based quasi-3-D FE approaches has been used by many researchers<sup>126, 127, 128, 129</sup>. Another stress-function based numerical approach was first employed by Tang<sup>130</sup> and Tang and Levy<sup>131</sup> by introducing Lekhnitskii's stress-functions<sup>132</sup>. This stress-based boundary layer approach was extensively applied to this Pipes-Pagano problem, e.g., by Ting *et al.*<sup>133, 134</sup>, Wang *et al.*<sup>135, 136</sup> and many others<sup>137, 138, 139, 140</sup>. They were focusing mainly on revealing the natures of singularities of the boundary stress field in Pipes-Pagano problems.

Pipes-Pagano problem is the free-edge effect at the straight edges. Other types of the free-edge effect were also studied in the literature. Griffin, Jr. *et al.*<sup>141</sup> analyzed interlaminar thermal stresses distributions around the free corner of angle-ply laminates (free-corner effect) by using 3-D continuum solid element. On the other hand, the curved free-edge problems have also been investigated by many researchers such as Raju *et al.*<sup>142</sup>, Lucking *et al.*<sup>143</sup> and Hu *et al.*<sup>144</sup>. Most of them analyzed interlaminar stresses around the circular holes by using 3-D continuum solid element.

In the context of the current research attentions for the free-edge problems, fully three-dimensional analysis of free-edge stresses along arbitrary shaped free edges are highly required. Since the most suitable FE model for this purpose is plate/shell models, a few attempts<sup>145, 146</sup> for application of plate/shell element to free-edge problems has been carried out, most of which used layered configuration of ESL-based plate elements and special interfacial transverse shear elements. On the other hand, applications of ML-based plate/shell elements like the present layerwise higher-order FE to the free-edge problems are relatively rare. However, as Moriya<sup>71</sup> and then Robbins, Jr. and Reddy<sup>96</sup> pointed out, ML-based plate/shell models are considerably suitable for free-edge problems as well as structural analysis and design, because they are equipped with both simple geometry of ESL and accuracy of 3-D continuum solid.

Consequently, the practicability of the present finite element will be very high, and applications of the present finite element to the free-edge problem will be demonstrated later on.



### Modeling of delaminations

Composite laminates exhibit a variety of failure phenomena which conventional homogeneous, isotropic materials do not experience, such as fiber breakage, matrix cracking, delamination and their combinations. Figure 5.2 schematically illustrates these failures and damages in composite materials and in composite laminates. Among these failures, delamination is one of the most feared failures for structural reliability of composite laminates. The initiations and then the growth of delaminations originate mainly from a large magnitude of interlaminar stresses at free edges or delamination fronts, i.e., the aforementioned free-edge stresses. Therefore, most of the numerical models valid for the free-edge problems can be straightforwardly extended and applied to studies on the delamination phenomena as well.

After several qualitative investigations on the relations between free-edge stresses and global strength of laminates<sup>147, 148, 149, 150</sup> were made, Kim and Soni<sup>151</sup> proposed "Average stress method", in which interlaminar normal stresses near the free edge are averaged over a certain finite width for predicting the edge-delamination onset load.

Although it was reported that Average stress method could accurately predict the onsets of edge delamination, a majority of researches on delamination phenomena have focussed on another sort of more rigorous quantities such as the stress intensity factors ( $K_I$ ,  $K_{II}$  and  $K_{III}$ ) and the strain energy release rate ( $G$ ). For example, Wang<sup>152, 153</sup> extended and applied his boundary-layer-stress models in conjunction with Lekhnitskii's stress functions and boundary-collocation technique, to edge-delamination problems in angle-ply laminates. He employed the stress intensity factors and the strain energy release rate as criterion of edge delaminations.

In particular, the strain energy release rate is well suited to such an approximate numerical model as displacement-based finite elements and hence the literature on this issue is very large. First attempt was made by Rybicki *et al.*<sup>154, 155</sup>. They calculated the strain energy release rate in the edge-delaminated laminate strip under tension load by using quasi-three-dimensional (quasi-3-D) finite element and the virtual crack closure integral (VCCI), the concept of which were first contended by Irwin<sup>156</sup>. Many researchers followed Rybicki *et al.* such as Wang and Crossman<sup>157</sup>, Kim and Hong<sup>158</sup> and Aoki and Kondo<sup>159</sup>, all of whom similarly used quasi-3-D finite elements and VCCI. Salpekar, Raju and O'Brien<sup>160</sup> who investigated delamination in a tapered laminate by two-dimensional (2-D) plane-strain element and VCCI and, more lately, Whitcomb<sup>161</sup> and Salpekar, O'Brien and Shivakumar<sup>162</sup> who successfully employed fully three-dimensional (3-D) continuum brick elements for local analysis of the energy release rate similarly using VCCI. Furthermore, because of the practical

interest in delamination properties of fully 3-D, arbitrary shaped composite laminates with various kinds of delamination failures, some research efforts for applications of ESL-based plate elements to the energy release rate calculation have been made by Whitcomb and Shivakumar<sup>163</sup>, Davidson and Schapery<sup>164</sup>, Gim<sup>165</sup> and Pavier and Clarke<sup>166</sup>. They used multi-point constraints (MPC) for representing delaminations by ESL-based plate elements.

The strain energy release rate (denoted by  $G$ ) is calculated as follows,

$$G = \frac{\partial \mathcal{W}}{\partial A} - \frac{\partial \mathcal{U}}{\partial A} \quad (5.27)$$

whereas  $\mathcal{W}$ ,  $\mathcal{U}$  and  $A$  are work by external forces, strain energy in the total system and delamination area, respectively.

It is certainly possible to directly evaluate these quantities in Equation (5.27) and then calculate the energy release rate  $G$ . However, in finite element approximations, the virtual crack closure integral (VCCI) are commonly used for the energy release rate calculation. According to VCCI approach, the energy release rate  $G$  (without the change of  $\mathcal{W}$ ) can be given as,

$$\begin{aligned} G &= -\frac{\partial \mathcal{U}}{\partial A} = -\lim_{\Delta A \rightarrow 0} \frac{\Delta \mathcal{U}}{\Delta A} \\ &= \lim_{\Delta A \rightarrow 0} \frac{1}{2\Delta A} \int_A^{A+\Delta A} \mathbf{u}_R^T \mathbf{X} d\Omega \end{aligned} \quad (5.28)$$

in which  $\mathbf{u}_R$  and  $\mathbf{X}$ , respectively, stand for the relative displacements after and prior to crack extension and interfacial tractions at any point in the virtual crack extension area  $\Delta A$ . Figure 5.3 illustrates this concept of VCCI. In order to sustain the generality of the concept, local coordinate system  $(x', y', z')$  is used in accordance with the conventional notation in the fracture mechanics. As illustrated in Figure 5.3, the components of  $\mathbf{u}_R$  and  $\mathbf{X}$  in the local coordinate system are defined as the following,

$$\mathbf{u}_R = (u'_R, v'_R, w'_R)$$

$$\mathbf{X} = (X', Y', Z')$$

One of the advantages of VCCI over the direct calculation of  $G$  via the overall energy balance is that, during VCCI process, one can decompose  $G$  into the three modes of fracture, i.e.,

$$G = G_{\text{total}} = G_I + G_{II} + G_{III} \quad (5.29)$$

whereas

$$\left. \begin{aligned} \text{mode I : Opening} \quad G_I &= \lim_{\Delta A \rightarrow 0} \frac{1}{2\Delta A} \int_A^{A+\Delta A} v_R' Y' d\Omega \\ \text{mode II : In-plane shearing} \quad G_{II} &= \lim_{\Delta A \rightarrow 0} \frac{1}{2\Delta A} \int_A^{A+\Delta A} u_R' X' d\Omega \\ \text{mode III : Out-of-plane tearing} \quad G_{III} &= \lim_{\Delta A \rightarrow 0} \frac{1}{2\Delta A} \int_A^{A+\Delta A} w_R' Z' d\Omega \end{aligned} \right\} \quad (5.30)$$

As for finite element implementation of VCCI, a further approximation of Equation (5.30) has been taken by converting pointwise  $u_R$  and  $X$  values at any point on the crack extension area  $\Delta A$ , into nodal values and then omitting the area integrals such that,

$$\left. \begin{aligned} G_I &\approx \frac{1}{2\Delta A} \{ (v_{b_v}' - v_{b_L}') Y_b' + (v_{c_v}' - v_{c_L}') Y_c' \} \\ G_{II} &\approx \frac{1}{2\Delta A} \{ (u_{b_v}' - u_{b_L}') X_b' + (u_{c_v}' - u_{c_L}') X_c' \} \\ G_{III} &\approx \frac{1}{2\Delta A} \{ (w_{b_v}' - w_{b_L}') Z_b' + (w_{c_v}' - w_{c_L}') Z_c' \} \end{aligned} \right\} \quad (5.31)$$

in which nodal displacement vectors such as  $(u_{b_v}', v_{b_v}', w_{b_v}')$  and  $(u_{b_L}', v_{b_L}', w_{b_L}')$  and, nodal force vectors such as  $(X_b', Y_b', Z_b')$  are given in Figure 5.4(a).

On the other hand, Figure 5.4(b) is a schematic of the multi-point constraints (MPC) scheme for modeling a delamination and then calculating  $G$  by ESL-based plate elements. Although MPC scheme is quite effective in such a problem as delamination buckling, at least three plate elements are required for modeling a specific delamination and cumbersome constraint conditions should be satisfied at the tip of the delamination.

In the context with respect to delamination modelings and the strain energy release rate calculation, ML-based plate/shell elements like the present layerwise higher-order element will serve as one of the most attracting models for this purpose. Recently, Barbero and Reddy<sup>167</sup> developed a delamination finite element model using the general layerwise plate theory of Reddy<sup>97</sup>. They employed the Heaviside step functions for representing delaminated layer-interfaces and the Jacobian derivative method, previously developed by them<sup>168</sup>, for the strain energy release rate analysis. They also successfully conducted a variety of numerical examples by the developed layerwise delaminated element and, as a consequence, demonstrated the validity and superiority over the conventional models of ML-based plate/shell elements for delamination modelings and the energy release rate calculations.



Henceforth, a new scheme for delamination modeling and the energy release rate calculation by the present layerwise higher-order element is devised.

In the present formulation, instead of detaching nodal points like in the conventional schemes, delaminations and crack extensions for VCCI are modeled by setting specific penalty numbers at the delaminated layer-interface equal to zero or considerably small, such that,

$$\alpha_i^{(k)} \rightarrow 0, \quad i = x', y', z' \quad (5.32)$$

where it is assumed that a delamination occurs at the interface between  $k^{\text{th}}$  and  $(k+1)^{\text{th}}$  layers. This modeling scheme were first employed by Fuehne and Engblom<sup>169</sup> in their finite element analysis by using 20-node 3-D continuum solid element. In their work, they investigated the free-edge stress problems with debonds by similarly setting the penalty number equal to zero. However, they did not mention anything about crack extension for VCCI and hence the energy release rate calculation. Therefore, to the author's best knowledge, the present scheme is the first attempt for applying the penalty method to the delamination modelings and crack extensions for VCCI. The advantages of the present scheme are many, for instance,

- The penalty number has a physical meaning as spring constant, which has already illustrated in Figure 3.4. Therefore, one can easily visualize both of perfectly adhered state of the layer interface by setting the penalty numbers very large and delaminated discontinuous state by setting them nearly equal to zero. Note that adhesion and delamination can be modeled by merely changing the magnitude of the penalty numbers and any iteration or any non-linear consideration is not required.
- One can easily control delamination modes, which has been difficult in the conventional schemes. For instance, when one wishes to model mode II delamination alone, then one can set only  $\alpha_{x'}^{(k)}$  equal to zero and leave the others unchanged. In the cases that mode I stress  $\sigma_{y'}$  exhibits negative values (i.e. compression) around the tip of delamination front, mode I delamination will not occur (otherwise adjacent layers will overlap) and hence one should set only  $\alpha_{x'}^{(k)}$  and  $\alpha_{z'}^{(k)}$  equal to zero and leave  $\alpha_{y'}^{(k)}$  unchanged.
- In the penalty method, there is a possibility for modeling the interfacial properties for the "interphases" in laminates by setting the penalty numbers some finite magnitude, neither very large nor nearly equal to zero. However, further investigation on this issue will be made elsewhere.



In addition to the aforementioned flexible and rational delamination and crack extension modelings by the penalty numbers, the virtual crack closure integral (VCCI) scheme is also sophisticated in the present formulation. In a customary finite element implementation of VCCI, nodal values of  $\mathbf{u}_R$  and  $\mathbf{X}$  are used for the energy release rate calculation as already described in Equation (5.31) and Figure 5.4. This approximation requires substantially fine meshes in the vicinity of the delamination front and virtual crack area  $\Delta A$  because this scheme omits the area integrals. Although this conventional VCCI scheme is possibly employed, more precise VCCI is also possible in the present formulation. Recalling the meanings of  $\mathbf{u}_R$  and  $\mathbf{X}$  in Equation (5.28), it is easy to realize that  $\mathbf{u}_R$  and  $\mathbf{X}$  are identical to the gap vector  $\mathbf{g}^{(k)}$  after crack extension in Equation (5.13) and the interlaminar stresses  $\lambda^{(k)}$  in Equation (5.14), respectively. Therefore the exact integral in Equation (5.30) can be carried out as follows,

$$\left. \begin{aligned} G_I^{(k)} &= \lim_{\Delta A \rightarrow 0} \frac{1}{2\Delta A} \int_A^{A+\Delta A} g_{y'}^{(k)} \lambda_{y'}^{(k)} d\Omega \\ G_{II}^{(k)} &= \lim_{\Delta A \rightarrow 0} \frac{1}{2\Delta A} \int_A^{A+\Delta A} g_{x'}^{(k)} \lambda_{x'}^{(k)} d\Omega \\ G_{III}^{(k)} &= \lim_{\Delta A \rightarrow 0} \frac{1}{2\Delta A} \int_A^{A+\Delta A} g_{z'}^{(k)} \lambda_{z'}^{(k)} d\Omega \end{aligned} \right\} \quad (5.33)$$

where  $g_{x'}^{(k)}$ ,  $g_{y'}^{(k)}$  and  $g_{z'}^{(k)}$  are the gaps after crack extension, while  $\lambda_{x'}^{(k)}$ ,  $\lambda_{y'}^{(k)}$  and  $\lambda_{z'}^{(k)}$  are the reaction forces (i.e. interlaminar stresses) prior to crack extension. In the actual evaluation of above integrals, numerical integration of  $3 \times 3$  Gauss rule can be adopted.

The delamination modeling and the energy release rate calculation presented herein will be validated in the last part of the next section.

## 5.3 Numerical examples

Finite element calculations is conducted on Hitachi MP5800/320 mainframe of Computer Centre of the University of Tokyo, equipped with 1024 MB main core storage and in double precision arithmetic for representing real numbers. In order to avoid any numerical instability in solving the linear equation system, scaling and partial pivoting schemes are applied during gaussian elimination.

### 5.3.1 Accuracy and convergence check

First of all, a comparative study will be shown to check the accuracy and the convergence of the developed finite element.

## bending of a cross-ply square laminate

The problem considered herein is the  $[0/90/0]_L$  cross-ply square laminated plate with its all four edges fully simply-supported and the sinusoidal lateral pressure is applied on the upper surface. Schematics of the problem definitions are given in Figure 5.5.

For this example, exact elasticity analytical solutions by Pagano<sup>26</sup> are available. The elastic properties are as follows:

$$\begin{aligned} E_L/E_T &= 25, & \nu_{LT} &= \nu_{TT} = 0.25 \\ G_{LT}/E_T &= 0.5, & G_{TT}/E_T &= 0.2 \end{aligned}$$

in which  $L$  denotes the fiber direction and  $T$ , the transverse direction to  $L$ .

In accordance with Pagano, obtained values are non-dimensionalized as follows:

$$\text{for displacements: } \bar{w} = \left( \frac{100E_T}{q_0 h S^4} \right) w \quad \bar{u} = \left( \frac{100E_T}{q_0 h S^3} \right) u$$

$$\text{for stresses: } \bar{\sigma}_x = \left( \frac{1}{q_0 S^2} \right) \sigma_x \quad \bar{\tau}_{xy} = \left( \frac{1}{q_0 S^2} \right) \tau_{xy} \quad \bar{\tau}_{zx} = \left( \frac{1}{q_0 S} \right) \tau_{zx} \quad \bar{\sigma}_z = \left( \frac{1}{q_0} \right) \sigma_z$$

where  $S = l/h$ ,  $l$  = span length and  $h$  = total thickness of the laminate, and  $q_0$  denotes load intensity. In addition,  $\bar{z} = z/h$  is also defined as the normalized coordinates through the thickness measured from the middle plane of the laminate, and  $\bar{x} = x/l$  and  $\bar{y} = y/l$ , as the normalized in-plane coordinates. Besides every penalty number in the three directions is set equal to the same value  $\alpha$ .

The central deflections and the in-plane normal stresses for various penalty parameters in the case of the span-to-thickness ratio  $S = 4$ , are plotted against square mesh refinements in Figures 5.6 and 5.7, respectively. The results are normalized with the Pagano's exact solutions. The rapid convergence to the exact values is observed for both deflections and in-plane normal stresses when the penalty number's magnitude:

$$p = \log \left( \frac{\alpha}{h \sqrt{E_L E_T}} \right)$$

is in the range of 3 to 8. The results obtained by setting  $p$  less than 3 converge to overestimated values, while in the cases that  $p$  is greater than 8, the results diverge. It is postulated that in the case of too small magnitudes of the penalty numbers, displacement continuity requirements at the layer-interfaces will not be achieved sufficiently, while the excessively large value of the penalty number will cause numerical

errors in solving the linear equations. Therefore it is concluded that the penalty numbers should be chosen so that neither broken interlayer displacement continuities nor numerical errors will occur, and in this study,  $p = 5$  will be adopted hereafter.

Figure 5.8 shows the in-plane displacement distributions through the thickness at  $(\bar{x}, \bar{y}) = (0, 1/2)$  in the case of  $S = 4$ . In addition to Pagano's exact solution, analytical solutions by CLT are also reproduced. It is observed that the present FE solution is almost identical to Pagano's exact solution. On the other hand, CLT solutions provide different distributions from the Pagano's exact solution and the present FE solutions. Figures 5.9 and 5.10 show the through-the-thickness distributions of the in-plane normal stress at  $(\bar{x}, \bar{y}) = (1/2, 1/2)$  and in-plane shear stress at  $(\bar{x}, \bar{y}) = (0, 0)$ , respectively. For the in-plane shear stress, results by the present FE is obtained at the nearest Gauss point from the actual evaluation point. It is also observed that for both in-plane normal and shear stresses the present FE solutions agree very much with the exact solutions while CLT solutions do not.

Figures 5.11 and 5.12 show the transverse shear stress at  $(\bar{x}, \bar{y}) = (0, 1/2)$  and the transverse normal stress at  $(\bar{x}, \bar{y}) = (1/2, 1/2)$ , respectively. In the present FE solutions, the pointwise values of interlayer stresses can be evaluated from Equation (5.26), therefore these values are also plotted (two black solid marks at the layer interfaces in the graphs). For transverse stresses, distributions of results obtained by the present FE agree fairly good with the exact solutions in that they are evaluated directly from the constitutive equations without the aid of the post-processing by the 3-D equilibrium equations. Although these results derived from the constitutive equations dose not rigorously satisfy the equilibrium conditions at the layer interfaces and on the loaded or the traction-free surfaces, they will be sufficiently precise for global and/or approximate structural analyses and designs. Besides, the interlaminar stresses evaluated from the penalty numbers are almost identical to the exact values. Therefore, it will be possible to perform pointwise interlaminar strength analysis if any confidential interfacial strength is obtained.

### 5.3.2 Interlaminar stress evaluations

For laminated composites, it is well-known that interlaminar stresses play a significant role in not only local but also global failures. Hence, as the next example, the free-edge effect problem are picked up.



### Infinitely long laminated strip under uniform axial extension

An angle-ply symmetric laminated strip  $[(45/-45)_s]$  under uniform axial extension is considered. The strip is assumed to be infinitely long compared to the width and the thickness so that the end effect can be neglected in the regions sufficiently far from the loaded ends by virtue of Saint Venant's principle. Hence, this problem is not fully three-dimensional (3-D) but quasi-three-dimensional (quasi-3-D) and therefore it might be unsuitable for the assessment of the present FE. However, this example, pioneered by Puppo and Evensen<sup>118</sup> and then Pipes and Pagano<sup>119</sup>, has been extensively studied for the last two or three decades and hence it has plenty of numerical reports with which to compare.

As illustrated in Figure 5.13, the laminated strip discretized into 144 finite elements with the meshing biased along width directions so that narrow area in the vicinity of the free edges has finer meshes. The material data for the numerical simulation are listed as follows:

$$\begin{aligned} E_L &= 137.9 \text{ GPa } (20.0 \times 10^6 \text{ psi}), & E_T &= 14.48 \text{ GPa } (2.1 \times 10^6 \text{ psi}) \\ \nu_{LT} &= \nu_{TT} = 0.21 \\ G_{LT} &= G_{TT} = 5.86 \text{ GPa } (0.85 \times 10^6 \text{ psi}) \end{aligned}$$

Figures 5.14 through 5.17 present the variations of stresses along the width coordinate direction at the interface between  $+45$  and  $-45$  layers  $z \rightarrow h_0$  ( $z > h_0$ ). Very precise stress-based numerical solutions by Wang *et al.*<sup>135</sup> who employed Lekhnitskii's stress-functions<sup>132</sup> and boundary-collocation method, are also plotted as a baseline for numerical accuracy.

As shown in Figure 5.14, distributions of in-plane stresses  $\sigma_x$  and  $\tau_{xy}$  by the present FE solutions are almost identical to the results by Wang *et al.* except for a slight difference near the free edge.

In Figure 5.15, it is observed that the transverse shear stress  $\tau_{xz}$  which is directly evaluated from the constitutive equations agrees well with the results by Wang *et al.* in practical use, while the interlaminar shear stress derived from the small gaps between the adjacent layers and the penalty numbers, somehow fluctuates, probably oscillates.

In Figures 5.16 and 5.17, it is observed that distributions of  $\sigma_z$  from the constitutive equations and  $\tau_{yz}$  derived from the gaps and the penalty numbers give reasonable results compared with results by Wang *et al.* On the other hand,  $\sigma_z$  derived from the penalty numbers and the gaps and  $\tau_{yz}$  from the constitutive equations provide poor results. The fluctuating (probably oscillating) behaviors of  $\tau_{xz}$  and  $\sigma_z$  from the gaps



and the penalty numbers is probably caused by their singular natures on the free edge, although any mathematically rigorous proof is impossible because the present results are approximate ones.

### Infinitely long laminated strip with resin films

Much attention has recently been paid to the existence of interlayer in laminated composites on account of its toughening mechanism. For example, a newly developed interlayer toughened graphite/epoxy has demonstrated excellent compression after impact (CAI) strength in which interlayer is composed of a mixture of thermoplastic particles and thermoset base resin selectively localized between laminae as a thin resin film.

The next example is a  $[45/(\text{resin-film})/-45]_s$  angle-ply laminated strip under uniform axial extension, as illustrated in Figure 5.18.

The material data for CFRP layers is the same as that in the foregoing problem, and for the isotropic resin films it is assumed as follows:

$$E = 13.79 \text{ GPa } (2.0 \times 10^6 \text{ psi}), \quad \nu = 0.3$$

Figure 5.19 through 5.22 present the variations of stresses along the width coordinate direction at the interface between  $+45$  layer and the resin film layer  $z \rightarrow h_0 + t$  ( $z > h_0 + t$ ). For comparison, results without the resin film layers (i.e.  $t = 0$ ) is plotted again.

Figure 5.19 shows that in-plane stresses distributions are slightly different from those in the case  $t = 0$ .

Distributions of the transverse shear  $\tau_{zx}$  and the transverse normal  $\sigma_z$  stresses calculated from the constitutive equations are plotted in Figures 5.20 and 5.21, respectively. It is shown that the magnitude of stresses in the vicinity of free edge decreases as the thickness of the resin film layer increases. For  $\tau_{zx}$ , the values at  $y/b = 0.996$  decrease by 15.6 % for  $t = 0.1h_0$ , by 26.1 % for  $t = 0.25h_0$ . For  $\sigma_z$ , the values at  $y/b = 0.996$  decrease by 53.2 % for  $t = 0.1h_0$ , by 77.085 % for  $t = 0.25h_0$ .

In Figure 5.22, the interlaminar shear stresses  $\tau_{yz}$  evaluated from the small gaps and the penalty numbers are plotted. It is observed that when the resin film layers exist, rapid drops near the free edge occur. It is postulated that further fine meshing will be necessary for precise predictions of  $\tau_{yz}$ .

### 5.3.3 Strain energy release rate calculations

In the previous section, interlaminar stress evaluations are carried out by using the developed FE, and fairly satisfactory results are obtained in a practical point of view. However, it is also observed that the present displacement-based FE provides somehow unusual distributions of interlaminar stresses obtained from the small gaps of relative displacements of adjacent layers and the penalty numbers in the vicinity of free edge. This is probably because interlaminar stresses which are proven to become singular at the tip of the free edge or the delamination front can not be evaluated by such a displacement-based FE as the present.

However, this fact is not pessimistic at all. From a practical point of view, excessively precise predictions of interlaminar stress values at the tip of free edges are not always useful. In stead of interlaminar stresses, the strain energy release rate  $G$  becomes of significant interest because this quantity can be measured in experiments.

#### Infinitely long laminated strip with edge delaminations

Hence, in order to demonstrate the feasibility of the present FE for the strain energy release rate calculation, simple edge-delamination problem are investigated herein.

Consider a symmetric laminated rectangular strip with its both ends clamped and extended as illustrated in Figure 5.23. By virtue of Saint Venant's principle, quasi-3-D strain/stress state can be assumed in the area sufficiently far from the loaded ends. The laminate has straight edge delaminations along the free edges and delamination length (or delamination depth) are denoted by  $a$ . Three different types of the stacking sequence are considered, i.e., cross-ply  $[90/0]_s$ , angle-ply  $[45/-45]_s$ , and quasi-isotropic  $[45/-45/0/90]_s$ . Each of the dissimilar material laminae was precisely modeled by a specific layer and thus the total number of layers is 4 for the cross-ply and the angle-ply laminates, and 8 for the quasi-isotropic laminate. Symmetric edge delaminations are introduced by setting the penalty numbers equal to zero at the interfaces between 90 and 0 layers for the cross-ply, 45 and -45 layers for the angle-ply, and -45 and 0 layers for the quasi-isotropic laminate, respectively. For the rest of perfectly adhered interfaces, the penalty numbers are set equal to  $5 \times 10^5$  GPa/mm. The strain energy release rate  $G$  was calculated by using the virtual crack closure integral (VCCI) scheme presented in Equation (5.33). Note that the present VCCI scheme does not employ any kind of nodal values of relative displacements and forces, but interfacial gaps after crack extension and reaction forces prior to crack extension. The integrals for VCCI are exactly carried out by Gauss numerical integration.

Aoki and Kondo<sup>159</sup> examined this problem by using quasi-3-D isoparametric finite element analysis. In accordance with Aoki and Kondo, material data and laminate thickness are as follows:

$$\begin{aligned} 2h &= 1.12 \text{ mm} \\ E_L &= 130.9 \text{ GPa}, \quad E_T = 8.934 \text{ GPa} \\ \nu_{LT} &= 0.3213, \quad G_{LT} = G_{TT} = 4.648 \text{ GPa} \end{aligned}$$

Finite element meshes are produced for each of the three cases, so that the virtual crack length  $\Delta a$  is set equal to 0.025 mm when the delamination length  $a$  is less than or equal to 0.1 mm and 0.05 mm when  $a$  is greater than 0.1 mm. It should be noted that, in order to achieve the quasi-3-D state of the problem by the present fully 3-D layerwise plate element, only one quadrant of the laminates can be considered and only one finite element division in the axial direction are used in the case of the cross-ply laminate, while in the cases of the angle-ply and the quasi-isotropic laminate, the entire laminate are considered and fairly fine meshing in the axial direction are required because of the dominance of mode III.

Figures 5.24 through 5.26 present the strain energy release rate  $G$  against edge-delamination length  $a$  for cross-ply, angle-ply and quasi-isotropic laminates, respectively. These results consistently indicate that the results by the present FE agree fairly well to the results by Aoki and Kondo. Consequently, it is ensured that the present finite element can be successfully applied to the strain energy release rate calculation.

#### finite-length laminated coupon with edge delaminations

The present finite element is the fully 3-D model and therefore it can analyze the distributions of the energy release rate along the delamination front.

Figure 5.27 shows a typical grid work of finite element meshes in the finite-length laminated coupon with the straight edge delaminations. In order to simulate uniform axial extension around the central part apart from the ends, both ends are prescribed with respect to axial displacement  $u^{(k)}$ , that is,

$$U_0^{(k)} = \text{constant}, \quad U_1^{(k)} = U_2^{(k)} = U_3^{(k)} = 0$$

Since the angle-ply and the quasi-isotropic laminates exhibit mode III (i.e. out-of-plane tearing) strain/stress states, the end effect will become noticeable if the length of the coupon is not so large compared to the width and the thickness.



Figures 5.28 and 5.29, respectively, show distributions along the delamination front of the strain energy release rate  $G_{\text{total}}$  and  $G_{\text{III}}$  for the angle-ply laminate. Three cases of the delamination length,  $a = 0.03$  mm, 0.05 mm and 0.10 mm, are plotted. It is observed that  $G_{\text{total}}$  become small as the delamination front gets closer to the prescribed end. This is because mode III shearing are suppressed near the end as indicated in Figure 5.29. Similarly, Figures 5.30, 5.31 and 5.32 show distributions of  $G_{\text{total}}$ ,  $(G_{\text{II}} + G_{\text{III}})$  and  $G_{\text{I}}$  for the quasi-isotropic laminate, respectively. As for the quasi-isotropic, three cases of the delamination length,  $a = 0.05$  mm, 0.20 mm and 0.50 mm, are examined. In Figure 5.30, intense rises of  $G_{\text{total}}$  is observed near the end for every case of the delamination length. This is due to the steep rise of  $G_{\text{I}}$  near the end (it is ensured that  $\sigma_z$  is positive before the crack extension). This fact alerts a possibility of severe edge delaminations near the gripped ends in the tensile test coupons of this sort of stacking sequence for the quasi-isotropic laminates.

## 5.4 Discussion

A very accurate FE for N-layup laminated plate was developed, based on the displacement-based layerwise higher-order assumptions with the use of the penalty method.

The developed finite element was first applied to bending of a cross-ply laminate and the accuracy and the convergence property of the finite element were confirmed. The valid range of magnitude of the penalty numbers were also investigated.

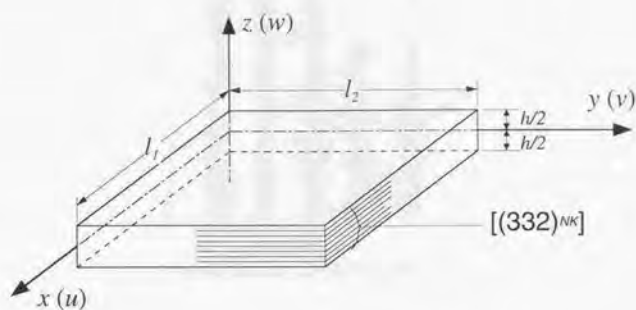
Next interlaminar stress evaluations were performed in the case of an angle-ply symmetric laminated strip under uniform axial extension. Fairly good agreements with the very precise boundary layer solutions based on the two-dimensional stress-function method are observed in a practical point of view. For the purpose of pursuing practical applications of the developed FE, interlaminar stress evaluations of a laminated strip with resin films inserted in the layer interfaces are carried out as well, and some interesting observations are obtained.

Finally, since the delamination phenomena in composite laminates are attracting much attention, a delamination modeling were proposed by setting the penalty numbers equal to zero. Furthermore, a new calculation scheme of strain energy release rates was also proposed. Comparative studies of developed FE and the existing numerical results shows the accuracy and validity of the proposed delamination modeling and the calculation scheme of strain energy release rates.

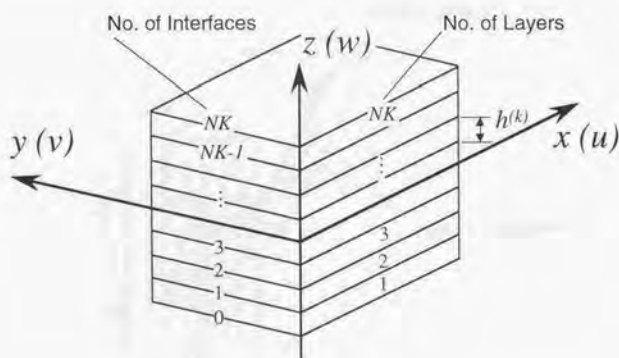
The present FE model is not a particular model for evaluating local stresses, but a



general and versatile model for fully three-dimensional structural analysis. Therefore, there are many practical cases considered to which the developed FE can be applied, such as calculations of stress fields and strain energy release rates for fully 3-D arbitrary shaped composite laminates.

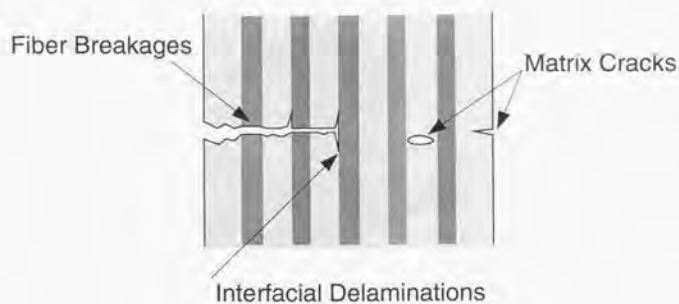


(a) geometry, coordinate and deformations

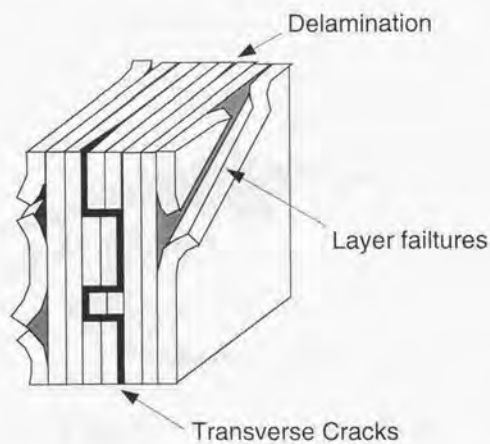


(b) through-the-thickness configurations

Figure 5.1 General laminated plate element – geometry and displacement assumptions

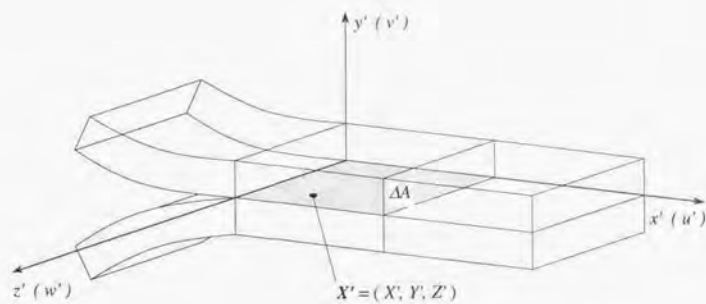


(a) Damages in a composite material

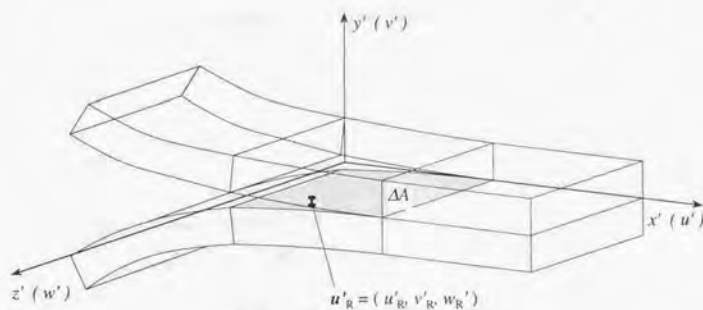


(b) Failures in a composite laminate

Figure 5.2 Various failures and damages in composite laminates



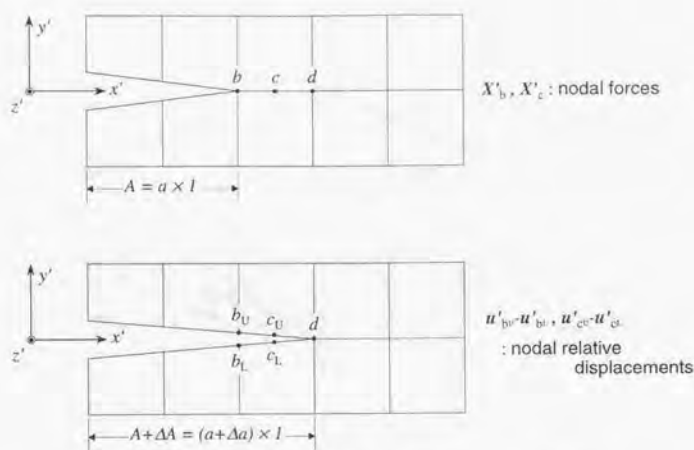
(a) prior to crack extension



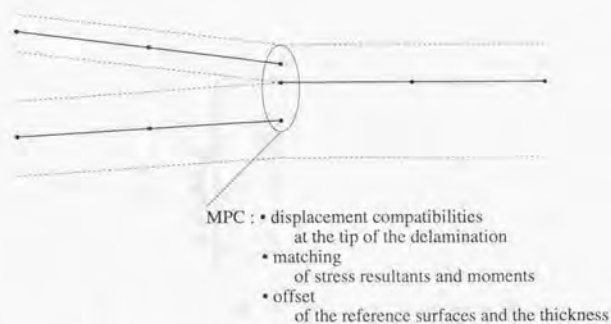
(b) after crack extension

Figure 5.3 Concept of virtual crack closure integral (VCCI)



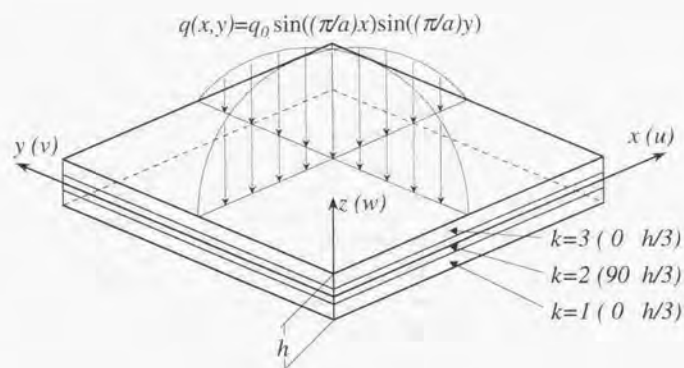


(a) Conventional VCCI by finite element analysis

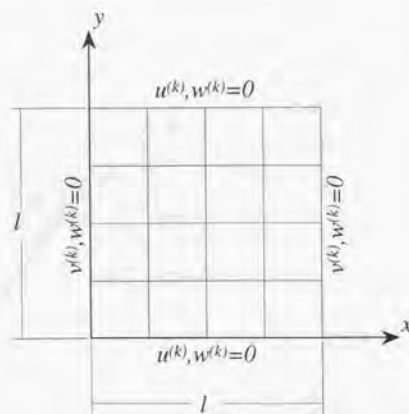


(b) Delamination modeling by ESL-based plate elements

Figure 5.4 Conventional modelings of delamination and crack extension in finite element analysis



(a) Perspective of the problem



(b) Top view of the problem and typical meshing and boundary conditions

Figure 5.5 Schematics of geometry, boundary conditions and finite element meshes for cross-ply square laminate under sinusoidal lateral load

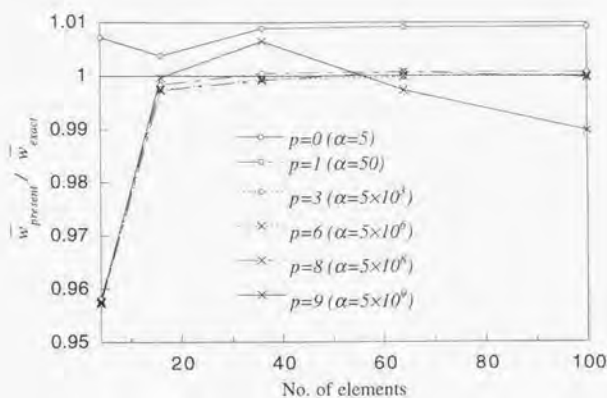


Figure 5.6 Central deflections at  $(1/2, 1/2, 0)$  against the square mesh refinement for various penalty numbers in case of  $S = 4$

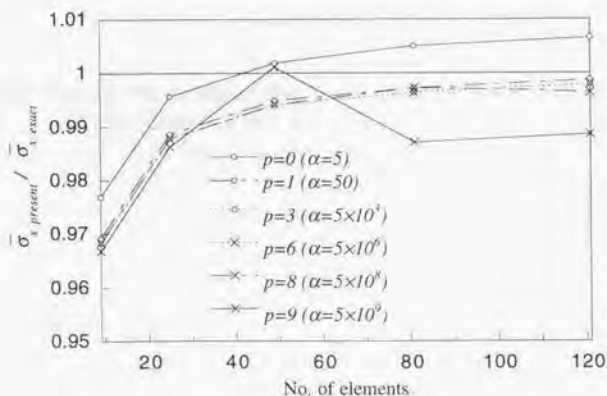


Figure 5.7 Central in-plane normal stresses at  $(1/2, 1/2, 1/2)$  against the square mesh refinement for various penalty numbers in case of  $S = 4$

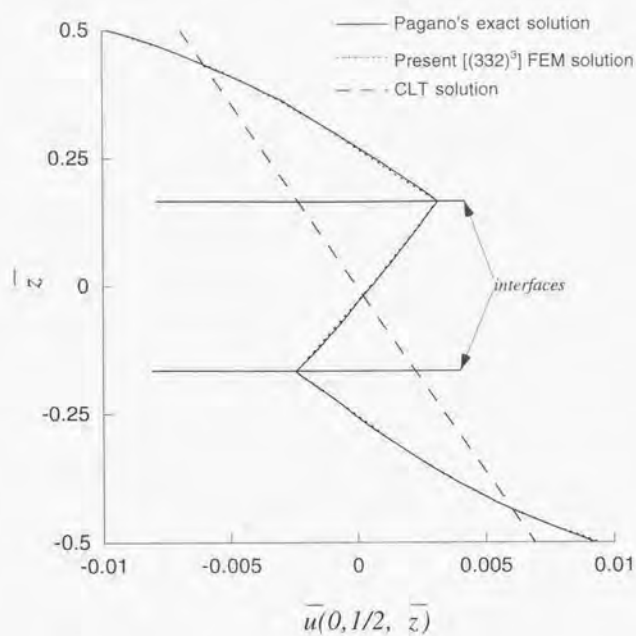


Figure 5.8 Through-the-thickness distributions of the in-plane displacement  $\bar{u}$  at  $(1/2, 1/2, z)$  in case of  $S = 4$



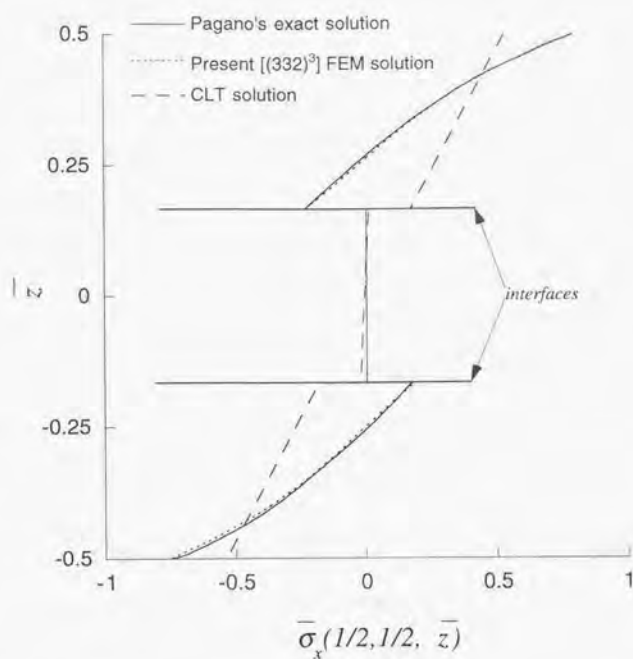


Figure 5.9 Through-the-thickness distributions of the in-plane normal stress  $\bar{\sigma}_x$  at  $(1/2, 1/2, \bar{z})$  in case of  $S = 4$

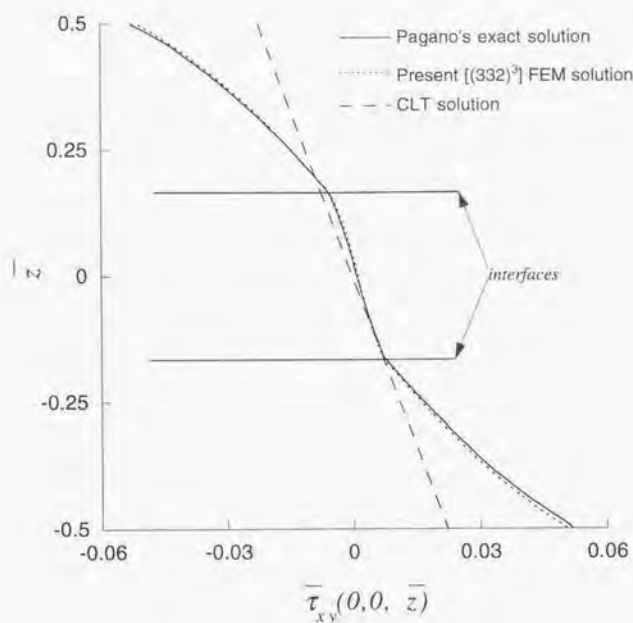
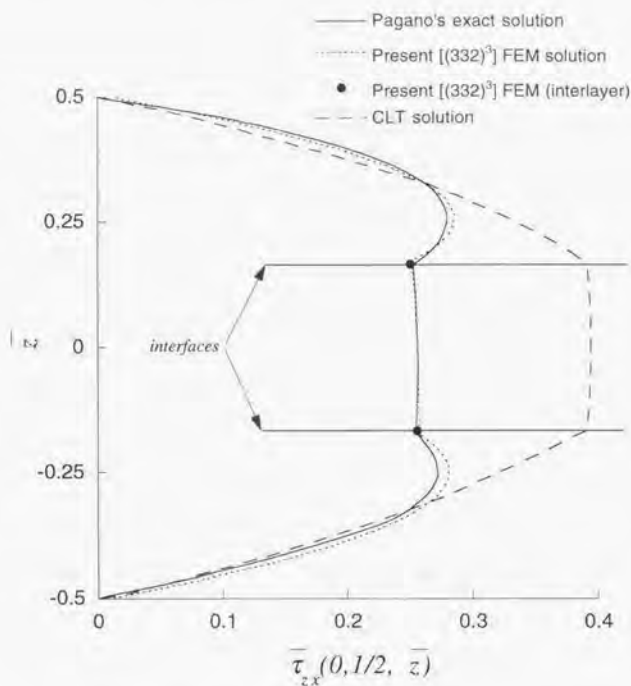


Figure 5.10 Through-the-thickness distributions of the in-plane shear stress  $\bar{\tau}_{xy}$  at  $(0,0,\bar{z})$  in case of  $S = 4$  (the present FEM solution is evaluated at the nearest Gauss point from the actual sampling point)



**Figure 5.11** Through-the-thickness distributions of the transverse shear stress and the interlaminar shear stress  $\bar{\tau}_{zx}$  at  $(0, 1/2, \bar{z})$  in case of  $S = 4$  (the present FEM solution is evaluated at the nearest Gauss point from the actual sampling point)

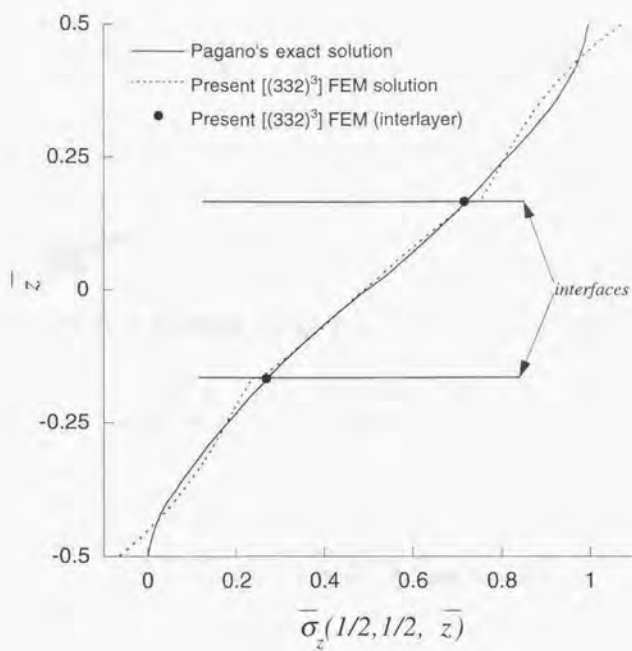
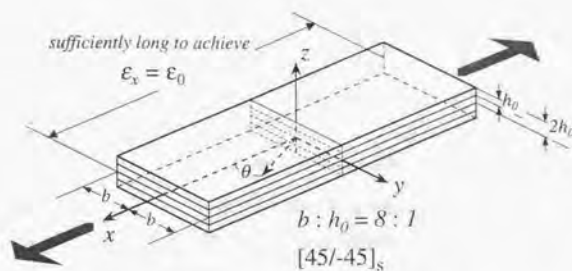


Figure 5.12 Through-the-thickness distributions of the transverse normal stress and the interlaminar normal stress  $\bar{\sigma}_z$  at  $(1/2, 1/2, \bar{z})$  in case of  $S = 4$

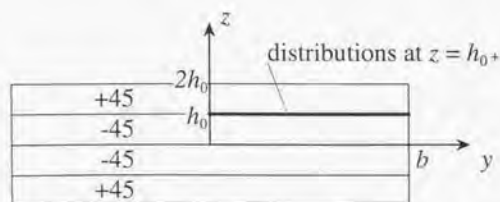




(a) Problem definition of angle-ply symmetric laminated strip



(b) Gridwork of finite element meshes



(c) Side view of the laminate and the evaluation interface

Figure 5.13 Problem definition for infinitely long laminated strip under uniform axial extension

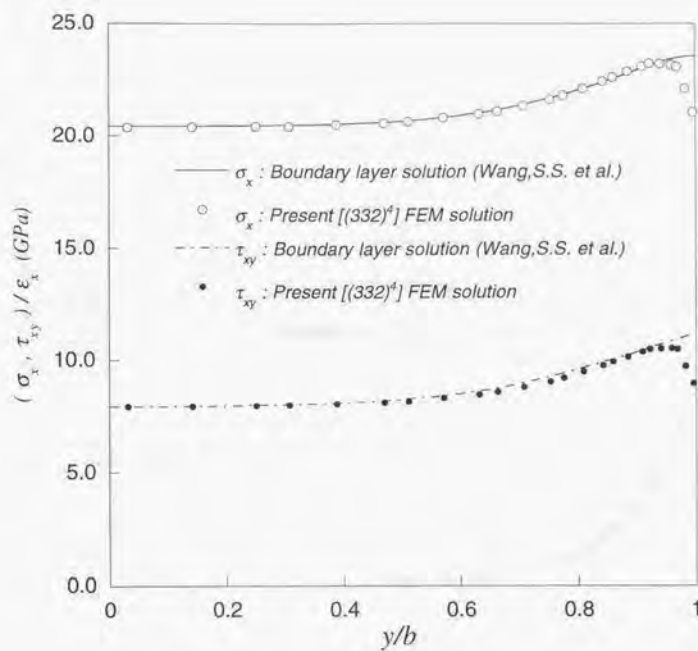
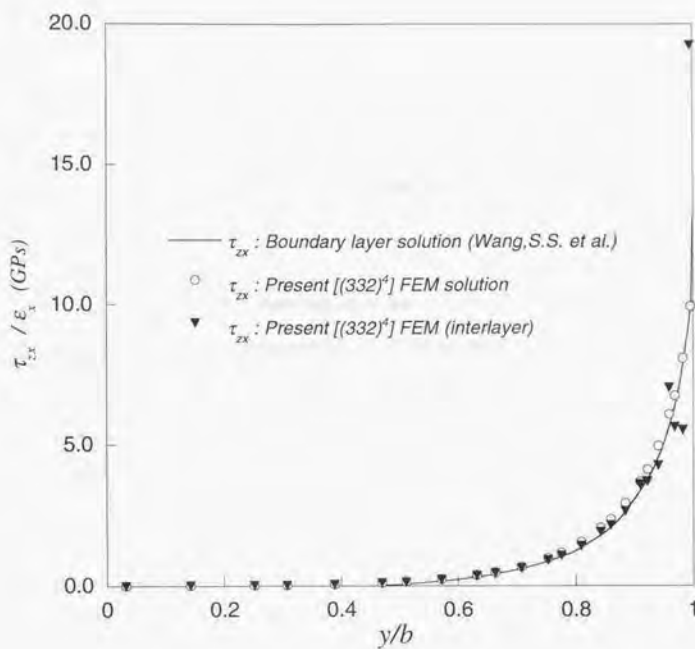


Figure 5.14 Variations of the in-plane stresses  $\sigma_x$  and  $\tau_{xy}$  at the layer interface along the width direction



**Figure 5.15** Variations of the interlaminar shear stress  $\tau_{zx}$  at the layer interface along the width direction

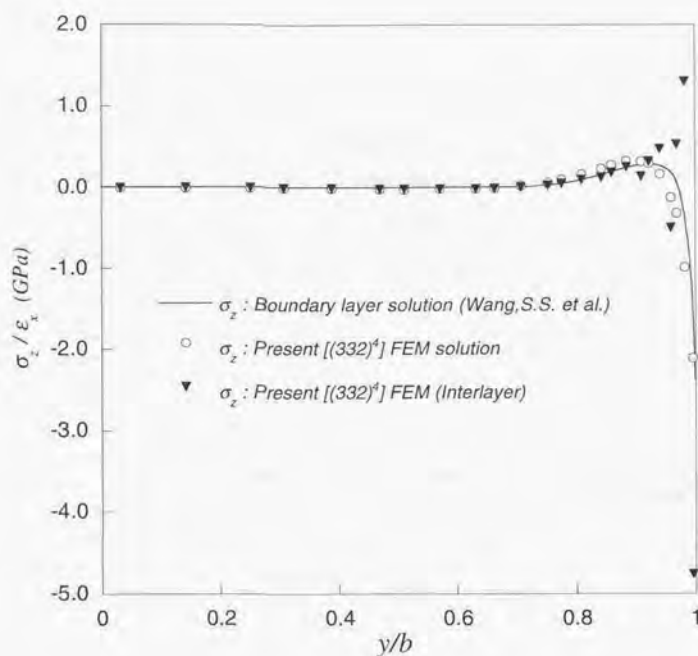


Figure 5.16 Variations of the interlaminar normal stress  $\sigma_z$  at the layer interface along the width direction



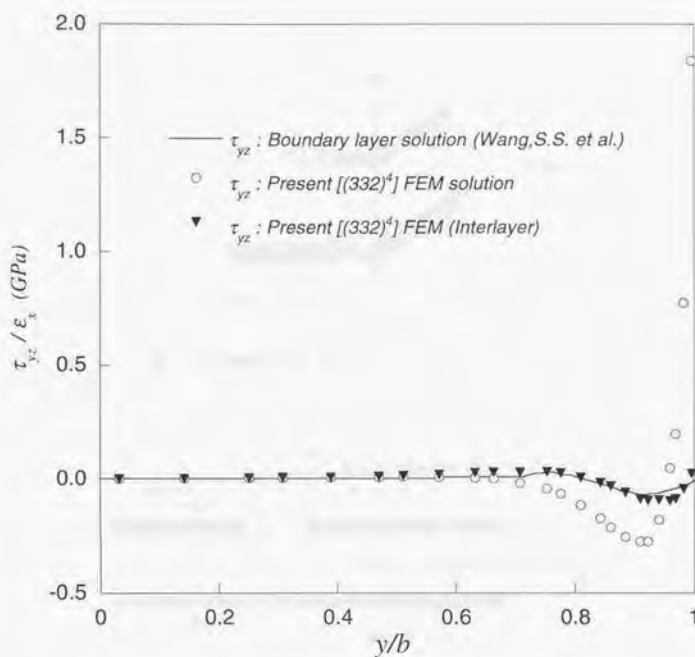
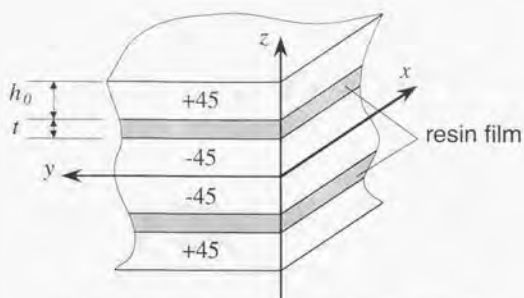
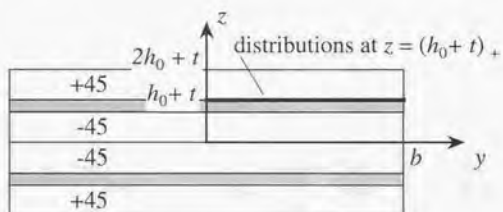


Figure 5.17 Variations of the interlaminar shear stress  $\tau_{yz}$  at the layer interface along the width direction



(a) Laminated strip with resin films inserted



(b) Side view of the laminate and the evaluation interface

**Figure 5.18** Schematics of through-the-thickness configurations of a laminated strip with resin films inserted

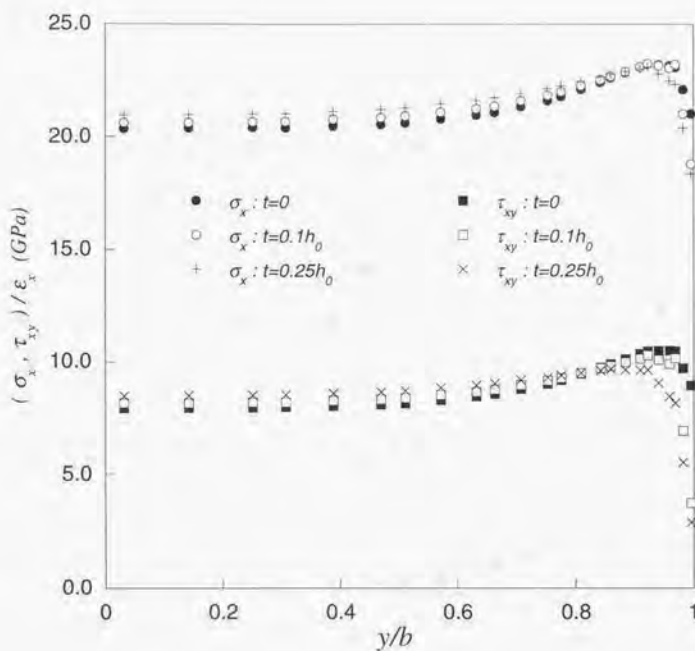


**Figure 5.19** Variations of the in-plane stresses  $\sigma_x$  and  $\tau_{xy}$  at the CFRP/resin-film interface along the width direction : solutions by the present [(332)<sup>6</sup>] FEM

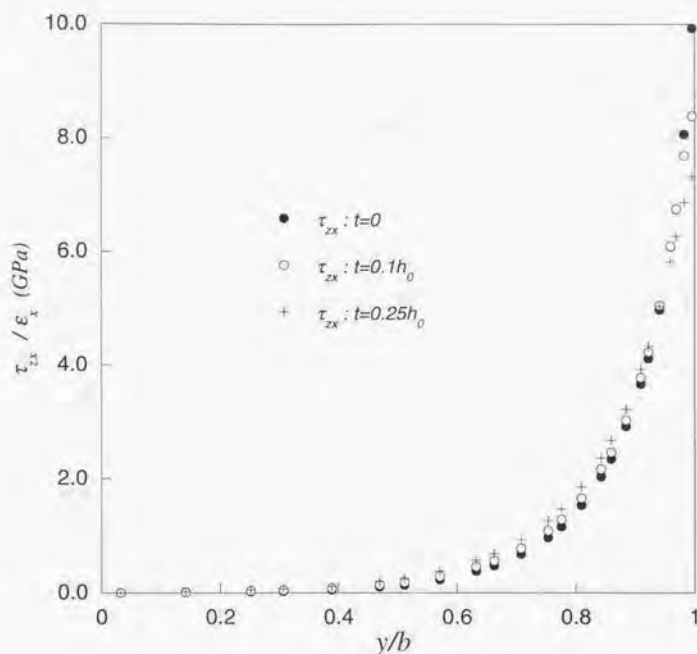
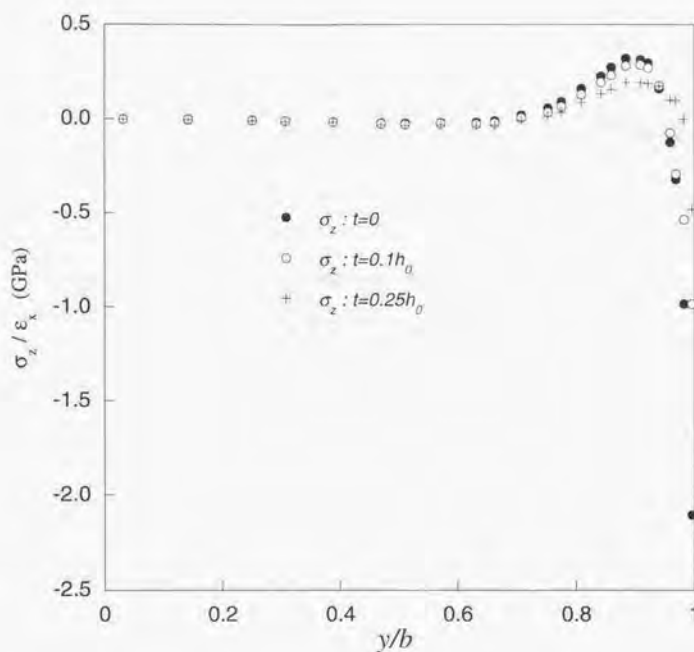
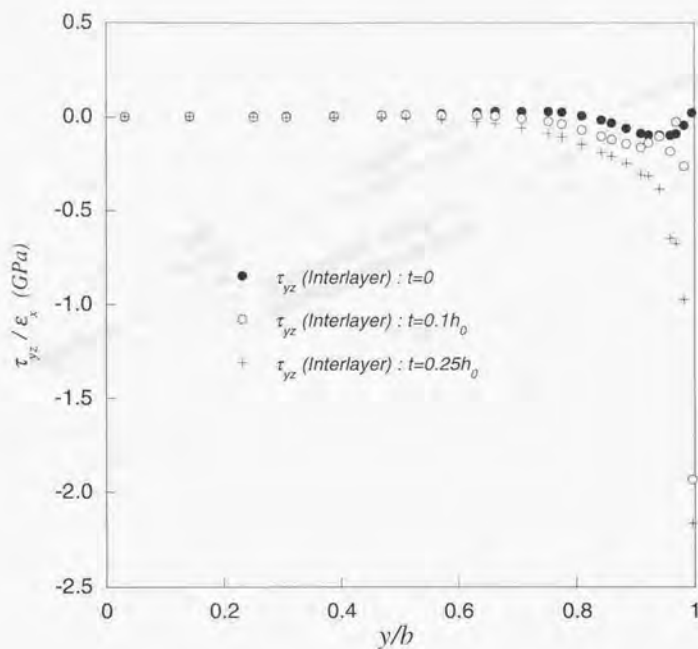


Figure 5.20 Variations of the interlaminar shear stress  $\tau_{zx}$  at the CFRP/resin-film interface along the width direction : solutions by the present [(332)<sup>6</sup>] FEM (evaluated from the constitutive equations)





**Figure 5.21** Variations of the interlaminar normal stress  $\sigma_z$  at the CFRP/resin-film interface along the width direction : solutions by the present [(332)<sup>6</sup>] FEM (evaluated from the constitutive equations)



**Figure 5.22** Variations of the interlaminar shear stress  $\tau_{yz}$  at the CFRP/resin-film interface along the width direction : solutions by the present [(332)<sup>6</sup>] FEM (directly evaluated from the displacement gaps and the penalty numbers)

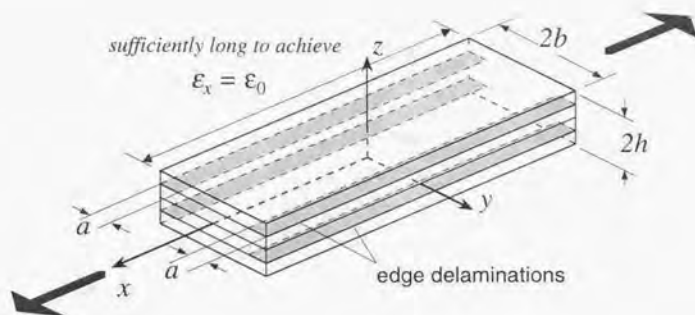


Figure 5.23 Problem definition of a infinitely long laminated strip with edge delaminations

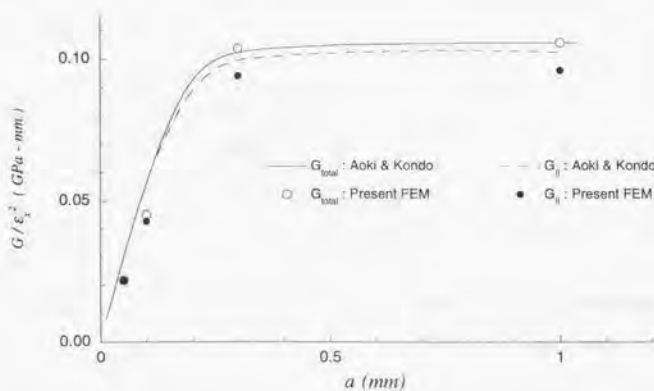


Figure 5.24 Strain energy release rate  $G$  versus delamination length  $a$  for cross-ply laminate  $(90/0)_s$ ,  $2h = 1.12$  mm; the present solutions are obtained by  $[(332)^4]$  FEM

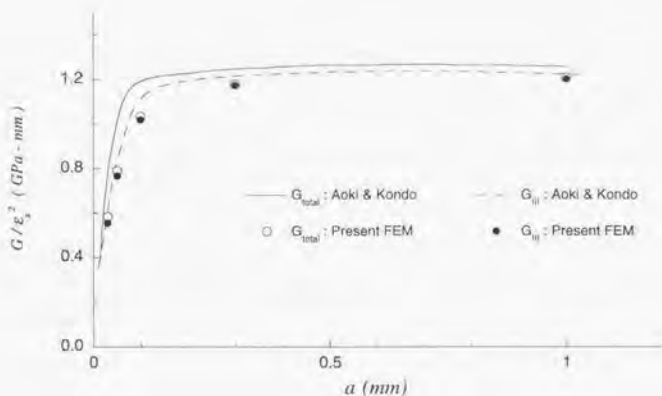


Figure 5.25 Strain energy release rate  $G$  versus delamination length  $a$  for angle-ply laminate  $(45/-45)_8$ ,  $2h = 1.12$  mm; the present solutions are obtained by  $[(332)^4]$  FEM

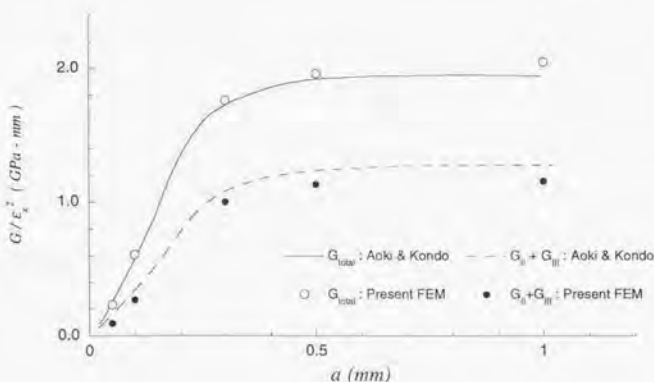
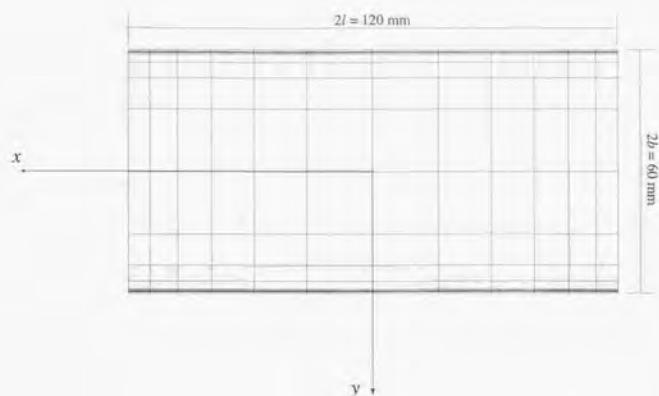


Figure 5.26 Strain energy release rate  $G$  versus delamination length  $a$  for quasi-isotropic laminate  $(45/-45/0/90)_8$ ,  $2h = 1.12$  mm; the present solutions are obtained by  $[(332)^8]$  FEM (delaminations assumed at  $-45/0$  interfaces)





**Figure 5.27** Typical gridwork of finite element meshes for finite-length laminate coupon with edge delamination in case of  $a = 0.3 \text{ mm}$

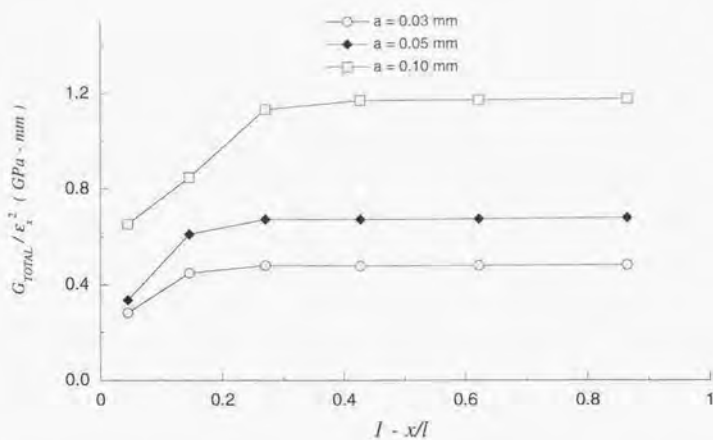
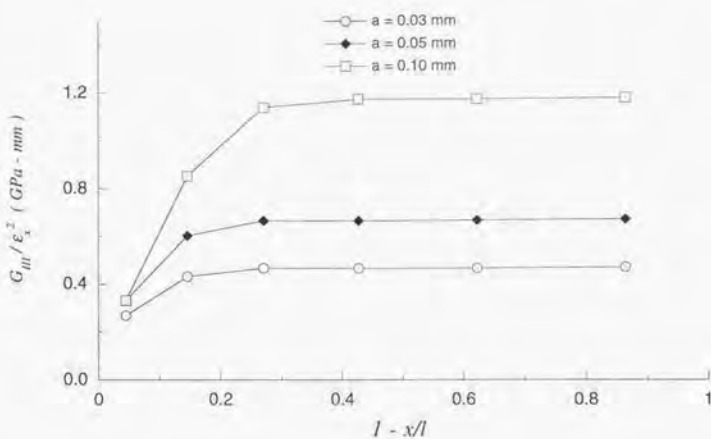
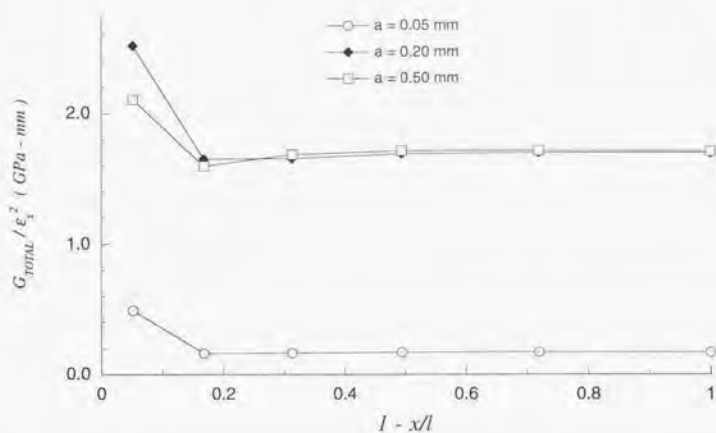


Figure 5.28 Distributions of the energy release rate  $G_{total}$  along the delamination front for several cases of delamination length  $a$  for angle-ply laminate  $(45/-45)_s$ ,  $2h = 1.12$  mm ; the present solutions are obtained by [(332)<sup>4</sup>] FEM



**Figure 5.29** Distributions of the energy release rate  $G_{III}$  along the delamination front for several cases of delamination length  $a$  for angle-ply laminate  $(45/-45)_s$ ,  $2h = 1.12$  mm; the present solutions are obtained by  $[(332)^4]$  FEM



**Figure 5.30** Distributions of the energy release rate  $G_{\text{total}}$  along the delamination front for several cases of delamination length  $a$  for quasi-isotropic laminate  $(45/-45/0/90)_s$ ,  $2h = 1.12$  mm; the present solutions are obtained by [(332)<sup>8</sup>] FEM (delaminations assumed at  $-45/0$  interfaces)



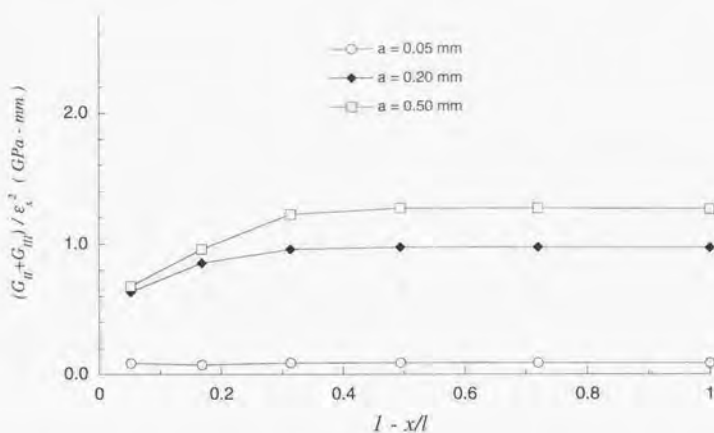


**Figure 5.31** Distributions of the energy release rate ( $G_{II} + G_{III}$ ) along the delamination front for several cases of delamination length  $a$  for quasi-isotropic laminate  $(45/-45/0/90)_s$ ,  $2h = 1.12$  mm; the present solutions are obtained by [(332)<sup>8</sup>] FEM (delaminations assumed at  $-45/0$  interfaces)

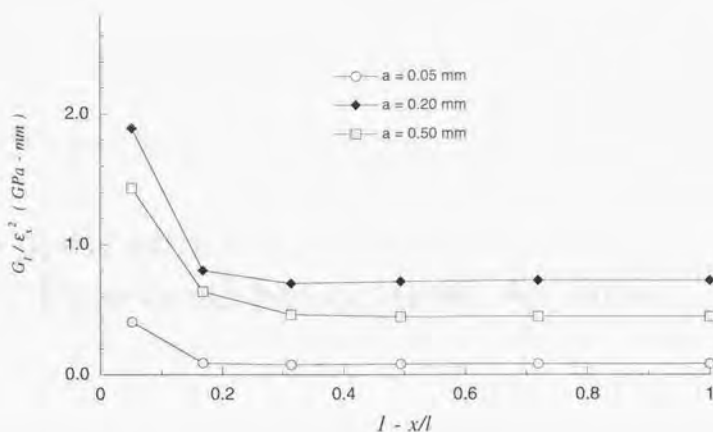


**Figure 5.32** Distributions of the energy release rate  $G_I$  along the delamination front for several cases of delamination length  $a$  for quasi-isotropic laminate  $(45/-45/0/90)_s$ ,  $2h = 1.12$  mm; the present solutions are obtained by  $[(332)^8]$  FEM (delaminations assumed at  $-45/0$  interfaces)

## Chapter 6

### Applications to Practical Structural Analysis

## 6.1 Introduction to this chapter

The recent widespread use of advanced composite materials (ACM) for the primary structural members in various industrial fields necessitates efficient analysis tools which is capable of more accurately predicting their mechanical attributes. Especially, precise evaluations of elastic response and initiation of failures peculiar to this inhomogeneous and anisotropic material under multi-axial service load conditions are highly required.

In this chapter, as the final examples derived from the layerwise higher-order model of the author, a couple of applications for practical structural analysis is to be shown.

## 6.2 Application to general shell laminates

Since almost all structural components made of composite laminates are fully three-dimensional (3-D) and arbitrary shaped shell structures, a general and versatile shell model for composite laminates is becoming of more and more importance.

Historical progress of numerical shell models for composite laminates is quite analogous to that of plate models, but a bit delayed. Detailed survey of analytical and numerical shell models for laminated composite material structures (composite laminates) up to the end of 1980's were made by Noor and Burton<sup>170</sup>. Early investigations on composite laminated shells had focuses on two dimensional (2-D) analytical shell models deduced from three-dimensional (3-D) elasticity theory. Following several proposals of membrane shell models for anisotropic and laminated shells, CPT models based on Love's first approximation<sup>171</sup> were applied to orthotropic laminated thin shells of simple geometry such as cylindrical shells by Ambartsumyan<sup>6</sup>, Dong, Pister and Taylor<sup>8</sup>, Cheng and Ho<sup>172</sup> and Whitney<sup>173</sup>. Applications of FOSDT models to laminated cylindrical shells were made by Gulati and Essenberg<sup>174</sup>, Zukas and Vinson<sup>175</sup>, Dong and Tso<sup>176</sup> and Bert *et al.*<sup>177, 178</sup>. Reddy<sup>179</sup> and Reddy *et al.*<sup>180</sup> established the analytical solutions of doubly-curved laminated shells based on FOSDT assumption.

As one of the earliest ESL-based higher-order models for laminated shells, HOT cylindrical shells based on Love's second approximation<sup>171</sup> was investigated by Whitney<sup>173</sup> and then Whitney and Sun<sup>43, 181</sup>. Later, Reddy and Liu<sup>182</sup> extended Reddy's third-order theory (HOT of Reddy)<sup>28</sup> to doubly-curved laminated shells. Kant and Menon<sup>183, 184</sup> and Mallikarjuna and Kant<sup>185</sup> also developed ESL-based cylindrical and doubly-curved shell finite element based on [(330)] HOT assumptions.



On the other hand, several efforts for ML-based laminated shell models were made by Hsu and Wang<sup>186</sup>, Barbero, Reddy and Teply<sup>187</sup>, Wu and Liu<sup>188</sup> for cylindrical laminated shells, and by Epstein and Glockner<sup>189</sup>, Di Sciuva<sup>190</sup>, Fraternali and Reddy<sup>191</sup>, Verijenko<sup>91,92</sup> and Cho *et al.*<sup>191</sup> for doubly curved laminated shells.

Although these classical and refined two-dimensional (2-D) shell models for composite laminates cited above are mathematically rigorous and substantially sophisticated in exchange for their rather complicated formulations, they are restricted to simple geometry like cylindrical and spherical shells and a few primitive load and boundary conditions, and hence they are not always attractive for the analysis and design of composite laminates from an engineering point of view.

On the other hand, since a fully three-dimensional (3-D) versatile shell element which is degenerated from the 3-D continuum solid representation was given birth to by Ahmad, Irons and Zienkiewicz<sup>4</sup> and then refined with several research efforts<sup>5, 192, 193, 194, 195</sup>, this degenerated 3-D shell element have been dominantly used for single-layer isotropic shells. And hence it was not long before this versatile shell element was extended to composite laminates. Following the first attempt made by Panda and Natarajan<sup>196</sup> who straightforwardly extended this 3-D shell element to composite laminates, numerous contributions to its refinement and further extension have been made in the literature<sup>197, 198, 199, 200, 201, 202</sup>. Corresponding to the progress of the laminated plate models and the laminated 2-D shell models, the refinement of the laminated degenerated 3-D shell element has also been directed towards higher-order<sup>203</sup> and multi-layer<sup>71, 61, 63, 204</sup> considerations.

In this section, a layerwise laminated degenerated 3-D shell element is developed for fully 3-D and arbitrary shaped composite laminates. The accuracy and convergence property of the developed shell element are ensured in the case of simply-supported cross-ply spherical shells.

### 6.2.1 Layerwise laminated degenerated 3-D shell element

The present degenerated 3-D shell element can be viewed as an extension of the general laminated plate element presented in the previous chapter, that is:

- The present FE can exactly model a laminated shell composed of the unlimited number of different material layups (N-layered shell model);
- The displacement assumption  $[(332)^{NK}]$  is employed.
- The interfacial displacement constraints are approximated by the penalty method;

- The interlaminar stresses are directly evaluated from the small displacement gaps and the penalty numbers at the interfaces between the adjacent layers.

The degenerated shell element concept is used in the formulation of the present arbitrary curved layerwise laminated shell element.

### shell geometry

In Figure 6.1, the present eight-node degenerated 3-D shell element is schematically shown. The geometry of the element is defined by interpolating the nodal point coordinates at mid-surface of the laminate as follows:

$$\begin{Bmatrix} x \\ y \\ z \end{Bmatrix}^{(k)} = \sum_{J=1}^8 \Phi_J \begin{Bmatrix} x_J \\ y_J \\ z_J \end{Bmatrix}^{(k)} + \sum_{J=1}^8 \Phi_J \frac{h_J^{(k)}}{2} \zeta \hat{\mathbf{V}}_{nJ} \quad (6.1)$$

where

$(\xi, \eta, \zeta)$  : natural curvilinear coordinates

$\Phi_J(\xi, \eta)$ ;  $J = 1, 2, \dots, 8$  : shape functions

$\begin{Bmatrix} x_J \\ y_J \\ z_J \end{Bmatrix}^{(k)}$  : sub-nodal coordinates for the mid-surface of the  $k^{\text{th}}$  layer

$h_J^{(k)}$  : sub-nodal thickness of the  $k^{\text{th}}$  layer

and  $\hat{\mathbf{V}}_{nJ}$  is the nodal unit vector normal to the mid-surface of the laminate. In this formulation,  $\hat{\mathbf{V}}_{nJ}$  is defined by input data so as to exactly be normal to the actual mid-surface of the laminated shell, not to the elemental mid-surface generated in the program from the nodal coordinate as defined by the first term of the right-hand side in Equation (6.1). Note that this modification enforces the compatibility of the generalized displacement components adjacent elemental boundaries.

The nodal unit vectors  $\hat{\mathbf{V}}_{LJ}$  and  $\hat{\mathbf{V}}_{TJ}$  tangential to the mid-surface of the laminate are also introduced. Similarly to the case of  $\hat{\mathbf{V}}_{nJ}$ ,  $\hat{\mathbf{V}}_{LJ}$  is defined by input data so that it coincides with a reference principal direction for orthotropic materials (i.e. 0 deg. direction). On the other hand,  $\hat{\mathbf{V}}_{TJ}$  which is perpendicular to both  $\hat{\mathbf{V}}_{nJ}$  and  $\hat{\mathbf{V}}_{LJ}$  can be obtained from the following vector product:

$$\hat{\mathbf{V}}_{TJ} = \hat{\mathbf{V}}_{nJ} \times \hat{\mathbf{V}}_{LJ}$$

These mutually perpendicular vectors  $\hat{\mathbf{V}}_{LJ}$ ,  $\hat{\mathbf{V}}_{TJ}$  and  $\hat{\mathbf{V}}_{nJ}$  constitute a orthogonal coordinate axes at the nodal point, and then nodal direction cosine matrix  $\boldsymbol{\mu}_J$  is defined

as follows:

$$\mu_J = [\hat{V}_{L,J} \quad \hat{V}_{T,J} \quad \hat{V}_{n,J}] = \begin{bmatrix} l_{L,J} & l_{T,J} & l_{n,J} \\ m_{L,J} & m_{T,J} & m_{n,J} \\ n_{L,J} & n_{T,J} & n_{n,J} \end{bmatrix} \quad (6.2)$$

After nodal coordinate system is defined, next the local coordinate system  $(x', y', z')$  should also be defined for describing local components of displacements, strains and stresses at any point within the shell element.

In the original scheme <sup>4, 196</sup>, the local coordinate base axes at any point  $(\xi, \eta)$  are defined with respect to the natural curvilinear coordinates such that:

$$V'_n = \frac{V_\xi \times V_\eta}{|V_\xi \times V_\eta|} \quad (6.3)$$

in which

$$V_\xi = \left\{ \frac{\partial x}{\partial \xi} \quad \frac{\partial y}{\partial \xi} \quad \frac{\partial z}{\partial \xi} \right\}^T$$

$$V_\eta = \left\{ \frac{\partial x}{\partial \eta} \quad \frac{\partial y}{\partial \eta} \quad \frac{\partial z}{\partial \eta} \right\}^T \quad (6.4)$$

and

$$V'_{L,J} = \frac{V_\xi}{|V_\xi|}, \quad V'_{T,J} = \frac{V'_n \times V_\xi}{|V'_n \times V_\xi|} \quad (6.5)$$

This local coordinate system in the original scheme are, however, can not represent locally varying material directions, i.e., "the drapability effect" which has been underlined in Chapter 2.

In order to include "the drapability effect" in the formulation, an alternative scheme of the author <sup>23, 199</sup> for defining local coordinate axes is introduced in the present formulation. The local coordinate system can be obtained by interpolating into any point  $(\xi, \eta)$  on the mid-surface the foregoing nodal orthogonal vectors  $\hat{V}_{L,J}$ ,  $\hat{V}_{T,J}$  and  $\hat{V}_{n,J}$ , such that:

$$[\hat{V}'_{L,J} \quad \hat{V}'_{T,J} \quad \hat{V}'_{n,J}] = \sum_{J=1}^8 \Phi_J [\hat{V}_{L,J} \quad \hat{V}_{T,J} \quad \hat{V}_{n,J}] \quad (6.6)$$

and then local direction cosine matrix  $\mu'$  is defined as follows:

$$\mu' = [\hat{V}'_{L,J} \quad \hat{V}'_{T,J} \quad \hat{V}'_{n,J}] = \begin{bmatrix} l'_L & l'_T & l'_n \\ m'_L & m'_T & m'_n \\ n'_L & n'_T & n'_n \end{bmatrix} \quad (6.7)$$

Although the number of the functions for evaluating the element stiffness matrix increases if the locally varying material directions are taken into consideration, as

presented in Equation (6.3), the present scheme is more flexible than the original in that it is capable of modeling the "drapability effect" of composite laminates as illustrated in Figure 6.1(c) and it is indispensable for satisfactory analysis and design of composite laminates.

Finally, any first derivative regarding to global coordinate  $(x, y, z)$  are obtained by:

$$\frac{\partial}{\partial(x, y, z)} = [\mathbf{J}]^{-1} \frac{\partial}{\partial(\xi, \eta, \zeta)} \quad (6.8)$$

where the Jacobian matrix  $\mathbf{J}$  is defined as:

$$\mathbf{J} = \frac{\partial(x, y, z)}{\partial(\xi, \eta, \zeta)} \quad (6.9)$$

and then any first derivative with respect to local coordinate  $(x', y', z')$  can be obtained by using the transformation relation between the local and global coordinates as follows:

$$\frac{\partial}{\partial(x', y', z')} = [\boldsymbol{\mu}']^T \left[ \frac{\partial}{\partial(x, y, z)} \right] [\boldsymbol{\mu}'] \quad (6.10)$$

It should be supplemented that, when a quantity regarding to the local coordinate is independent of the normal direction (i.e.  $z'$ ), then the two-dimensional Jacobian is available which is defined as,

$$\mathbf{J}^{2D} = \begin{bmatrix} \mathbf{V}_\xi \cdot \hat{\mathbf{V}}'_L & \mathbf{V}_\xi \cdot \hat{\mathbf{V}}'_T \\ \mathbf{V}_\eta \cdot \hat{\mathbf{V}}'_L & \mathbf{V}_\eta \cdot \hat{\mathbf{V}}'_T \end{bmatrix} \quad (6.11)$$

and in that case, derivatives regarding to the local coordinate can be simplified as follow:

$$\left\{ \frac{\partial}{\partial x'} \right\} = \left\{ I_{11} \frac{\partial}{\partial \xi} + I_{12} \frac{\partial}{\partial \eta} \right\}$$

$$\left\{ \frac{\partial}{\partial y'} \right\} = \left\{ I_{21} \frac{\partial}{\partial \xi} + I_{22} \frac{\partial}{\partial \eta} \right\} \quad (6.12)$$

whereas  $I_{ij}$ ;  $i, j = 1, 2$  are the components of the inverse of the 2-D Jacobian:

$$[\mathbf{J}^{2D}]^{-1} = \begin{bmatrix} I_{11} & I_{12} \\ I_{12} & I_{22} \end{bmatrix}$$

### $[(332)^{NK}]$ displacement assumption

The displacement components at any point in the  $k^{\text{th}}$  layer can be obtained as follows:

$$\begin{Bmatrix} u \\ v \\ w \end{Bmatrix}^{(k)} = \boldsymbol{\mu}' \begin{Bmatrix} u' \\ v' \\ w' \end{Bmatrix}^{(k)}$$



$$= \sum_{J=1}^8 \Phi_J \mu_J \left[ \begin{Bmatrix} U'_0 \\ V'_0 \\ W'_0 \end{Bmatrix}_J + \left(\frac{h_J}{2}\zeta\right) \begin{Bmatrix} U'_1 \\ V'_1 \\ W'_1 \end{Bmatrix}_J + \left(\frac{h_J}{2}\zeta\right)^2 \begin{Bmatrix} U'_2 \\ V'_2 \\ W'_2 \end{Bmatrix}_J + \left(\frac{h_J}{2}\zeta\right)^3 \begin{Bmatrix} U'_3 \\ V'_3 \\ 0 \end{Bmatrix}_J \right]^{(k)} \quad (6.13)$$

and hence the local displacements  $(u', v', w')$  measured in the local coordinate system are

$$\begin{Bmatrix} u' \\ v' \\ w' \end{Bmatrix}^{(k)} = \sum_{J=1}^8 \Phi_J [\mu_J]^T \mu_J \left[ \begin{Bmatrix} U'_0 \\ V'_0 \\ W'_0 \end{Bmatrix}_J + \left(\frac{h_J}{2}\zeta\right) \begin{Bmatrix} U'_1 \\ V'_1 \\ W'_1 \end{Bmatrix}_J + \left(\frac{h_J}{2}\zeta\right)^2 \begin{Bmatrix} U'_2 \\ V'_2 \\ W'_2 \end{Bmatrix}_J + \left(\frac{h_J}{2}\zeta\right)^3 \begin{Bmatrix} U'_3 \\ V'_3 \\ 0 \end{Bmatrix}_J \right]^{(k)} \quad (6.14)$$

The generalized displacement vector  $\delta'$  are defined as,

$$[\delta']^T = \left\{ [\delta^{(1)}]^T \dots [\delta^{(k)}]^T \dots [\delta^{(NK)}]^T \right\} \quad (6.15)$$

in which the  $k^{\text{th}}$  sub-vector in  $\delta'$  are

$$[\delta^{(k)}]^T = \{U'_0 \ V'_0 \ W'_0 \ U'_1 \ V'_1 \ W'_1 \ U'_2 \ V'_2 \ W'_2 \ U'_3 \ V'_3\}^{(k)} \quad (6.16)$$

The strain-displacement relations, the constitutive equations and then the interface continuity constraints via the penalty method can be obtained from almost the same procedure as in the case of the  $[(332)^{NK}]$  layerwise plate element already described in the previous chapter, and hence they will not be repeated here. Similarly, the rest of the finite element development procedure is already established and is not necessary for improvement in the present formulation, and hence it will not be repeated as well. One can refer to the precedent literature such as the works of Ahmad *et al.*<sup>4</sup>, Panda *et al.*<sup>196</sup> and Chao and Reddy<sup>197</sup> for further details of the degenerated 3-D shell element and its application to composite laminates.

### 6.2.2 Spherical shell under uniformly distributed pressure

For demonstrating the validity of the developed general shell element, a simple numerical example which is analogous to that of the preceding plate element is shown here. That is the  $[0/90/0]_t$  cross-ply spherical shell with its all four edges fully simply-supported and the uniformly lateral pressure is applied on the upper surface. Schematics of the problem definitions are given in Figure 6.2.



The same elastic properties as in the case of the foregoing plate example are used:

$$\begin{aligned} E_L/E_T &= 25, & \nu_{LT} &= \nu_{TL} = 0.25 \\ G_{LT}/E_T &= 0.5, & G_{TT}/E_T &= 0.2 \end{aligned}$$

In consistence with Pagano's manner, obtained results are non-dimensionalized as follows:

$$\text{for displacements: } \bar{w}' = \left( \frac{1000E_T}{q_0 h S^4} \right) w' \quad \bar{u}' = \left( \frac{100E_T}{q_0 h S^3} \right) u'$$

$$\text{for in-plane stresses: } \bar{\sigma}_{x'} = \left( \frac{1}{q_0 S^2} \right) \sigma_{x'} \quad \bar{\tau}_{x'y'} = \left( \frac{1}{q_0 S^2} \right) \tau_{x'y'}$$

$$\text{for transverse stresses: } \bar{\tau}_{z'x'} = \left( \frac{1}{q_0 S} \right) \tau_{z'x'} \quad \bar{\tau}_{y'z'} = \left( \frac{1}{q_0 S} \right) \tau_{y'z'} \quad \bar{\sigma}_{z'} = \left( \frac{1}{q_0} \right) \sigma_{z'}$$

where  $S = l/h$ ,  $l$  = span length,  $h$  = total thickness of the laminate and  $p_0$  is the uniformly distributed lateral load.  $\bar{z}' = z'/h$  is also defined as the normalized local coordinates through the thickness measured from the middle plane of the laminate, and  $\bar{x}' = x'/l$  and  $\bar{y}' = y'/l$ , as the normalized local in-plane coordinates. Besides every penalty number in the three directions is set equal to the same value  $\alpha$ .

Unfortunately, in this case of the spherical shell, exact elastic solutions to be compared with as in the case of the plate are not available. Instead of exact elastic solutions, ESL-based closed-form solutions were obtained by Reddy<sup>179</sup> for FOSDT and by Reddy and Liu<sup>182</sup> for HOT of Reddy, and hence they will also be, if available, shown for comparison.

The normalized deflections  $\bar{w}'$  at the center point  $(x', y', z') = (1/2, 1/2, 0)$  and the in-plane normal stresses  $\bar{\sigma}_{x'}$  at the quarter point  $(x', y', z') = (1/4, 1/4, 1/2)$  for various penalty parameters in the case of the span-to-thickness ratio  $S = 10$ , are plotted against square mesh refinements in Figures 6.3 and 6.4, respectively. The results indicate the same tendency as in the case of the plate. The rapid convergence to a certain specific values is observed for both deflections and in-plane normal stresses when the penalty number's magnitude:

$$p = \log \left( \frac{\alpha}{h \sqrt{E_L E_T}} \right)$$

is in the range of 3 to 8. The results obtained by setting  $p$  less than 3 converge to overestimated values because the displacement gaps at the layer-interfaces become prominent, while in the cases that  $p$  is greater than 8, the results diverge because of

numerical errors in solving the linear equations. All the following results are obtained by setting  $p = 5$ .

In Table 6.1, the non-dimensionalized central deflections obtained from various models are compared for a couple of radius-to-span  $R/l$  and span-to-thickness  $S = l/h$  ratios. In case of  $S = 10$  (that is thick shell), influence of multi-layer and higher-order deformation is evident, for the present FE provide larger deflections than FOSDT and HOT of Reddy.

Figure 6.5 shows the in-plane displacement distributions through the thickness at  $(\bar{x}', \bar{y}') = (1/4, 1/4)$  in the case of  $S = 10$  for three cases of radius-to-span ratios, i.e.,  $R/l = 1$  (deep), 10 (middle) and 100 (shallow). It is observed that in case of deep shell  $R/l = 1$ , membrane contribution is dominant, and as  $R/l$  is smaller, results become closer to that of the plate.

Figures 6.6 and 6.7 show the through-the-thickness distributions of the in-plane normal stress  $\bar{\sigma}_{x'}$  and in-plane shear stress  $\bar{\tau}_{x'y'}$  at  $(\bar{x}', \bar{y}') = (1/4, 1/4)$ , respectively. On the other hand, Figures 6.8 through 6.10 show the through-the-thickness distributions of the transverse stresses  $\bar{\tau}_{z'x'}$ ,  $\bar{\tau}_{y'z'}$  and  $\bar{\sigma}_{z'}$ , respectively, at  $(\bar{x}', \bar{y}') = (1/4, 1/4)$ . For the transverse stresses, in addition to the intralayer stresses evaluated from the constitutive equations, the pointwise values of interlayer stresses can be evaluated from the small gaps and the penalty numbers therefore these values are also plotted (two black solid marks at the layer-interfaces in the graphs). It is notable that these results consistently show that deep shell (i.e.,  $R/l = 1$ ) exhibit substantially different through-the-thickness distributions of displacement and stresses from those in case of  $R/l = 10$  and 100.

### 6.3 Application to structural joint in laminates

Joints are one of the most challenging aspects for engineers and designers in the analysis and design of composite laminates. No composite products are free from joints, even though the number of portions to be jointed will be substantially decreased compared to that of metallic counterparts. For composite laminates, two distinct types of joint are available, that is, mechanical joint and adhesive joint. Mechanical joints such as bolted and rivet joints usually need cutouts in the laminates, and this will cause severe stress concentrations and free-edge stresses around the cutouts. For the structural joints of composite laminates, therefore, adhesive joint has been preferably used.

Since the overall structural strength of composite products is dominantly governed

by strength of jointed regions, nowadays the context of experimental and numerical investigations of joints are very active. For instance, recently Kimpara *et al.* including the author<sup>205, 206</sup> have conducted a series of static strength tests of adhesively jointed GFRP for several cases of different adhesives and bonding processes. Figures 6.11 and 6.12 are photographic views of the actual tests conducted by Kimpara *et al.* including the author.

As for the numerical analysis of Joint regions, numerous attempts have been made by many researchers such as Roy and Reddy<sup>207</sup>, Barbero *et al.*<sup>208</sup> and many others<sup>209, 210</sup>. Especially, Sheno *et al.*<sup>211, 212, 213, 214</sup> have been extensively performing detailed studies on structural composite T-joints in marine structures by using both experimental and numerical approaches.

In this section, the layerwise higher-order model of the author is modified and applied to stress analysis of a structural joint in laminates. From a comparative study with experimental results available in the precedent literature, the validity of the layerwise higher-order model for such a challenging problem in the analysis and design of composite laminates is demonstrated.

### 6.3.1 Stress analysis of T-joint test specimen

Stress analysis of a T-Joint test specimen by the layerwise higher-order finite element will be demonstrated herein.

The structural T-joint picked up here is schematically shown in Figure 6.13. The T-Joint comprises a 560 mm flange and a 260 mm web which are 15 mm thick and made of 17 lay-ups of glass fiber woven roving (WR) cloth set. The flange and the web are connected by a resin fillet with a radius of 50 mm. The fillet is overlaid to form boundary angles. The boundary angles form 12 layup laminates, the detail of which is given in Figure 6.14. Delieu-Smith *et al.*<sup>215</sup> have quantitatively obtained stress distributions across the thickness of the boundary angles by thermoelastic stress analysis. As the experimental equipment for the thermoelastic stress analysis, they used the SPATE (Stress Pattern Analysis by the measurement of Thermal Emissions) system. The test set-up for loading and SPATE scan area in the joint are illustrated in Figure 6.15. Further details of the thermoelastic stress analysis of this T-joint construction can be found in the original work of Delieu-Smith *et al.*<sup>215</sup>.

In the present study,  $[(332)^5]$  and  $[(332)^3]$  elements are used for modeling the T-joint. Each of the web, the boundary layers and the fillet layers is individually represented by a specific layer. Elastic properties used for the present finite element



analysis are, if any, taken from the original works of Delieu-Smith *et al.* and given in Figure 6.14. Figure 6.16 shows the gridwork of finite element meshes and boundary conditions for the present finite element analysis.

In order to compare the present finite element results to the experimental results in the original work, stress values are transformed into  $\sigma_p + \alpha\sigma_t$ . The directions of  $\sigma_p$  and  $\sigma_t$  are schematically shown in Figure 6.14 as well.  $\alpha$  is a experimentally determined constant and according to Delieu-Smith,  $\alpha$  is set equal to 3.1 in this case.

In Figures 6.17 through 6.20, thermoelastic stress distributions along Line 1 through Line 4, which are shown in Figure 6.15(b), are compared. In addition to the present finite element results and the experimental results by SPATE system, Delieu-Smith *et al.* also obtained numerical results by 2-D continuum plain-strain element in ANSYS package, and therefore, they will also be shown for comparison. It is observed that the present FE results as well as the results by the 2-D continuum element indicate fairly satisfactory predictions of the stress distributions across the thickness compared to the experimental results. Therefore, the applicability of the present FE to detailed stress analysis of structural joints in composite laminates are, if partly, ensured.

Applications of the layerwise higher-order models to joint problems are quite beneficial to the efficient analysis and design of composite laminates. The example shown here implies that, by using the layerwise higher-order models alone, designer can evaluate almost all design quantities precisely, and conduct a satisfactory design of composite laminates.

## 6.4 Discussion

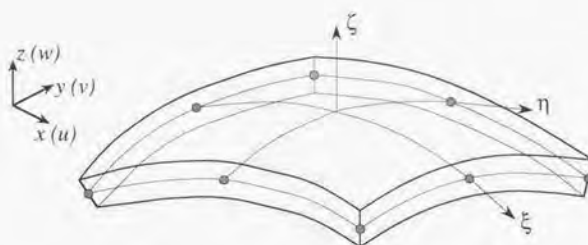
In this chapter, as the final examples derived from the layerwise higher-order model of the author, its two practical applications for structural analysis of composite laminates were presented.

In the first case, i.e., the extension of the layerwise higher-order plate element to the degenerated 3-D shell element, the finite element formulation was successfully performed coupled with a few refinements or adjustments to the layerwise higher-order assumption. It should be highlighted that the developed 3-D shell element is capable of representing the locally varying material principal directions (drapability effect) as well as transverse deformations (due to weaker properties over the thickness) and layerwise deformations (due to laminate-like inhomogeneity through the thickness), and hence this shell model will be one of the right answer to the three questions posed in Chapter 2. The developed 3-D shell element was applied to bending of a cross-ply spherical

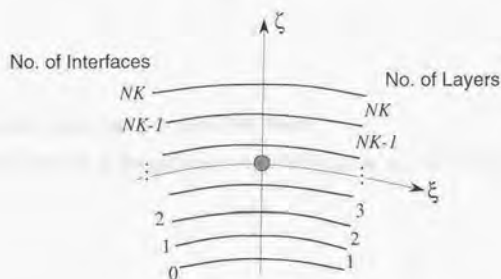


shell and the accuracy and the convergence property of the element were confirmed. The valid range of magnitude of the penalty numbers were also shown just like the case of the plate element in the previous chapter. The benefits of the developed 3-D shell element is many, and it is believed that in near future such a layerwise and higher-order shell element will be commonly used in the ordinary structural analysis and design of composite laminates.

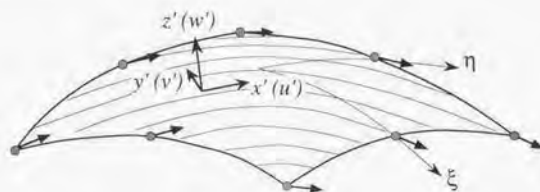
Next, in order to demonstrating the versatility of the layerwise higher-order model of the author, structural T-joint analysis by the layerwise element was conducted. The comparative study of the results by the present element to the experimental results certainly indicated that the accuracy and then the validity of the present model for such a challenging aspect in the structural analysis and design of composite laminates.



(a) Eight-node degenerated shell element

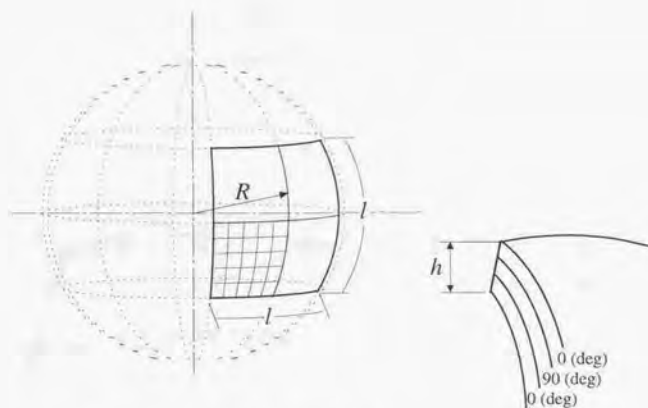


(b) Cross-section view of the shell element



(c) Definition of local coordinate system by interpolating nodal reference axes

Figure 6.1 Schematics of layerwise laminated degenerated 3-D shell element



*simply supported for all four edges*

*uniformly distributed lateral load ( $q_0$ ) on upper surface*

Figure 6.2 Schematics of geometry, boundary conditions and finite element meshes

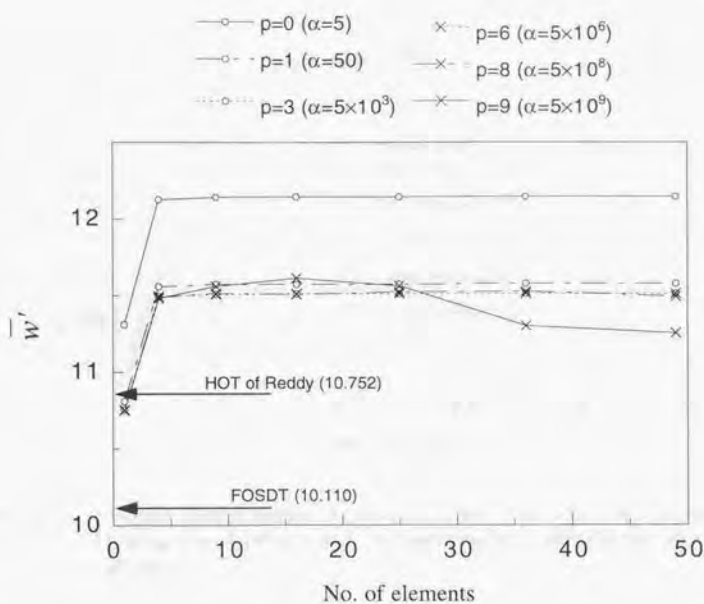


Figure 6.3 Deflections  $\bar{w}'$  at the center point  $(1/2, 1/2, 0)$  against the square mesh refinement for various penalty numbers in case of  $S = 10$  and  $R/l = 10$



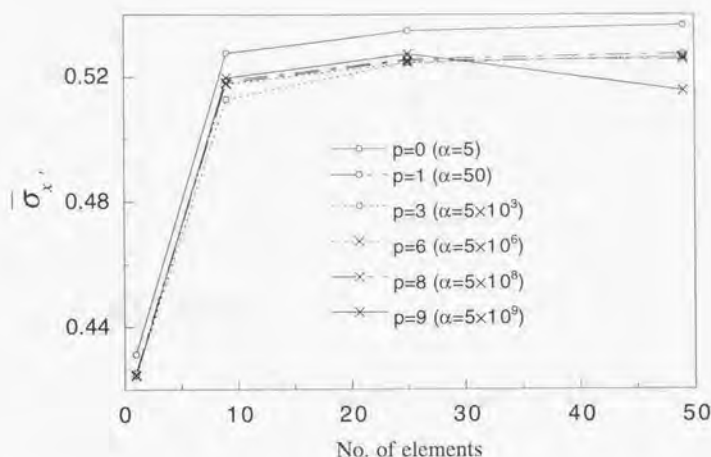


Figure 6.4 In-plane normal stresses  $\bar{\sigma}_{xx}$  at the quarter point  $(1/4, 1/4, 1/2)$  against the square mesh refinement for various penalty numbers in case of  $S = 10$  and  $R/l = 10$

Table 6.1 Non-dimensionalized central deflections  $\bar{w}'$  of the cross-ply spherical shell

$R/l$	source	$S = l/h = 10$	$S = l/h = 100$
1	FOSDT <sup>†</sup>	4.8173	0.0718
	HOT of Reddy <sup>‡</sup>	—	—
	present FE	5.5933	0.0713
10	FOSDT	10.110	3.6445
	HOT of Reddy	10.752	3.6426
	present FE	11.511	3.6803
100	FOSDT	10.218	6.6421
	HOT of Reddy	10.898	6.6496
	present FE	11.550	6.7442

<sup>†</sup> Reddy <sup>179</sup> in 1984

<sup>‡</sup> Reddy and Liu <sup>182</sup> in 1985

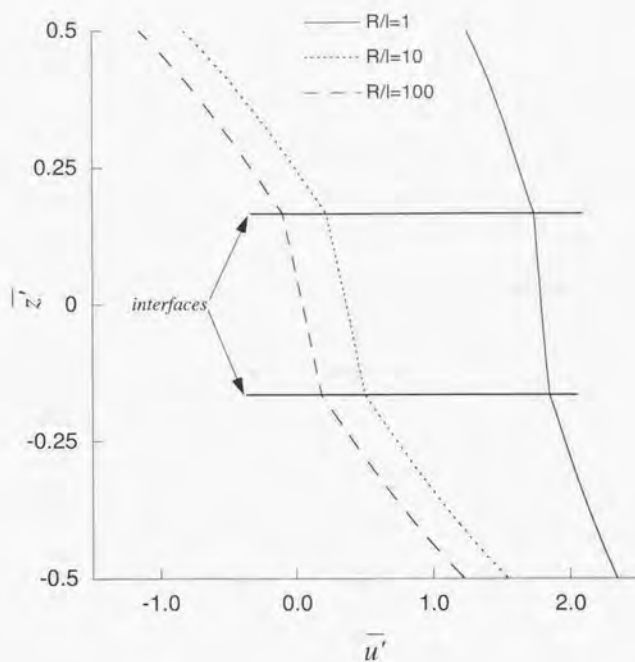


Figure 6.5 Through-the-thickness distributions of the in-plane displacement  $\bar{u}'$  at  $(1/4, 1/4, z')$  in case of  $S = 10$

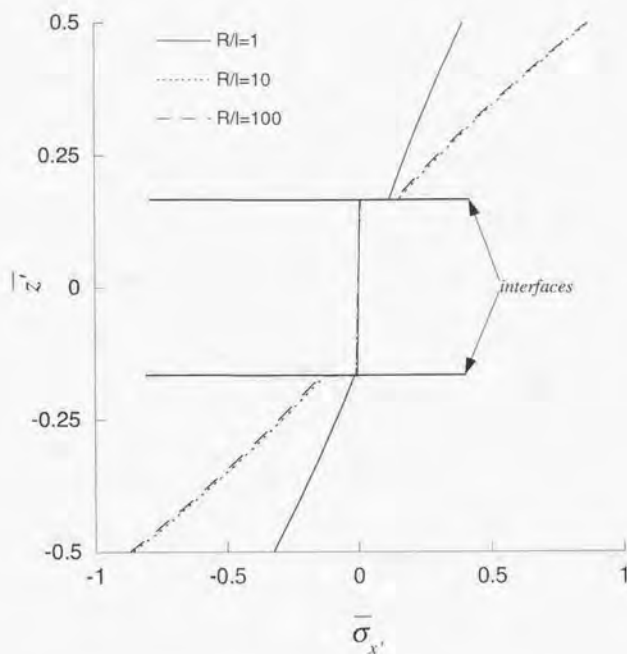


Figure 6.6 Through-the-thickness distributions of the in-plane normal stress  $\bar{\sigma}_{x'}$  at  $(1/4, 1/4, \bar{z}')$  in case of  $S = 10$

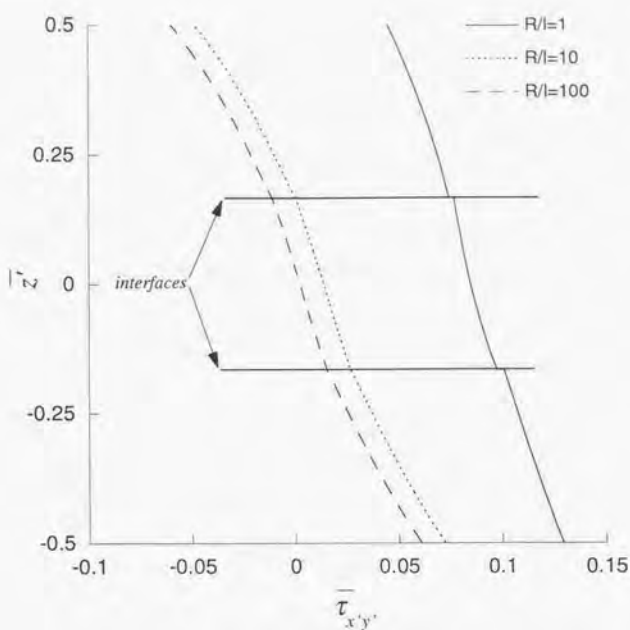


Figure 6.7 Through-the-thickness distributions of the in-plane shear stress  $\bar{\tau}_{x'y'}$  at  $(1/4, 1/4, z')$  in case of  $S = 10$



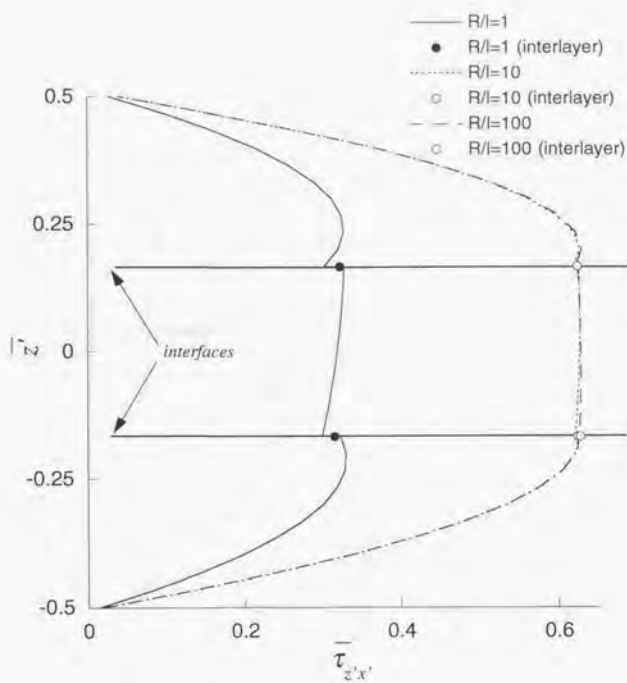


Figure 6.8 Through-the-thickness distributions of the transverse shear stress  $\bar{\tau}_{z'x'}$  at  $(1/4, 1/4, z')$  in case of  $S = 10$

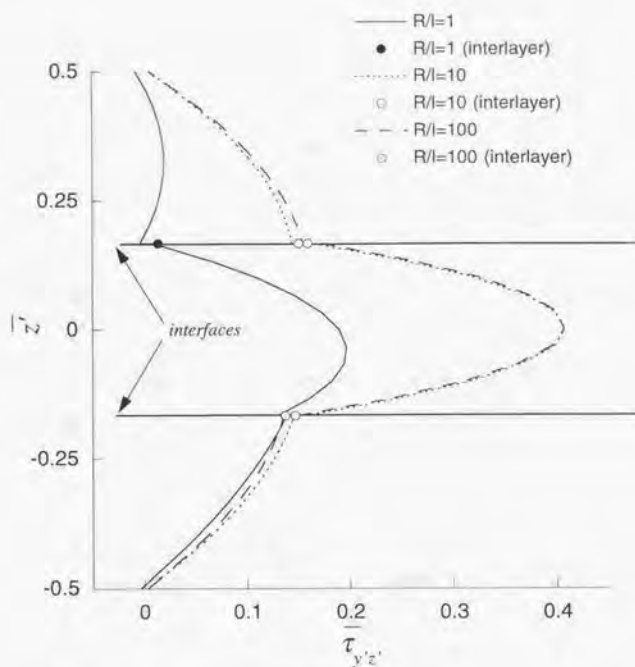


Figure 6.9 Through-the-thickness distributions of the transverse shear stress  $\bar{\tau}_{y'z'}$  at  $(1/4, 1/4, \bar{z})$  in case of  $S = 10$

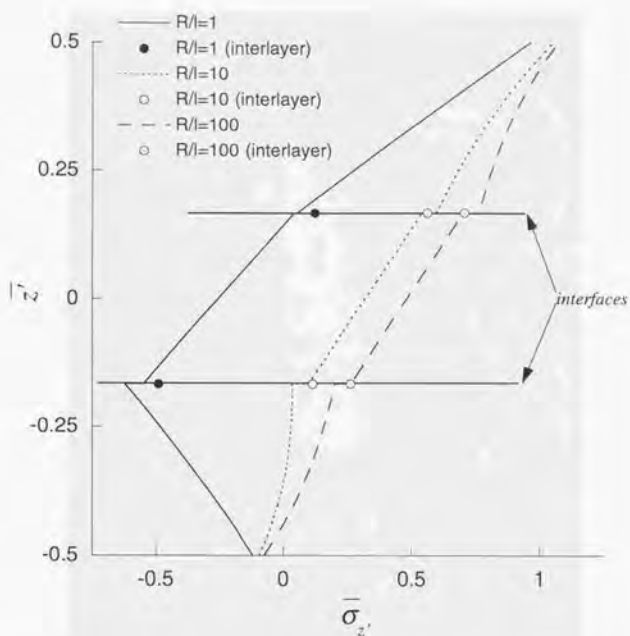
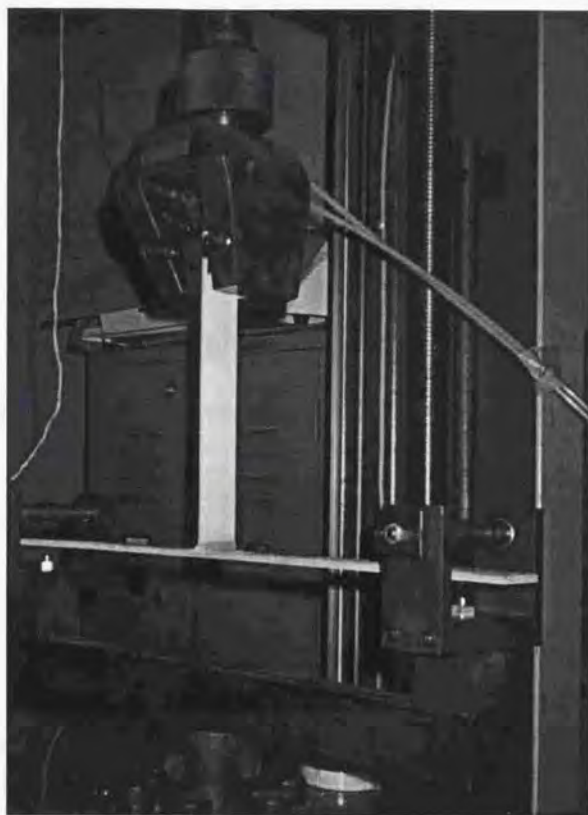


Figure 6.10 Through-the-thickness distributions of the transverse normal stress  $\bar{\sigma}_{z'}$  at  $(1/4, 1/4, \bar{z}')$  in case of  $S = 10$



Figure 6.11 Photographic view of Lap-Joint static tension-shear test  
(source : I. Kimpara, T. Suzuki and K. Suzuki <sup>206</sup>)





**Figure 6.12** Photographic view of T-Joint test  
(source : I. Kimpara, T. Suzuki and K. Suzuki <sup>206</sup>)

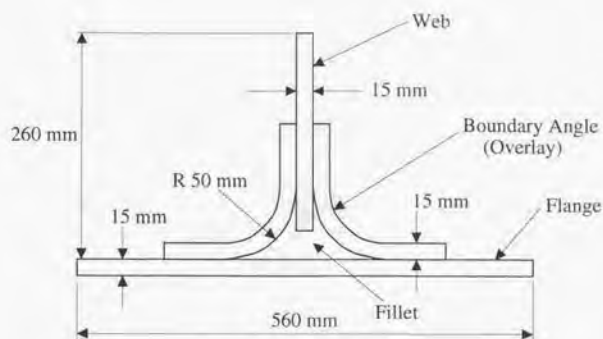


Figure 6.13 T-Joint construction (source : Dulieu-Smith *et al.* <sup>215</sup>)

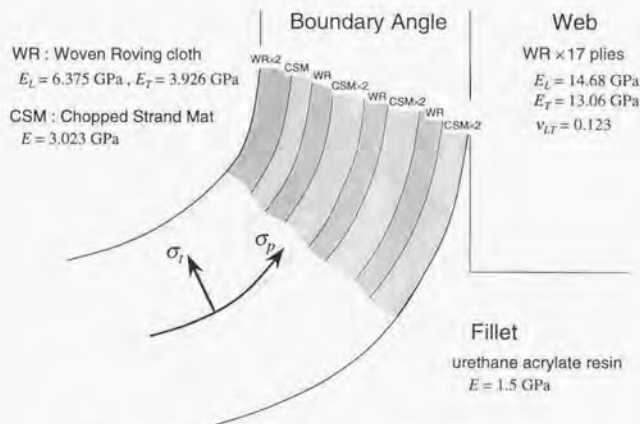
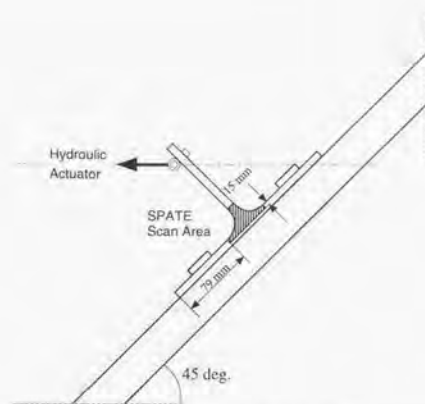


Figure 6.14 Design details of T-Joint construction

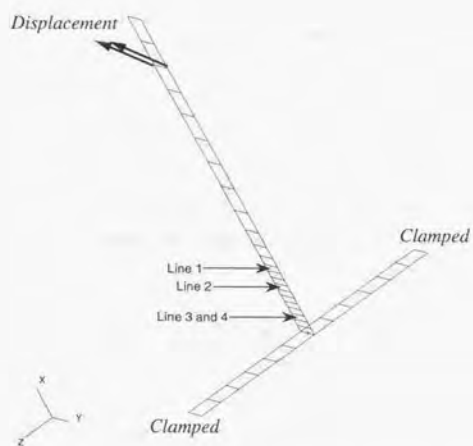


(a) Loading configuration

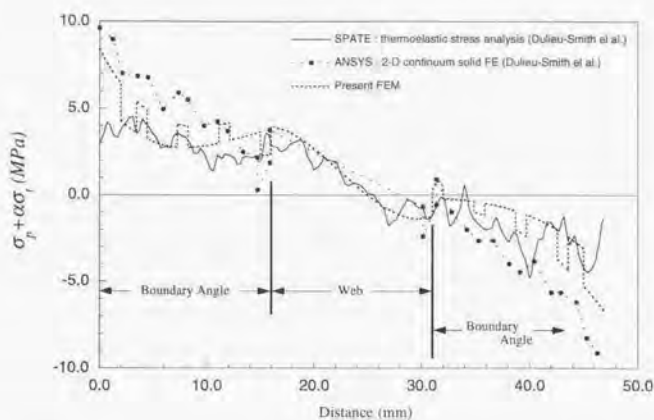
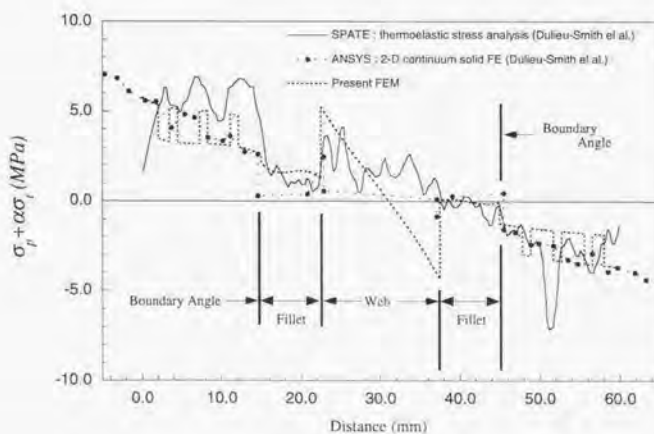


(b) Scan Area

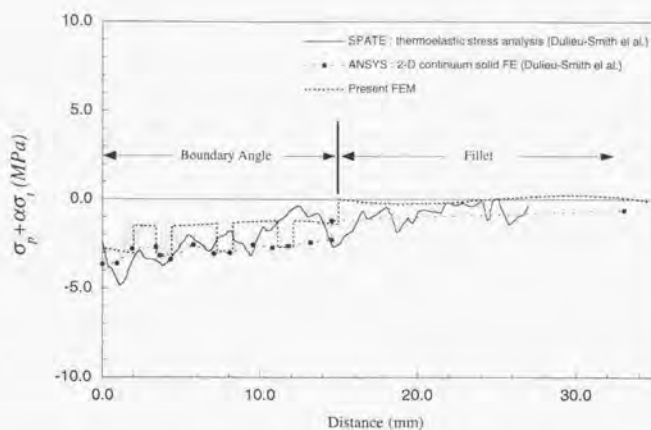
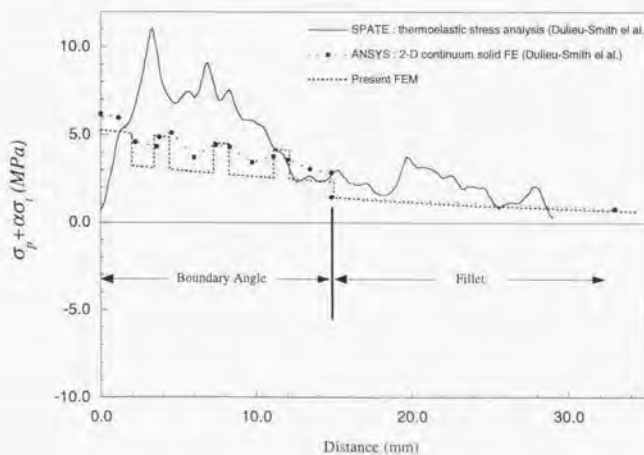
**Figure 6.15** Thermoelastic stress analysis by SPATE  
(source : Dulieu-Smith *et al.*<sup>215</sup>)



**Figure 6.16** Gridwork of finite element meshes and boundary conditions

Figure 6.17 Thermoelastic stress distribution across the thickness along *Line 1*Figure 6.18 Thermoelastic stress distribution across the thickness along *Line 2*



Figure 6.19 Thermoelastic stress distribution across the thickness along *Line 3*Figure 6.20 Thermoelastic stress distribution across the thickness along *Line 4*

## Chapter 7

## Conclusion

## 7.1 Conclusion to this thesis

Prior to the general concluding remarks on this thesis research, first briefly summarized is the whole.

1. Since laminated composite material structures (composite laminates) is seeking for their proper numerical model, which alternates the conventional model for isotropic homogeneous materials, the major goal of the present thesis research was placed on establishing proper and efficient numerical models for composite laminates.
2. The restrictions, limitations and deficiencies of the conventional numerical models were revealed through several case studies in which the author was actually involved during the early period of the thesis course. It was also highlighted that the three specific aspects of composite laminates, that is, anisotropic properties; weakness in the transverse direction; laminate-like, through-the-thickness inhomogeneity, are the primary obstacles which make numerical modelings for composite materials more complicated and skillful.
3. As a candidate for the numerical model suitable for composite laminates, the layerwise higher-order deformation theory was proposed and then its theoretical formulation was presented. The proposed theory identifies itself from other similar theories in that (a) the number of discretized layers is independent of the number of the actual laminae; (b) the orders of polynomial series of displacements assumed for each layer can be different from each other; (c) displacement continuity requirements at the layer interfaces are included by using either the direct elimination method or the penalty method as a specific approximation of Lagrange multiplier.
4. By using the proposed layerwise higher-order deformation theory, flexible and versatile numerical modeling methodology for composite laminates was established. The proposed methodology is inherently inductive and hence its validity should be confirmed through actual numerical applications step by step.
5. As the first example of the layerwise higher-order model of the author, selective layerwise sandwich element was developed. Through a couple of numerical examples, the validity and the superiority over the conventional models of the developed element were confirmed. On the other hand, the developed sandwich element employs direct elimination scheme for introducing interfacial displacement continuities. This fact restricts the applications of the element.

6. As the second example deduced from the layerwise higher-order model of the author,  $[(332)^{NK}]$  general laminated plate finite element was developed. In the finite element formulation, the penalty method were introduced for achieving interfacial displacement continuities. The accuracy and convergence property of the element was confirmed through a series of numerical results for a simple problem. The valid range of magnitude of the penalty numbers were also investigated. Furthermore, interlaminar stress evaluations and strain energy release rate calculations by the developed element were also demonstrated.
7. As the final examples derived from the layerwise higher-order model of the author, two cases of practical applications were conducted. The first case is the extension of the  $[(332)^{NK}]$  plate element to the layerwise degenerated 3-D shell element. After several key features of the developed 3-D shell element were shown, a simple numerical example was investigated by the developed shell element and its validity and practicability was ensured.
8. The latter case of the final examples is the application to the structural T-joint analysis. The layerwise higher-order finite element was modified and applied to the stress analysis of a T-joint. By comparing the present numerical model to the experimental results, beneficial potentials of the present models for such kind of challenging problems were partly demonstrated.

In consequence of these results summarized above, it is surely believed that primary purposes of the present thesis research have been accomplished to fairly satisfactory extent.

Nowadays, in the context of computational engineerings, studies on finite element modelings are regarded as something old-fashioned, however in finite element modelings for composite laminates, there are so much possibilities invoked towards their satisfactory analysis and design. Hence they will continue to be an active research subject.

The final goal of the present research is to break the deadlock in the analysis and design of composite laminates by the existing commercial finite element analysis packages. Certainly, the layerwise higher-order finite element models require large scale computations, but, on the opposite side, if one wish to analyze composite laminates precisely, then substantially large scale computations can not be avoided. On the other hand, the recent accelerating advancements of computational facilities symbolized by massive parallel computers equipped with vary large extensional core storages are allowing quite large scale structural analysis. Therefore, it is believed that the present



study will be highlighted in near future.

## 7.2 Future research proposals

As the final remarks on this thesis research, some future research proposals relevant to the present study are made herein.

Although it is possibly conducted a global structural analysis of composite laminates by using a specific layerwise higher-order model alone, more sophisticated and efficient analysis can be made by using a couple of different types of the models. The typical example is the global/local analysis scheme<sup>216, 217, 218</sup>. In this scheme, almost all regions of the structure is modeled by global models such as a ESL-based, first-order model while the limited critical regions such as free-edge regions and jointed parts are modeled by a few of local models like the layerwise higher-order models. Adjacent ESL-based elements and layerwise higher-order elements can be jointed by transition element models. This scheme will be easy to integrate into the program and quite effective without loss of accuracy. Recently, Reddy has proposed a global-local stress analysis scheme by superpositioning the results obtained from the ESL, and the Reddy's layerwise HOT solutions<sup>21</sup>.

Another attracting research is parallel computations of the layerwise higher-order finite elements. In the layerwise finite elements, one should evaluate elemental stiffness matrices layer by layer, and this will cause increase of computational time as the number of the layer increases. If the same number of processor elements (PE) as that of layers are available, one will need only one do-loop for evaluating the all of the layer contributions of elemental stiffness matrices. Furthermore, in the linear equation solver, one can also use these PE for solving the linear equations<sup>219</sup>. Thus, very fast and efficient computation will be achieved by parallel computations for the layerwise higher-order finite element analysis.



## Reference

1. Reissner, E., The effect of transverse shear deformation on the bending of elastic plates, *ASME JOURNAL OF APPLIED MECHANICS* **12** (1945), pp.69-77.
2. Bollé, E., Contribution au probleme lineaire de flexion d'une plaque elastique, *Bull. Technique de la Suisse Romande* **73** (1947), pp.281-285, 293-298.
3. Mindlin, R.D., Influence of rotatory inertia and shear on flexural motions of isotropic, elastic plates, *ASME JOURNAL OF APPLIED MECHANICS* **18** (1951), pp.31-38.
4. Ahmad, S., Irons, B.M. and Zienkiewicz, O.C., Analysis of thick and thin shell structures by curved finite elements, *International Journal for Numerical Methods in Engineering* **2** (1970), pp.419-451.
5. Zienkiewicz, O.C., Taylor, R.L. and Too, J.M., Reduced integration technique in general analysis of plates and shells, *International Journal for Numerical Methods in Engineering* **3** (1971), pp.275-290.
6. Ambartsumyan, S.A., *Theories of Anisotropic Shells*, Nauka, Moscow, (1961) and also available in *NASA TT F-118* (1964).
7. Reissner, E and Stavsky, Y., Bending and stretching of certain types of heterogeneous anisotropic elastic plates, *ASME JOURNAL OF APPLIED MECHANICS* **28**(3) (1961), pp.402-408.
8. Dong, S.B., Pister, K.S. and Taylor, R.L., On the theory of laminated anisotropic shells and plates, *Journal of the Aero/space Sciences* **29**(8) (1962), pp.969-975.
9. Whitney, J.M. and Leissa, A.W., Analysis of heterogeneous anisotropic plates, *ASME JOURNAL OF APPLIED MECHANICS* **36**(2) (1969), pp.261-266.
10. Whitney, J.M., The effect of boundary conditions on the response of laminated composites, *Journal of COMPOSITE MATERIALS* **4**(October) (1970), pp.192-203.
11. Ashton, J.E. and Whitney, M.J., *Theory of laminated plates*, Technomic, Wesport CT, (1970).
12. Yang, P.C., Norris, C.H. and Stavsky, Y., Elastic wave propagation in heterogeneous plates, *International Journal of Solids and Structures* **2** (1966), pp.665-684.
13. Whitney, J.M., The effect of transverse shear deformation in the bending of laminated plates, *Journal of COMPOSITE MATERIALS* **3** (1969), pp.534-547.
14. Whitney, J.M., Stress analysis of thick laminated composite and sandwich plates, *Journal of COMPOSITE MATERIALS* **6**(October) (1972), pp.426-440.
15. Whitney, J.M., Shear correction factors for orthotropic laminates under static load, *ASME JOURNAL OF APPLIED MECHANICS* **40**(1) (1973), pp.302-304.
16. Whitney, J.M. and Pagano, N.J., Shear deformation in heterogeneous anisotropic plates, *ASME JOURNAL OF APPLIED MECHANICS* **37**(4) (1970), pp.1031-1036.
17. Pryor, C.W. and Barker, R.M., A finite-element analysis including transverse shear effects for application to laminated plates, *AIAA Journal* **9** (1971), pp.912-917.

18. Reddy, J.N., A penalty plate-bending element for the analysis of laminated anisotropic composite plates, *International Journal for Numerical Methods in Engineering* **15** (1980), pp.1187-1206.
19. Reddy, J.N. and Chao, W.C., A comparison of closed-form and finite element solutions of thick laminated anisotropic rectangular plates, *Nuclear Engineering and Design* **64** (1981), pp.153-167.
20. Reddy, J.N. and Chao, W.C., Non-linear bending of thick rectangular, laminated composite plates, *International Journal of Non-Linear Mechanics* **16**(3/4) (1981), pp.291-301.
21. Reddy, J.N., An evaluation of equivalent-single-layer and layerwise theories of composite laminates, *Composite Structures* **25** (1993), pp.21-35.
22. *MARC Reference Library - Rev. K.5.2*, MARC Analysis Research Corp., California, (1993).
23. 高戸谷 健, 鈴木 浩治, 金原 勲, 影山 和郎, 先進複合材料によるマリンスラックチャの設計・製作支援システムの開発 (第3報, 異方性積層材料に適した有限要素法の適用), 日本造船学会論文集/日本造船学会 **178** (1996), pp.593-599.  
Takatoya, T., Suzuki, K., Kimpara, I. and Kageyama, K., Development of computer aided design and manufacturing system for advanced composite marine structures (3rd report : Application of finite element analysis for anisotropic laminated materials), *Journal of the Society of Naval Architects of Japan* **178** (1996), pp.593-599.
24. 金原 勲, 影山 和郎, 鈴木 浩治, 異方性積層板の高次変形を考慮した数値解析モデルについて, 日本複合材料学会講演会予稿集/日本複合材料学会 (1996), 5月, 東京, pp.39-40.  
Kimpara, I., Kageyama, K. and Suzuki, K., Numerical analysis models of anisotropic laminates considering higher-order deformations, *Proceedings of the Annual Research Meeting on Composite Materials / the Japan Society for Composite Materials* (1996), May, Tokyo, pp.39-40.
25. Pagano, N.J., Exact solutions for composite laminates in cylindrical bending, *Journal of COMPOSITE MATERIALS* **3** (1969), pp.398-411.
26. Pagano, N.J., Exact solutions for rectangular bidirectional composites and sandwich plates, *Journal of COMPOSITE MATERIALS* **4** (1970), pp.20-34.
27. Srinivas, S. and Rao, A.K., Bending, vibration and buckling of simply supported thick orthotropic rectangular plates and laminates, *International Journal of Solids and Structures* **6** (1970), pp.1463-1481.
28. Reddy, J.N., A simple higher-order theory for laminated composite plates, *ASME JOURNAL OF APPLIED MECHANICS* **51** (1984), pp.745-742.
29. 鈴木 浩治, 金原 勲, 影山 和郎, 積層複合材料構造の不均質レベルに応じた有限要素解析手法の提案, 第26回 FRP シンポジウム講演論文集/日本材料学会 (1997), 3月, 京都, pp.140-143.  
Suzuki, K., Kimpara, I. and Kageyama, K., An appropriate finite element analysis of laminated composite structures with consideration of their inhomogeneities, *JCOM : JSMS COMPOSITES-26* (1997), March, Kyoto, pp.140-143.
30. Engblom, J.J. and Ochoa, O.O., Thru-the-thickness stress predictions for laminated plates of advanced composite materials, *International Journal for Numerical Methods in Engineering* **21** (1985), pp.1759-1776.
31. Engblom, J.J. and Ochoa, O.O., Finite element formulation including interlaminar stress calculations, *Computers and Structures* **23**(2) (1986), pp.241-249.
32. Spencer, B.E., Composite drive shafting applications, *Proceedings of International SAMPE Symposium and Exhibition* **32**, Covina, CA, (1987), pp.650-661.
33. Nordstrand, T.M. and Carlsson, L.A., Evaluation of transverse shear stiffness of structural core sandwich plates, *Composite Structures* **37** (1997), pp.145-153.
34. M. Heder, Buckling of sandwich panels with different boundary conditions - A comparison between FE-analysis and analytical solutions, *Composite Structures* **19** (1991), pp.313-332.
35. *COMPOSIC V2.8 Reference Manual - Rev.C*, FRAMASOFT+CSI, Paris, (1995).

36. Reissner, E., Reflections on the theory on bending of elastic plates, *Applied Mechanics Reviews / the American Society of Mechanical Engineers* **38**(11) (1985), pp.1453-1464.
37. Reddy, J.N., A review of the literature on finite element modeling of laminated composite plates, *Shock and Vibration Digest* **17**(4) (1985), pp.3-8.
38. Reddy, J.N., A review of refined theories of laminated composite plates, *Shock and Vibration Digest* **22**(7) (1990), pp.3-17.
39. Noor, A.K. and Burton, W.S., Assessment of shear deformation theories for the multilayered composite plates, *Applied Mechanics Reviews / the American Society of Mechanical Engineers* **42**(1) (1989), pp.1-13.
40. 成田 吉弘, 複合材料構造物のモデリングと振動問題における研究展望, 日本機械学会論文集 (C 編) / 日本機械学会 **59** 巻 565 号 (1993), pp.2593-2599.  
Narita, Y., Modeling of composite structures and overview on the related vibration problems, *Transactions of the Japan Society of Mechanical Engineers. Series C* **59**(565) (1993), pp.2593-2599.
41. Naghdi, P.M., On the theory of thin elastic shells, *Quarterly of Applied Mathematics* **14** (1957), pp.369-380.
42. Librescu, L., On the theory of anisotropic elastic shells and plates, *International Journal of Solids and Structures* **3** (1967), pp.53-68.
43. Whitney, J.M. and Sun, C.T., A higher order theory for extensional motion of laminated anisotropic shells and plates, *Journal of Sound and Vibration* **30**(1) (1973), pp.85-97.
44. Nelson, R.B. and Lorch, D.R., A refined theory for laminated orthotropic plates, *ASME JOURNAL OF APPLIED MECHANICS* **41**(1) (1974), pp.177-183.
45. Reissner, E., On transverse bending of plates, including the effects of transverse shear deformation, *International Journal of Solids and Structures* **11**(5) (1975), pp.569-573.
46. Krishna Murty, A.V., Higher-order theory for vibrations of thick plates, *AIAA Journal* **15**(12) (1977), pp.1823-1824.
47. Lo, K.H., Christensen, R.H. and Wu, E.M., A higher-order theory plate deformation, Part 1: homogeneous plates, Part 2: Laminated plates, *ASME JOURNAL OF APPLIED MECHANICS* **44**(4) (1977), pp.663-676.
48. Lo, K.H., Christensen, R.M. and Wu, E.M., Stress solution determination for high order plate theory, *International Journal of Solids and Structures* **14** (1978), pp.655-662.
49. Bhimaraddi, A. and Stevens, L.K., A higher order theory for free vibration of orthotropic, homogeneous, and laminated rectangular plates, *ASME JOURNAL OF APPLIED MECHANICS* **51** (1984), pp.745-752.
50. Di Sciuva, M., Bending, vibration and buckling of simply supported thick multilayered orthotropic plated: an evaluation of a new displacement model, *Journal of Sound and Vibration* **105**(3) (1986), pp.425-442.
51. Kant, T., Numerical analysis of thick plates, *Computer Methods in Applied Mechanics and Engineering* **31**(1) (1982), pp.1-18.
52. Pandya, B.N. and Kant, T., Higher-order shear deformable theories for flexure of sandwich plates - finite element evaluations, *International Journal of Solids and Structures* **24** (1988), pp.1267-1286.
53. Kant, T., Arora, C.P. and Varaiya, J.H., Finite element transient analysis of composite and sandwich plates based on a refined theory and a mode superposition method, *Composite Structures* **22** (1992), pp.109-120.
54. Reddy, J.N., A refined nonlinear theory of plates with transverse shear deformation, *International Journal of Solids and Structures* **20**(9/10) (1984), pp.881-896.



55. Putcha, N.S. and Reddy, J.N., Stability and natural vibration analysis of laminated plates by using a mixed element based on a refined plate theory, *Journal of Sound and Vibration* **104**(2) (1984), pp.633-638.
56. Reddy, J.N. and Phan, N.D., Stability and vibration of isotropic, orthotropic and laminated plates according to a higher-order shear deformation theory, *Journal of Sound and Vibration* **98**(2) (1985), pp.157-170.
57. Librescu, L. and Reddy, J.N., A few remarks concerning several refined theories of anisotropic composite laminated plates, *International Journal of Engineering Science* **27** (1989), pp.515-527.
58. Reddy, J.N., A general non-linear third-order theory of plates with transverse shear deformation, *International Journal of Non-linear Mechanics* **25** (1990), pp.677-686.
59. Mau, S.T., Tong, P. and Pian, T.H.H., Finite element solutions for laminated thick plates, *Journal of Composite Materials* **6** (1972), pp.304-311.
60. Pian, T.H.H., Derivation of element stiffness matrices by assumed stress distributions, *AIAA Journal* **2** (1964), p.1333.
61. Lion, W.J. and Sun, C.T., A three-dimensional hybrid stress isoparametric element for the analysis of laminated composite plates, *Computers and Structures* **25**(2) (1987), pp.241-249.
62. Rao, K.M. and Meyer-Piening, H.R., Analysis of sandwich plates using a hybrid-stress finite element, *AIAA Journal* **29** (1991), pp.1498-1506.
63. Han, J. and Hoa, S.V., A three-dimensional multilayer composite finite element for stress analysis of composite laminates, *International Journal for Numerical Methods in Engineering* **36** (1993), pp.3903-3914.
64. Spilker, R.L., Chou, S.C. and Orringer, O., Alternate hybrid-stress elements for analysis of multilayer composite plates, *Journal of Composite Materials* **11** (1977), pp.51-70.
65. Spilker, R.L., Hybrid-stress eight-node elements for thin and thick multilayer laminated plates, *International Journal for Numerical Methods in Engineering* **18** (1982), pp.801-828.
66. Spilker, R.L., An invariant eight-node hybrid-stress element for thin and thick multilayer laminated plates, *International Journal for Numerical Methods in Engineering* **20**(3) (1984), pp.573-582.
67. Spilker, R.L. and Engelmann, B.E., Hybrid-stress isoparametric elements for moderately thick and thin multilayer plates, *Computer Methods in Applied Mechanics and Engineering* **56**(3) (1986), pp.339-361.
68. Pagano, N.J., Stress field in composite laminates, *International Journal of Solids and Structures* **14**(4) (1978), pp.385-401.
69. Yeom, C.H. and Lee, S.W., An assumed strain finite element model for large deflection composite shells, *International Journal for Numerical Methods in Engineering* **28** (1978), pp.1749-1768.
70. Reissner, E., On a variational theorem in elasticity, *Journal of Mathematics and Physics* **29**(2) (1950), pp.90-95.
71. 守屋 一政, 繊維強化積層複合材から成る平板およびかくの有限要素解析について, 日本機械学会論文集 (A編) / 日本機械学会 **52** 巻 478 号 (1986), pp.1600-1607.  
Moriya, K., Laminated plate and shell elements for finite element analysis of advanced fiber reinforced composite structures, *Transactions of the Japan Society of Mechanical Engineers, Series A* **52**(478) (1986), pp.1600-1607.
72. Washizu, K., *Variational Methods in Elasticity and Plasticity*, 3rd. ed., Pergamon Press, Oxford/New York, (1982).
73. Murakami, H., A laminated composite plate theory with improved in-plane responses, *ASME JOURNAL OF APPLIED MECHANICS* **53**(3) (1986), pp.661-666.

74. Toledano, A. and Murakami, H., A high-order laminated plate theory with improved in-plane responses, *International Journal of Solids and Structures* **23**(1) (1987), pp.111-131.
75. Toledano, A. and Murakami, H., A composite plate theory for arbitrary laminate configurations, *ASME JOURNAL OF APPLIED MECHANICS* **54**(1) (1987), pp.181-189.
76. Reissner, E., On a certain mixed variational principle and a proposed application, *International Journal for Numerical Methods in Engineering* **20** (1984), pp.1366-1368.
77. Reissner, E., On a mixed variational theorem and on shear deformable plate theory, *International Journal for Numerical Methods in Engineering* **23** (1986), pp.193-198.
78. Bhaskar, K. and Varadan, T.K., Reissner's new mixed variational principle applied to laminated cylindrical shells, *Transactions of the ASME. Journal of Pressure Vessel Technology* **114** (1992), pp.115-119.
79. Sun, C.T. and Whitney, J.M., Theories for the dynamic response of laminated plates, *AIAA Journal* **11**(2) (1973), pp.178-183.
80. Mau, S.T., A refined laminated plate theory, *ASME JOURNAL OF APPLIED MECHANICS* **40**(2) (1973), pp.606-607.
81. Srinivas, S., A refined analysis of composite laminates, *Journal of Sound and Vibration* **12**(2) (1973), pp.187-199.
82. Epstein, P.S. and Huttelmaier, H.P., A finite element formulation for multilayered and thick plates, *Computers and Structures* **16**(5) (1983), pp.645-650.
83. Owen, D.R.J. and Li, Z.H., A refined analysis of laminated plates by finite element displacement methods — I. Fundamentals and static analysis. — II. Vibration and stability, *Computers and Structures* **26**(6) (1987), pp.907-923.
84. Chaudhuri, R.A. and Seide, P., Triangular finite element for analysis of thick laminated plates, *International Journal for Numerical Methods in Engineering* **24**(6) (1987), pp.1203-1244.
85. Chaudhuri, R.A. and Seide, P., An approximate method for prediction of transverse shear stresses in a laminated shell, *International Journal of Solids and Structures* **23**(8) (1987), pp.1145-1161.
86. Soldatos, K.P.A., A general laminated plate theory accounting for continuity of displacements and transverse shear stresses at material interfaces, *Composite Structures* **20** (1992), pp.195-211.
87. Wu, C.P. and Kuo, H.C., Interlaminar stresses analysis for laminated composite plates based on a local high order lamination theory, *Composite Structures* **20** (1992), pp.237-247.
88. Wu, C.P. and Kuo, H.C., An interlaminar stress mixed finite element method for the analysis of thick laminated composite plates, *Composite Structures* **24** (1993), pp.29-42.
89. Wu, C.P., Analysis of sandwich plates using a mixed finite element, *Composite Structures* **25** (1993), pp.397-405.
90. Wu, C.P. and Hsu, C.S., A new local high-order laminate theory, *Composite Structures* **25** (1993), pp.439-448.
91. Verijenko, V.E., Nonlinear analysis of laminated composite plates and shells including the effects of shear and normal deformation, *Composite Structures* **25** (1993), pp.173-185.
92. Verijenko, V.E., Geometrically nonlinear higher order theory of laminated plates and shells with shear and normal deformation, *Composite Structures* **29** (1994), pp.161-179.
93. Reddy, J.N., On the generalization of displacement-based laminate theories, *Appl. Mech. Rev.* **42** (1989), pp.213-222.
94. Reddy, J.N., Barbero, E.J. and Teply, J.L., A plate bending element based on a generalized laminate plate theory, *International Journal for Numerical Methods in Engineering* **28** (1989), pp.2275-2292.



95. Barbero, E.J. and Reddy, J.N., An accurate determination of stresses in thick laminates using a generalized plate theory, *International Journal for Numerical Methods in Engineering* **29** (1990), pp.1-14.
96. Robbins, Jr., D.H. and Reddy, J.N., Modelling of thick composite using a layerwise laminate theory, *International Journal for Numerical Methods in Engineering* **36** (1993), pp.655-677.
97. Reddy, J.N., A generalization of two-dimensional theories of laminated composite plates, *Communications in Applied Numerical Methods* **3** (1987), pp.173-180.
98. Vinson, J.R., Sierakowski, R.L. 著, 福田 博, 野村 靖一, 武田 展雄 訳, 複合材料の構造力学, 日刊工業新聞社, 東京, (1987).  
Vinson, J.R. and Sierakowski, R.L., *The Behavior of Structures Composed of Composite Material*, Martinus Nijhoff, Dordrecht, (1986).
99. Kimpara, I., Takehana, M. and Yabe, S., Finite element analysis of sandwich composite structures, *FUKUGO ZAIRYO KENKYU Composite Materials and Structures* **3**(2) (1974), pp.9-17.
100. Ascione, L. and Fraternali, F., A penalty model for the analysis of curved composite beams, *Computers and Structures* **45**(5/6) (1992), pp.985-999.
101. Fraternali, F. and Reddy, J.N., A penalty model for the analysis of laminated composite shells, *International Journal of Solids and Structures* **30** (1993), pp.3337-3355.
102. Oden, J.T. and Kikuchi, N., Finite element methods for constrained problems in elasticity, *International Journal for Numerical Methods in Engineering* **18** (1982), pp.701-825.
103. 矢川 元基, 平山 浩, 三好 昭生, 安藤 良夫, ベナルティ関数を用いた殻の接触解析, 日本機械学会論文集 (A編) / 日本機械学会 **48** 巻 428 号 (1982), pp.454-466.  
Yagawa, G., Hirayama, H., Miyoshi, A. and Ando, Y., *Transactions of the Japan Society of Mechanical Engineers. Series A* **48**(428) (1982), pp.454-466.
104. Kant, Y. and Yagawa, G., A dynamic contact buckling analysis by the penalty finite element method, *International Journal for Numerical Methods in Engineering* **29** (1990), pp.755-774.
105. 金原 勲, 影山 和郎, 鈴木 浩治, 高戸谷 健, 高次要素による複合材料構造の有限要素法解析, 第 19 回 複合材料シンポジウム講演要旨集 / 日本複合材料学会 (1994), 1 2 月, 東京, pp.145-148.  
Kimpara, I., Kageyama, K., Suzuki, K. and Takatoya, T., Finite element analysis of composite laminated structures by high-degree elements, *Proceedings of the 19th Symposium on Composite Materials / the Japan Society for Composite Materials* (1994), December, Tokyo, pp.145-148.
106. Reissner, E., Small bending and stretching of sandwich-type shells, *NACA TN - 1832* (1949), pp.1-89.
107. Ha, K.H., Finite element analysis of sandwich plates: an overview, *Computers and Structures* **37** (1990), pp.397-403.
108. Rao, D.K., Buckling coefficients for FRP faced sandwich panels under combined loading, *AIAA Journal* **25** (1987), pp.733-739.
109. Manjunatha, B.S. and Kant, T., New theories for symmetric/unsymmetric composite and sandwich beams with  $C^0$  finite elements, *Composite Structures* **23** (1993), pp.61-73.
110. Dobyns, A.L., The analysis of simply-supported orthotropic plates subjected to static and dynamic loads, *AIAA Journal* **19** (1981), pp.642-650.
111. Allen, H.G., *Analysis and design of sandwich panels*, Pergamon Press, Oxford/New York, (1969).
112. 影山 和郎, 複合材料の破壊力学 (I), 日本複合材料学会誌 / 日本複合材料学会 **18**(2) (1992), pp.83-89.  
Kageyama, K., *Journal of the Japan Society for Composite Materials* **18**(2) (1992), pp.83-89.
113. 影山 和郎, 複合材料の破壊力学 (II), 日本複合材料学会誌 / 日本複合材料学会 **18**(4) (1992), pp.158-165.  
Kageyama, K., *Journal of the Japan Society for Composite Materials* **18**(4) (1992), pp.158-165.

114. 影山 和郎, 複合材料の破壊力学 (III), 日本複合材料学会誌/日本複合材料学会 18(5) (1992), pp.208-214.  
Kageyama, K., *Journal of the Japan Society for Composite Materials* 18(5) (1992), pp.208-214.
115. Hayashi, T., Analytical study of interlaminar shear stresses in a laminated composite plate, *Transactions of the Japan Society for Aeronautical Engineering and Space Sciences* 10(17) (1967), p.43.
116. Sierakowski, R.L. and Ebcioğlu, I.K., On interlaminar shear stresses in composites, *Journal of COMPOSITE MATERIALS* 4 (1970), pp.144-149.
117. Salamon, N.J., An assessment of the interlaminar stress problem in laminated composites, *Journal of COMPOSITE MATERIALS Supplement* 14 (1980), pp.177-194.
118. Puppo, A.H. and Evensen, H.A., Interlaminar shear in laminated composites under generalized plane stress, *Journal of COMPOSITE MATERIALS* 4 (1970), pp.204-220.
119. Pipes, R.B. and Pagano, N.J., Interlaminar stresses in composite laminates under uniform axial extension, *Journal of COMPOSITE MATERIALS* 4 (1970), pp.538-548.
120. Pipes, R.B., Moiré analysis of the interlaminar shear edge effect in laminated composites, *Journal of COMPOSITE MATERIALS* 5 (1971), pp.255-259.
121. Pagano, N.J., On the calculation of interlaminar normal stress in composite laminate, *Journal of COMPOSITE MATERIALS* 8 (1974), pp.65-82.
122. Pipes, R.B. and Pagano, N.J., Interlaminar stresses in composite laminates - An approximate elasticity solution, *ASME JOURNAL OF APPLIED MECHANICS* 41 (1974), pp.668-672.
123. Rybicki, E.F., Approximate three-dimensional solutions for symmetric laminates under inplane loading, *Journal of COMPOSITE MATERIALS* 5 (1971), pp.354-360.
124. Wang, A.S.D. and Crossman, F.W., Some new results on edge effect in symmetric composite laminates, *Journal of COMPOSITE MATERIALS* 11 (1977), pp.92-106.
125. Wang, A.S.D. and Crossman, F.W., Edge effects on thermally induced stresses in composite laminates, *Journal of COMPOSITE MATERIALS* 11 (1977), pp.300-312.
126. Raju, I.S. and Crews, J.R., J.H., Interlaminar stress singularities at a straight free edge in composite laminates, *Computers and Structures* 14(1-2) (1981), pp.21-28.
127. Whitcomb, J.D., Raju, I.S. and Gorre, J.G., Reliability of the finite element method for calculating free edge stresses in composite laminates, *Computers and Structures* 15 (1982), pp.23-37.
128. Whitcomb, J.D. and Raju, I.S., Superposition method for analysis of free-edge stresses, *Journal of COMPOSITE MATERIALS* 17 (1983), pp.492-507.
129. Yeh, J.R. and Tadjbakhsh, I.G., Stress singularity in composite laminates by finite element method, *Journal of COMPOSITE MATERIALS* 20(July) (1986), pp.347-364.
130. Tang, S., A boundary layer theory - Part I: Laminated composites in plane stress, *Journal of COMPOSITE MATERIALS* 9(January) (1975), pp.33-41.
131. Tang, S. and Levy, A., A boundary layer theory - Part II: Extension of laminated finite strip, *Journal of COMPOSITE MATERIALS* 9(January) (1975), pp.42-45.
132. Lekhnitskii, S.G., *Theory of Elasticity of an Anisotropic Elastic Body*, Holden-Day, San Francisco, (1963).
133. Ting, T.C.T. and Chou, S.C., Edge singularities in anisotropic composites, *International Journal of Solids and Structures* 17(11) (1981), pp.1057-1068.
134. Ting, T.C.T., Explicit solution and invariance of the singularities at an interface crack in anisotropic composites, *International Journal of Solids and Structures* 22(9) (1986), pp.965-983.

135. Wang, S.S. and Choi, I., Boundary-layer effects in composite laminates: Part 1 — Free-edge stress singularities, Part 2 — Free-edge stress solutions and basic characteristics, *ASME JOURNAL OF APPLIED MECHANICS* **49** (1982), pp.541-560.
136. Wang, S.S. and Yuan, F.G., A singular hybrid finite element analysis of boundary-layer stresses in composite laminates, *International Journal of Solids and Structures* **19** (1983), pp.825-837.
137. Yoseph, P.B. and Pian, T.H.H., Calculation of interlaminar stress concentration in composite laminates, *Journal of COMPOSITE MATERIALS* **15** (1981), pp.225-239.
138. Yoseph, P.B., On the accuracy of interlaminar stress calculation in laminated plates, *Computer Methods in Applied Mechanics and Engineering* **36** (1983), pp.309-329.
139. Zwiars, R.L., Ting, T.C.T. and Spilker, R.L., On the logarithmic singularity of free-edge stress in laminated composites under uniform extension, *ASME JOURNAL OF APPLIED MECHANICS* **49** (1982), pp.561-569.
140. Yin, W.L., Interlaminar stress analysis of composite laminates using a sublaminar/layer model, *International Journal of Solids and Structures* **31**(11) (1994), pp.1549-1564.
141. Griffin, Jr., O.H. and Roberts, J.C., Numerical/experimental correlation of three-dimensional thermal stress distributions in graphite/epoxy laminates, *Journal of COMPOSITE MATERIALS* **17**(November) (1983), pp.539-548.
142. Raju, I.S. and Crews, J.H., Three-dimensional analysis of  $[0/90]_S$  and  $[90/0]_S$  laminates with a central circular hole, *Composites Technol. Rev.* **4**(4) (1982), pp.116-124.
143. Lucking, W.M., Hoa, S.V. and Sankar, T.S., The effect of geometry on interlaminar stresses of  $[0/90]_S$  composite laminates with circular holes, *Journal of COMPOSITE MATERIALS* **17**(March) (1984), pp.188-198.
144. Hu, F.Z., Soutis, C. and Edge, E.C., Interlaminar stresses in composite laminates with a circular hole, *Composite Structures* **37** (1997), pp.223-232.
145. Isakson, G. and Levy, A., Finite-element analysis of interlaminar shear in fibrous composites, *Journal of COMPOSITE MATERIALS* **5**(April) (1971), pp.273-276.
146. Barsoum, R.S. and Freese, C.E., An iterative approach for the evaluation of delamination stresses in laminated composites, *International Journal for Numerical Methods in Engineering* **20** (1984), pp.1415-1431.
147. Pagano, N.J. and Pipes, R.B., The influence of stacking sequence on laminate strength, *Journal of COMPOSITE MATERIALS* **5** (1971), pp.50-57.
148. Pipes, R.B., Kaminski, B.E. and Pagano, N.J., Influence of the free edge upon the strength of angle-ply laminates, analysis of the test methods for high modulus fibers and composites, *ASTM STP* 521 (1973), American Society for Testing and Materials, pp.218-228.
149. Rotem, A. and Hashin, Z., Failure modes of angle ply laminates, *Journal of COMPOSITE MATERIALS* **9** (1975), pp.191-206.
150. Herakovich, C.T., Influence of layer thickness on the strength of angle-ply laminates, *Journal of COMPOSITE MATERIALS* **16**(May) (1982), pp.216-227.
151. Kim, R.Y. and Soni, S.R., Experimental and analytical studies on the onset of delamination in laminated composites, *Journal of COMPOSITE MATERIALS* **18**(January) (1984), pp.70-80.
152. Wang, S.S., Fracture mechanics for delamination problems in composite materials, *Journal of COMPOSITE MATERIALS* **17** (1983), pp.210-223.
153. Wang, S.S., Edge delamination in angle-ply composite laminates, *AIAA Journal* **22**(2) (1984), pp.256-264.
154. Rybicki, E.F. and Kanninen, M.F., A finite element calculation of stress-intensity factors by a modified crack-closure integral, *Engineering Fracture Mechanics* **9** (1977), pp.931-938.



155. Rybicki, E.F., Schmueser, D.W. and Fox, J., An energy release rate approach for stable crack growth in the free-edge delamination problem, *Journal of COMPOSITE MATERIALS* **11** (1977), pp.470-487.
156. Irwin, G.R., Analysis of stresses and strains near the end of a crack traversing a plate, *ASME JOURNAL OF APPLIED MECHANICS* **24** (1957), pp.361-364.
157. Wang, A.S.D. and Crossman, F.W., Initiation and growth of transverse cracks and edge delamination in composite laminates: Part 1. An energy method: Part 2. Experimental correlation, *Journal of COMPOSITE MATERIALS Supplement* **14** (1980), pp.71-87, 88-108.
158. Kim, K.S. and Hong, C.S., Delamination growth in angle-ply laminated composites, *Journal of COMPOSITE MATERIALS* **20**(September) (1986), pp.423-438.
159. 青木 隆平, 近藤 恭平, 異方性複合材料積層板の層間剥離 (I) 理論的検討, 日本航空宇宙学会誌/日本航空宇宙学会 第37巻 第420号 (1989), pp.29-38.  
Aoki, T. and Kondo, K., Free-edge delamination of anisotropic composite laminates (I) Theoretical approach, *Journal of the Japan Society for Aeronautical Space Sciences* **37**(420) (1989), pp.29-38.
160. Salpekar, S.A., Raju, I.S. and O'Brien, T.K., Strain-energy-release rate analysis of delamination in a tapered laminate subjected to tension load, *Journal of COMPOSITE MATERIALS* **25**(February) (1991), pp.118-141.
161. Whitcomb, J.D., Three-dimensional analysis of a postbuckled embedded delamination, *Journal of COMPOSITE MATERIALS* **23**(September) (1989), pp.862-889.
162. Salpekar, S.A., O'Brien, T.K. and Shivakumar, K.N., Analysis of local delaminations caused by angle ply matrix cracks, *Journal of COMPOSITE MATERIALS* **30**(4) (1996), pp.418-440.
163. Whitcomb, J.D. and Shivakumar, K.N., Strain-energy release-rate analysis of a laminate with a postbuckled delamination, *NASA TM* 89091 (1987).
164. Davidson, B.D. and Schapery, R.A., A technique for predicting mode I energy release rates using a first-order shear deformable plate theory, *Engineering Fracture Mechanics* **36**(1) (1990), pp.157-165.
165. Gim, C.K., Plate finite element modeling of laminated plates, *Computers and Structures* **52**(1) (1994), pp.157-168.
166. Pavier, M.J. and Clarke, M.P., A specialized composite plate element for problems of delamination buckling and growth, *Composite Structures* **34** (1996), pp.43-53.
167. Barbero, E.J. and Reddy, J.N., Modeling of delamination in composite laminates using a layer-wise plate theory, *International Journal of Solids and Structures* **28**(3) (1991), pp.373-388.
168. Barbero, E.J. and Reddy, J.N., The jacobian derivative method for three-dimensional fracture mechanics, *Communications in Applied Numerical methods* **6** (1990), pp.507-518.
169. Fuehne, J.P. and Engblom, J.J., Finite element/penalty function method for computing stress near debonds, *AIAA Journal* **30**(6) (1992), pp.1625-1631.
170. Noor, A.K. and Burton, W.S., Assessment of computational models for multilayered composite shells, *Applied Mechanics Reviews / the American Society of Mechanical Engineers* **43**(4) (1991), pp.647-650.
171. Love, A.E.H., *A Treatise on the Mathematical Theory of Elasticity*, 4th Ed., Dover Publications, New York, (1944).
172. Cheng, S. and Ho, B.P.C., Stability of heterogeneous anisotropic cylindrical shells under combined loading, *AIAA Journal* **1**(4) (1963), pp.892-898.
173. Whitney, J.M., On the use of shell theory for determining stresses in composite cylinders, *Journal of COMPOSITE MATERIALS* **5**(July) (1971), pp.340-353.



174. Gulati, S.T. and Essenberg, F., Effects of anisotropy in axisymmetric cylindrical shells, *ASME JOURNAL OF APPLIED MECHANICS* **34** (1967), pp.650-666.
175. Zukas, J.A. and Vison, J.R., Laminated transversely isotropic cylindrical shells, *ASME JOURNAL OF APPLIED MECHANICS* **38**(June) (1971), pp.400-407.
176. Dong, S.B. and Tso, F.K.W., On a laminated orthotropic shell theory including transverse shear deformation, *ASME JOURNAL OF APPLIED MECHANICS* **39**(December) (1972), pp.1091-1097.
177. Bert, C.W. and Kumar, M., Vibration of cylindrical shells of bimodulus composite materials, *Journal of Sound and Vibration* **81**(1) (1982), pp.107-121.
178. Bert, C.W. and Reddy, V.S., Cylindrical shells of bimodulus material, *Journal of the Engineering Mechanics Division, ASCE* **8**(EM5) (1982), pp.675-688.
179. Reddy, J.N., Exact solutions of moderately thick laminated shells, *Journal of the Engineering Mechanics Division, ASCE* **110**(5) (1984), pp.794-808.
180. Reddy, J.N. and Chandrashekhara, K., Nonlinear analysis of laminated shells including transverse shear strains, *AIAA Journal* **23**(3) (1985), pp.440-441.
181. Whitney, J.M. and Sun, C.T., A refined theory for laminated anisotropic cylindrical shells, *ASME JOURNAL OF APPLIED MECHANICS* **41** (1974), pp.471-476.
182. Reddy, J.N. and Liu, C.F., A higher-order shear deformation theory of laminated elastic shells, *International Journal of Engineering Science* **23** (1985), pp.319-330.
183. Kant, T. and Menon, M.P., Higher-order theories for composite and sandwich cylindrical shells with  $C^0$  finite element, *Computers and Structures* **33**(5) (1989), pp.1191-1204.
184. Kant, T. and Menon, M.P., Estimation of interlaminar stresses in fibre reinforced composite cylindrical shells, *Computers and Structures* **38**(2) (1991), pp.131-147.
185. Mallikarjuna and Kant, T., A general fibre-reinforced composite shell element based on a refined shear deformation theory, *Computers and Structures* **42**(3) (1992), pp.381-388.
186. Hsu, T.M. and Wang, J.T.S., A theory of laminated cylindrical shells consisting of layers of orthotropic laminatae, *AIAA Journal* **8**(12) (1970), pp.2141-2146.
187. Barbero, E.J., Reddy, J.N. and Teply, J.L., General two-dimensional theory of laminated cylindrical shells, *AIAA Journal* **28**(3) (1990), pp.544-553.
188. Wu, C.P. and Liu, C.C., A local high-order deformable theory for thick laminated cylindrical shells, *Composite structures* **29** (1994), pp.69-87.
189. Epstein, M. and Glockner, P., Nonlinear analysis of multilayered shells, *International Journal of Solids and Structures* **13** (1977), pp.1081-1089.
190. Di Sciuva, M., An improved shear-deformation theory for moderately thick multilayered anisotropic shells and plates, *ASME JOURNAL OF APPLIED MECHANICS* **54** (1987), pp.589-596.
191. Cho, M., Kim, K.O. and Kim, M.H., Efficient higher-order shell theory for laminated composites, *Composite Structures* **34** (1996), pp.197-212.
192. Pawskey, S.F. and Clough, R.W., Improved numerical integration of thick shell finite elements, *International Journal for Numerical Methods in Engineering* **3** (1971), pp.575-586.
193. Malkus, D.S. and Hughes, T.J.R., Mixed finite element methods — Reduced and selective integration techniques : A unification of concepts, *Computer Methods in Applied Mechanics and Engineering* **15** (1978), pp.63-81.
194. Milford, R.V. and Schnobrich, W.C., Degenerated isoparametric finite elements using explicit integration, *International Journal for Numerical Methods in Engineering* **23** (1986), pp.133-154.
195. Vlachoutsis, S., Explicit integration for three-dimensional degenerated shell finite elements, *International Journal for Numerical Methods in Engineering* **29** (1990), pp.861-880.

196. Panda, S. and Natarajan, R., Analysis of laminated composite shell structures by finite element method, *Computers and Structures* **14**(3-4) (1981), pp.225-230.
197. Chao, W.C. and Reddy, J.N., Analysis of laminated composite shells using a degenerated 3-D element, *International Journal for Numerical Methods in Engineering* **20** (1984), pp.1991-2007.
198. Yunus, S.M., Kohnke, P.C. and Saigal, S., An efficient through-thickness integration scheme in an unlimited layer doubly curved isoparametric composite shell element, *International Journal for Numerical Methods in Engineering* **28** (1989), pp.2777-2793.
199. 鈴木 浩治, 積層型およびサンドイッチ型複合材料構造の有限要素解析モデル, 平成6年度東京大学修士論文 (1995) 第4章, pp.33-46.  
Suzuki, K., *Master's degree Thesis of Engineering* (1995), the University of Tokyo, Tokyo, Chapter 4, pp.33-46.
200. Kim, K.D., Buckling behaviour of composite panels using the finite element method, *Composite Structures* **36** (1996), pp.33-43.
201. Kumar, W.P.P. and Palaninathan, R., Finite element analysis of laminated shells with exact through-thickness integration, *Computers and Structures* **63**(1) (1997), pp.173-184.
202. Swaddiwudhipong, S. and Kiu, Z.S., Response of laminated composite plates and shells, *Composite Structures* **37**(1) (1997), pp.21-32.
203. Mallikarjuna and Kant, T., A general fiber-reinforced composite shell element based on a refined shear deformation theory, *Computers and Structures* **42** (1992), pp.381-388.
204. Barbero, E.J., A 3-D finite element for laminated composites with 2-D kinematic constraints, *Computers and Structures* **45**(2) (1992), pp.263-271.
205. 金原 勲, 鈴木 敏夫, 鈴木 浩治, FRP の接着工法に関する基礎試験と構造継手試験 その1 基礎試験, FRP 漁船 第208号 (1997), pp.3-15.  
Kimpura, I., Suzuki, T. and Suzuki, K., *FRP Gyo-sen* No.208 (1997), pp.3-15.
206. 金原 勲, 鈴木 敏夫, 鈴木 浩治, FRP の接着工法に関する基礎試験と構造継手試験 その2 構造継手試験, FRP 漁船 第209号 (1997), pp.18-26.  
Kimpura, I., Suzuki, T. and Suzuki, K., *FRP Gyo-sen* No.209 (1997), pp.18-26.
207. Roy, S. and Reddy, J.N., A finite element analysis of adhesively bonded composite joints with moisture diffusion and delayed failure, *Computers and Structures* **29**(6) (1988), pp.1011-1031.
208. Barbero, E.J., Luciano, R. and Sacco, E., Three-dimensional plate and contact/friction elements for laminated composite joints, *Computers and Structures* **54**(4) (1995), pp.689-703.
209. Skrna-Jakl, L.C., Stiftinger, M.A. and Rammerstorfer, F.G., Numerical investigations of an imperfect stringer-stiffened composite wing torsion box — an analysis concept, *Composites: Part B* **27B** (1996), pp.59-69.
210. Hassan, N.K., Mohamedien, M.A. and Rizkalla, S.H., Finite element analysis of bolted connections for PFRP composites, *Composites: Part B* **27B** (1996), pp.339-349.
211. Sheno, R.A. and Violette, F.L.M., A study of structural composite tee joints in small boats, *Journal of Composite Materials* **24**(June) (1990), pp.644-666.
212. Sheno, R.A. and Hawkins, G.L., Influence of material and geometry variations on the behaviour of bonded tee connections in FRP ships, *Composites* **23**(5) (1992), pp.335-345.
213. Dodkins, A.R., Sheno, R.A. and Hawkins, G.L., Design of joints and attachments in FRP ships' structures, *Marine Structures* **7** (1994), pp.365-398.
214. Sheno, R.A., Read, P.J.C.L. and Hawkins, G.L., Fatigue failure mechanisms in fibre-reinforced plastic laminated tee joints, *International Journal of Fatigue* **17**(6) (1995), pp.415-426.
215. Smith-Dulien, J.M., Quinn, S., Sheno, R.A., Read, P.J.C.L. and Moy, S.S.J., Thermoelastic stress analysis of a GRP tee joint, *Applied Composite Materials* **4** (1997), pp.283-303.

216. Pagano, N.J. and Soni, S.R., Global-local laminate variational model, *International Journal of Solids and Structures* **19** (1983), pp.207-228.
217. Feng, W. and Hoa, S.V., 3-D transition element formulation for the global/local analysis of laminated structures, *The International Conference on Design and Manufacturing using Composites*, Montreal, Canada, (1994).
218. Hoa, S.V. and Feng, W., Global/local approach using hybrid elements for composites, *Proceeding of the 5th International Conference on Computer Aided Design in Composite Material Technology*, Computational Mechanics Publications, (1996), pp.319-328.
219. Goehlich, D., Komzsik, L. and Fulton, R.E., Application of a parallel equation solver to static FEM problems, *Computers and Structures* **31** (1989), pp.121-129.







